



University of
Stavanger

Faculty of Science and Technology

MASTER'S THESIS

Study program/Specialization: Petroleum Geosciences Engineering	Spring, 2019 Open
Writer: Alexandra Elizabeth Tatayo Muzo	<hr/> (Writer's signature)
Faculty supervisor: Nestor Cardozo	
Title of thesis: Sediment growth around salt diapirs: Analysis and interpretation using full-azimuth seismic data from the Central Nordkapp Basin, SW Barents Sea.	
Credits (ECTS): 30	
Keywords: <ul style="list-style-type: none">• Salt diapirs• Growth strata• Minibasin• Nordkapp• Salt-sediment interaction	Pages: 93 Stavanger, 15 th June 2019

Copyright

by

Alexandra Elizabeth Tatayo Muzo

2019

**Sediment growth around salt diapirs: Analysis and interpretation
using full-azimuth seismic data from the Central Nordkapp Basin,
SW Barents Sea**

by

Alexandra Elizabeth Tatayo Muzo

Master Thesis

Presented to the Faculty of Science and Technology

The University of Stavanger

The University of Stavanger

June 2019

Acknowledgements

This master thesis is submitted in completion of the Master program in Petroleum Geosciences Engineering at the University of Stavanger.

I would like to express special gratitude to my thesis supervisor Nestor Cardozo and my co-supervisor Luis Alberto Rojo for their academic support and knowledge.

I would also like to thank the University of Stavanger for providing the workstation, and WesternGeco Multiclient (Schlumberger) for providing the amazing dataset.

Finally, I would like to express my gratitude to my parents and friends for the unconditional support through this time.

Abstract

Sediment growth around salt diapirs: Analysis and interpretation using full-azimuth seismic data from the Central Nordkapp Basin, SW Barents Sea

Alexandra E. Tatayo Muzo.

The University of Stavanger, 2019

Supervisor: Nestor Cardozo

The Nordkapp Basin (Norwegian Barents Sea) comprises a large number of salt structures developed during Late Paleozoic-Early Mesozoic. Salt diapirism is dominant in this basin, and it influences all aspects of the petroleum system. This thesis focuses on the analysis of the growth of four Triassic salt diapirs (D1-D4) that control the distribution of sediments in the central sub-basin of the Nordkapp basin. Salt-sediment interaction is analysed through $\Delta d/d$ (d:depth) plots constructed from interpreted horizons on a full-azimuth seismic cube in the central sub-basin. The $\Delta d/d$ technique allows (1) understanding the distribution and depositional environments of the Triassic sediments affected by the diapirs, (2) providing a growth history of the salt diapirs and, (3) identifying angular unconformities that can act as stratigraphic traps. The results indicate that although the four diapirs growth history is roughly common, not all diapirs formed at the same time and in the same way. Lower Triassic intervals show large salt evacuation that led mainly to the rise of diapirs D2 and D3 in the SE. Early to Middle Triassic minor salt movement resulted in the collapse of diapir D4 in the N. Middle

Triassic-Jurassic intervals display depocenter migration, with diapirs D1 and D4 in the NW growing more than diapirs D2 and D3 in the SE. Late Triassic gliding and contractional diapirism generated teardrop diapirs. Shortening is recognized during the Cretaceous and Cenozoic, and it allowed the rejuvenation and growth of the diapirs. Middle Triassic fluvial systems (meandering and braided) were influenced by the diapirs growth. In places where diapir growth is high, these river channels divert and are far away from the diapir. On the contrary, in places where diapir growth is low, the channels are located close to the diapirs and even bypass them. Furthermore, knowing the history of the diapir growth may conduct to better constrains on its dimensions and surrounding stress field, which could reduce risk for drilling close to diapirs. These results have implications for hydrocarbon exploration since they can help predicting the location and timing of maximum growth, and the highest petroleum potential intervals.

Table of Contents

List of Tables	x
List of Figures.....	xi
1. Introduction.....	1
1.1. Background of salt and salt-related basins.....	7
1.1.1. Salt.	7
1.1.2. Salt structures: geometry and classification.....	8
1.1.3. Diapirism formation processes	8
2. Geological Setting.....	14
2.1. Introduction.....	14
2.2. Stratigraphical and structural evolution of the Nordkapp Basin	16
3. Dataset and Methodology	21
3.1. Dataset.....	21
3.2. Methodology	22
3.2.1. Seismic interpretation	22
3.2.2. Stratigraphic framework.	25
3.2.3. Δ /depth method.	26
4. Results	32
4.1. Seismic Facies: Description and Interpretation.	32
Seismic Facies F1	32
Seismic Facies F2	33
Seismic Facies F3	34
Seismic Facies F4	34
4.2. Structural maps of study area	37
Top Sequence S1: Lower Triassic	37
Base Sequence S3: Lower to Middle Triassic	38
Top Sequence S5: Middle Triassic	39
Top Megasequence MS2: Jurassic.....	40
4.3. Thickness maps of sequences in the central sub-basin	41
Sequence S1: Lower Triassic.....	41
Sequence S3: Lower to Middle Triassic	42
Top Sequence S5: Middle Triassic	43
Top Megasequence MS2: Jurassic.....	44
4.4. Basin profiles of the central sub-basin	45
Profile 1 (focused on sequence S1).....	46
Profile 2 (focused on sequence S3).....	48
Profile 3.....	50
4.5. Minibasin Stratigraphy of the central sub-basin	52
Megasequence 1: Lower Triassic-Upper Triassic.....	52
4.6. Diapir growth according to Multiple Bischke Plots (MBP) during Triassic.	55
Diapir growth: Early Triassic.....	58
Diapir Growth: Early to Middle Triassic	61
Diapir Growth: Middle Triassic-Jurassic.....	63

5. Discussions	66
5.1. Diapir growth history in the central sub-basin	66
5.2. Influence of the diapirs growth on the distribution of Triassic fluvial systems.	67
5.3. Implication in the petroleum system.	69
6. Conclusions.....	70
7. References.....	72

List of Tables

Table 1. Summary of seismic horizons that bound the megasequences.	22
Table 2. Summary of the different seismic facies in the minibasins of the study area. All facies interpretations are based exclusively on seismic interpretation and previous work of Rojo and Escalona (2018) and Rojo et al., 2019	33

List of Figures

Figure 1. Horizons slices showing submarine channels with varying morphology (From Carter et al., 2016). (A) Fast vertical movement of salt dome 1 causes the channel migration away from the salt structure and with a straight morphology. (B) Channels belt width around salt dome 2, which grows less than salt dome 1.	1
Figure 2. Bathymetric and topographic image of Barents Sea (Modified after Rowan et al., 2017) showing its provinces: (1) SW Norwegian Barents Sea, and (2) SE Norwegian Barents Sea. Red circle indicates the location of the study area.	2
Figure 3. (A) Distribution of basins with salt diapirism induced by the mobilization of Pennsylvanian to lower Permian evaporites within the western Barents Sea. (B) Structural elements of the western Barents Sea region with focus on the Nordkapp Basin. The basin is divided in three sub-basins: western, central, and eastern sub-basins. The study area is underexplored. Black dots are explored wells. Red rectangle shows the location of the full azimuth 3D cube used in this study. Modified after Rojo et al., 2019.	4
Figure 4. Depth slices showing the position of channels respect to the salt diapirs. (A) Depth slice 1872 m displays a meandering river with adjacent overbank deposits. (B) Depth slice 2048 m shows the braided system along the northwestern minibasin.	5
Figure 5(A) Salt structures classification (Fossen (2010)). (B) Evolution of salt diapirs and related halokinetic sequences as function of sedimentation rate vs salt-supply rate. Modified from Guiles and Lawton (2002).	9
Figure 6. Salt diapir growth by Trusheim (1960). I: Primary rim synclines. II: Secondary rim synclines. III: Tertiary sim synclines.	11
Figure 7. Profiles of a diapir formed in an extensional model. The northern section intersects a reactive diapir. In the southern section, the diapir evolved further to form a passive diapir (Hudec and Jackson, 2007).	11
Figure 8 Contractional diapirism. (A) Reactivated salt diapir growing during shortening. (a) The roof is faulted and thinned. (b) Active diapir rise due to the combination of roof thinning and pressurization of the salt. The rotation and erosion of the diapir crest occurs as salt diapir pierce through the overburden. (c) The diapir extrudes at the surface and forms a salt glacier (Hudec and Jackson, 2007). (B) Contractional diapirism that may create salt structures like teardrop diapirs.	13
Figure 9. Diapir Collapse. Left: Uninterpreted detail of the salt diapir collapse and its sediment overburden separated by a high amplitude reflector. Right: Interpreted detail of sag or collapse of diapir D4 showing a salt horn and the fault associated to the flank of the salt diapir.	13
Figure 10. Structural elements of the Southern Barents Sea region. Modified after Mattingsdal et al., 2015.	15
Figure 11. Tectono-stratigraphic chart of the Nordkapp Basin (Rojo et al., 2019)	17
Figure 12. (A) Cross section showing uncertainty on the size and shape of salt diapirs and artifacts that resemble faults. (B) Depth-slice (1872m) displaying artifact (red dotted line) close to a channel (yellow discontinuous-line). Red line marks the position of the cross section Red arrow on Figure 12A shows the height at which the depth slice intersects the cross section.	21

Figure 13 Cross section displaying the interpreted seismic horizons truncating against the salt diapirs: D4, D1 and D2 (from the NW to the SE). The inset structural map on the bottom left shows the location of this seismic line in the study area within the central sub-basin of the Nordkapp Basin. MS1 = megasequence 1; MS2 = megasequence 2; MS3 = megasequence 3; MS4 = megasequence 4; S1 = sequence 1; S2 = sequence 2; S3 = sequence 3; S4 = sequence 4; S5 = sequence 5; S6 = sequence 6.23

Figure 14. (A) Time slice of the SW sub-basin of Nordkapp Basin (from Rojo, 2015), showing areas of uncertainty where the salt-sediment interface is not clear. (B) Depth slice within the study area displays the high quality seismic imaging that allows a more accurate interpretation close to diapirs.24

Figure 15. Detailed seismic analysis of the Triassic succession based on previous works (Rojo et al 2019) and observations of these seismic units, growth strata, onlaps, downlaps, and truncations, which were interpreted to establish the major periods of salt mobilization and quiescence.. Triassic sequences are bounded by angular unconformities close to the diapir that become laterally flooding surfaces towards the southeast.25

Figure 16. (A) Delta prograding over pre-growth section causing sediment accumulation at different levels that allows horizon correlation in order to construct the $\Delta d/d$ diagram. (B) The slope records the growth from the structurally higher well 1 to well 2. A positive slope or discontinuity indicates expanded sections. While (C) a negative slope or discontinuity indicates the presence of a condensed or reduced section (from the structurally lower well 2 to well 3). Flat slopes show pre-growth intervals (Bischke, 1994).26

Figure 17. Linear $\Delta d/\text{depth}$ diagram for two wells showing a rough linear correlation of the data points with an exception for correlation 27, which indicates a miscorrelation (red circle). Modified after Bischke, 1994.27

Figure 18. Large unconformities can produce positive or negative slopes that resemble faults. (A) Onlap create a positive slope, while (B) downlap generates a negative slope. As a rule, unconformities tend to remain in the same stratigraphic level. In this case, both profiles show missing sections between horizon 1-3 levels. Thus, this feature is interpreted as an unconformity instead of a fault (Bischke, 1994).28

Figure 19. (A). Map showing strike and dip on the Rob L horizon on the flank of a salt diapir in the northern Gulf of Mexico, USA. In this environment, geoscientist have difficulties attributing missing section to faults or to large unconformities. (B) The MBP for the structurally higher reference Well No. 6 versus the five off-structure comparison wells. A large unconformity is interpreted above the Rob L horizon. In Well No. 1 and 3 the Fault J produces about 250 and 340 ft of missing section, respectively (Bischke, 1994).29

Figure 20. Structural map showing the location of the 42 pseudo-wells around the salt diapirs (D1, D2, D3 and D4) in the salt-bearing minibasins. Pseudo-wells labeled in different colors for each diapir; D1 flank SE in purple; D1 flank NW in black, D2 in blue; D3 in brown and D4 in green.31

Figure 21. Seismic line showing the different seismic facies in the minibasin of the study area. Seismic facies F4 and F1 are the dominant in the study area. Seismic facies F1 become seismic facies F4 which onlaps onto seismic facies F3. Seismic

facies F2 downlaps onto the basal unconformity (green line). Note the high-amplitude reflector between the seismic facies F4 indicating the presence of a channel. Arrows indicates the position of depth slices of Figure 22.35

Figure 22. Depth slices showing the position of channels respect to the salt diapirs. (Left)) Depth slice 1872 m displays a meandering river with adjacent overbank deposits. (Right) Depth slice 2048 m shows the braided system along the northwestern minibasin. Red and green lines indicate the position of seismic line of Figure 21.....36

Figure 23. Top Sequence S1 elevation structural map showing the extension of salt diapir D4 in the north and diapir D1 in the central part. Note diapirs D2 and D3 are not recognized at this level.....37

Figure 24. Base Sequence S3 structural map. Diapirs D1 and D4 are longer and diapir D3 is already visible while diapir D2 does not appear in this period.38

Figure 25. Structural depth map showing all salt diapirs: D1-D4. Note the deepest point in the north.39

Figure 26. Top Megasequence MS2 elevation map showing the structural configuration of the study area in the Jurassic. All four diapirs reach the seabed at their top. Minibasins widen due to diapirs are thinner.40

Figure 27. Depth thickness map of sequence S1 (Lower Triassic). Strata around diapir D1 thicken against the southeastern flank. SE minibasin displays the deepest strata.41

Figure 28. Thickness map of sequence S3. Largest depocenter is located in the southernmost part. Towards the north, strata thin against diapirs D1, D3 and D4.42

Figure 29. Depth thickness map of sequence S5 showing thinning towards diapirs. During Middle Triassic thickness variations are roughly constant.....43

Figure 30. Thickness map of megasequence MS2 showing constant thickness in both minibasins. In the northern part, note the thickness variation of minibasin enclosed by diapir D4.44

Figure 31. Left: Structural maps of sequence S3 showing the location of profiles through the interpreted salt diapirs D1, D2, d3 and D4. Right: insert map showing the distribution of salt structures within the Nordkapp Basin. Red rectangle indicates the extent of the study area.45

Figure 32. Profile 1 showing the stratigraphic and structural configuration of the study area within the central sub-basin in the Nordkapp Basin. The inset structural map of sequence S1 on the bottom left shows the location of this seismic line. Evidence of salt tectonic is observed from the Middle Triassic until Quaternary (e.g. truncation and thinning occurring at the top of S4). In the SE flank of salt diapir D1, Triassic sequence S1 and S2 are delimited by an angular unconformity that becomes conformable towards the NW. MS1 = megasequence 1; MS2 = megasequence 2; MS3 = megasequence 3; MS4 = megasequence 4; S1 = sequence 1; S2 = sequence 2; S3 = sequence 3; S4 = sequence 4; S5 = sequence 5; S6 = sequence 6.....47

Figure 34. Profile 2 displays the stratigraphic and structural configuration of the study area within the central sub-basin in the Nordkapp Basin. The inset structural map of the sequence S3 on the bottom left shows the location of this seismic line. Salt diapirs growth occur from the Lower Triassic until Quaternary (e.g. truncation and

thinning occurring at the top of S1 and S4). The largest depocenter is located in the SE minibasin, in which a shift in salt withdrawal caused the minibasin inversion. Note the marked thickness variations of S3 in each minibasin and the presence of channels in S5. MS1 = megasequence 1; MS2 = megasequence 2; MS3 = megasequence 3; MS4 = megasequence 4; S1 = sequence 1; S2 = sequence 2; S3 = sequence 3; S4 = sequence 4; S5 = sequence 5; S6 = sequence 6.....49

Figure 35. Profile 3 showing the stratigraphic and structural configuration of minibasins enclosed by diapirs D4 and D3. The inset structural map of megasequence MS2 on the bottom left shows the location of the profile. Halokinesis is observed from Lower Triassic until Quaternary (e.g. thickness variation of S1). Note that the largest depocenter is located in the SE minibasin. Triassic strata are separated from Jurassic strata by an unconformity. MS1 = megasequence 1; MS2 = megasequence 2; MS3 = megasequence 3; MS4 = megasequence 4; S1 = sequence 1; S2 = sequence 2; S3 = sequence 3; S4 = sequence 4; S5 = sequence 5; S6 = sequence 6.51

Figure 36. . Top: graph showing the Multiple Bischke Plot for the structurally higher Reference Well No.1 respect to 42 wells around every salt diapir. Bottom: the inset map (Figure 20) displays the structural configuration of the study area. The MBP depicts the overall growth trend for each diapir. During the Lower Triassic, diapirs D2 and D3 show a greater growth than diapir D1 and D4. Through the Lower-Middle Triassic, the growth trend is the same, SE salt structures keep growing more than NW diapirs. In the Middle Triassic-Jurassic, migration of depocenters occurred because of diapirs located to the NW (D1 and D4) grew more than diapirs D2 and D3 in the SE due to the salt depletion in this part. Two unconformities are identified between (1) Lower Triassic sequences S1 and S2, and (2) Middle Triassic and Jurassic strata. Minibasin inversion observed in Lower Triassic sequences.57

Figure 37. MBP for diapir D2 showing the minibasin inversion during Lower Triassic. A general growth trend driven by passive diapirism is recognized after the unconformity between sequences S1 and S2. The inset map displays the position of wells respect to the reference well, which is located closer to diapir D2.....58

Figure 38. Two-dimensional (2-D) cross section restoration taken from Rojo and Escalona et al., 2019 corresponding to the study area of this master thesis. (G-I) Early Triassic minibasins inversion due to the sub-salt faulting responsible for the salt evacuation and the subsequent shift in salt withdrawal. (E-F) Early to Middle Triassic diapir collapse or sag in response to minor movement of sub-salt. (C-E) Middle Triassic-Jurassic depocenters migrating from the SE to the NW. (D) Late Triassic gravity gliding to induce contractional diapirism and to form teardrop diapirs. (C) Early Cretaceous-Cenozoic regional shortening leading to the rejuvenation and growth of salt diapirs.....60

Figure 39. Graph showing the growth rate of diapir D4. Observing the general negative trend of the $\Delta d/d$ curves the growth rate relate to this salt structure is the lowest compared with the others diapirs due to diapir D4 underwent an extension episode that led to diapir collapse (Figure 30E-F).62

Figure 40. Graph showing the MBP for the NW flank of diapir D1, according to the negative slope of its $\Delta d/d$ curves, in this zone diapir D1 grew less than southeastern salt structures during the Triassic period.63

- Figure 41. (Top) MBP for diapir D1 (SE flank) showing a positive growth trend during the Triassic interval compared with its NW flank (Figure 32), although $\Delta d/d$ curves of wells located towards the N (wells 22-24) are adopting a negative trend what means a smaller growth rate in this region. (Bottom) Plot of $\Delta d/d$ curves related to diapir D3. Note the marked positive slope in contrast diapir D1, which indicates that diapir D3 has a greater growth rate than diapir D1 on its SE flank.64
- Figure 42. Graph showing the Multiple Bischke Plot for the structurally higher Reference Well No.1 respect to five wells around every salt diapir. The MBP depicts the overall growth trend for each diapir. During the Lower Triassic, diapirs D2 and D3 show a greater growth than diapir D1 and D4. Through the Lower-Middle Triassic, the growth trend is the same, SE salt structures keep growing more than NW diapirs. In the Middle Triassic-Jurassic, migration of depocenters occurred because of diapirs located to the NW (D1 and D4) grew more than diapirs D2 and D3 in the SE due to the salt depletion in this part. Two unconformities are identified between (1) Lower Triassic sequences S1 and S2, and (2) Middle Triassic and Jurassic strata. Minibasin inversion observed in Lower Triassic sequences.66
- Figure 43. Depth slice analysis of spectral decomposition applied over sequence S5 strata (Middle Triassic). (A) Depth slices at 1872 m showing the trajectory of the meandering channel bypassing the diapir D1 to reach the diapir D4. (B) Depth slice at 1872 m displays the braided system along the NW minibasin enclosed by D1 and D4.68
- Figure 44. (A) Uninterpreted seismic analysis of the Lower Triassic. (B) Interpreted detailed seismic analysis showing the angular unconformity between Lower Triassic sequences S1 and S2, that resulted from the formation of a half turtle structure.69

1. INTRODUCTION

Salt-bearing sedimentary basins around the world are attractive areas for hydrocarbon exploration since the occurrence of salt and its subsequent mobilization influence all aspects of the petroleum system. Some examples of successful hydrocarbons provinces with the presence of salt are offshore Brazil, Gulf of Mexico, and the North Sea.

In view of the above, salt-sediment interaction should be analyzed since the growth of salt structures significantly controls the development of fluvial systems and resultant stratigraphic architecture (Venus et al., 2015). Carter et al., (2016) illustrates an example of this relationship. In places where diapir growth is high, submarine channels divert and are far away from the diapir leading to single-story channels (Figure 1A). On the other hand, in places where diapir growth is low, submarine channels rapidly aggrade and locate close to the diapirs and even can bypass them, developing multi story channel complexes (Figure 1B). This influences on the quality of potential reservoirs.

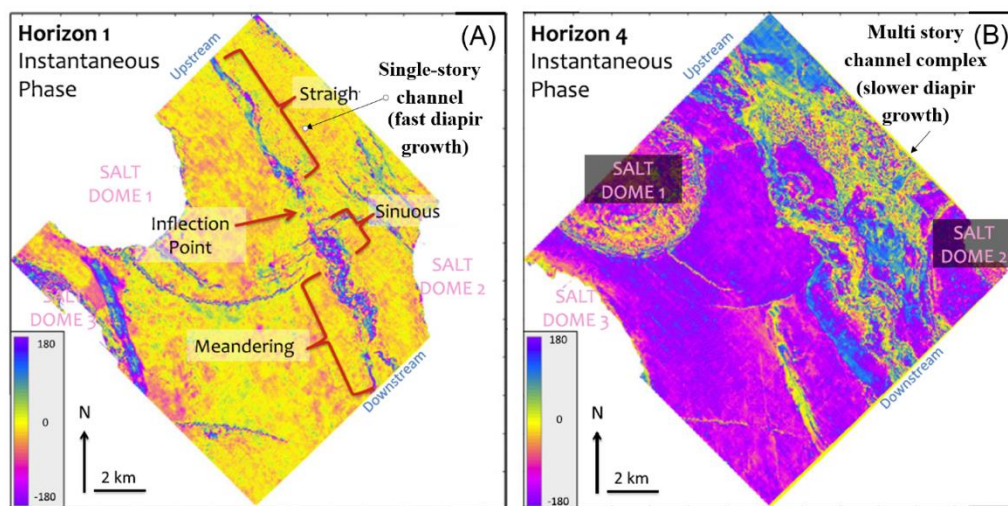


Figure 1. Horizons slices showing submarine channels with varying morphology (From Carter et al., 2016). (A) Fast vertical movement of salt dome 1 causes the channel migration away from the salt structure and with a straight morphology. (B) Channels belt width around salt dome 2, which grows less than salt dome 1.

The behavior of fluvial systems respect to the diapir growth rate has important implications for hydrocarbon exploration. For instance, in the second scenario of low diapir growth, there will be a higher chance for potential reservoirs on diapir flanks compared to the first situation of greater rate of salt diapir growth due to the distribution of reservoir-prone units around salt structures is better in terms of reservoirs connectivity.

This thesis focuses on an area located in the Nordkapp Basin, which is a confined salt-bearing basin in the southwest Barents Sea (Figure 2). The Nordkapp Basin is a NE-SW-trending basin (Figure 3A) developed during Late Paleozoic rifting. The Basin is divided in three sub-basins, the western, central, and eastern sub-basins.

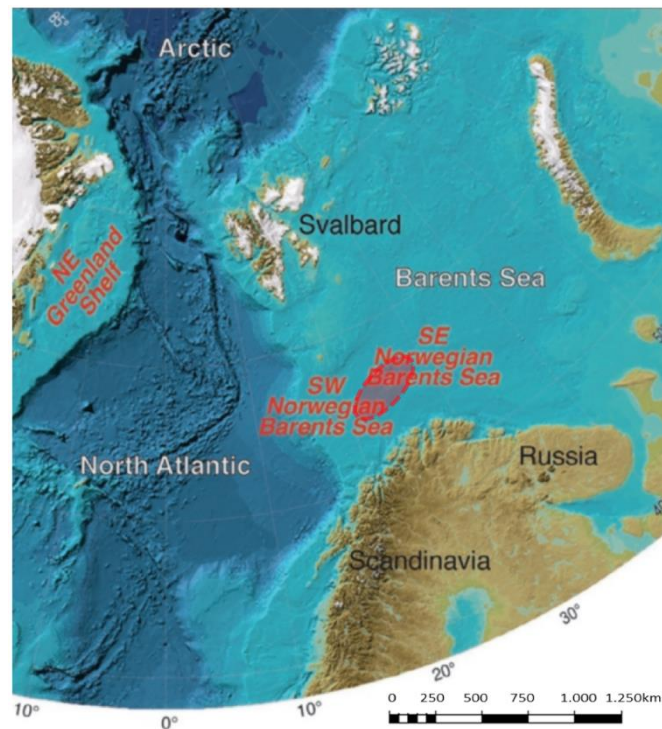


Figure 2. Bathymetric and topographic image of Barents Sea (Modified after Rowan et al., 2017) showing its provinces: (1) SW Norwegian Barents Sea, and (2) SE Norwegian Barents Sea. Red circle indicates the location of the study area.

This study focuses in the central sub-basin (Figure 3B). The central sub-basin remained closed for exploration for more than three decades (Koyi et al., 1993b). However, recently acquired seismic data allow testing hypotheses regarding the driving mechanisms of salt tectonics and their implications on the minibasins infill, with special focus on the Triassic (Rojo et al., 2019). During this period, salt growth generated topographic highs, which controlled sediment distribution pathways and acted as local sources of sediment for submarine debris flows and fan deltas developed adjacent to the salt structures (Rojo and Escalona, 2018). Likewise, salt depletion may have caused restricted sub-basins, favourable for organic-rich deposition (Bugge et al., 2002). From the interpretation of seismic data in these minibasins, it can be possible to recognize the influence of diapirs on the distribution of sediments and the relationship between diapir growth rate and sediment growth rate.

The study area within the central sub-basin of the Nordkapp Basin is covered by a 3D full-azimuth seismic cube kindly provided by WesternGeco/Schlumberger (Figure 3B). In this cube, there are four salt diapirs here named diapirs D1, D2, D3 and D4. Diapirs D1 and D3 are in the central zone of the data set, diapir D2 is in the east, and diapir D4 is in the west (Figure 3B). Two salt minibasins are surrounded by these salts structures forming large depocenters infilled with Triassic sediments. In depth slices, these sediments display fluvial systems characterized by intercalations of channels and overbank deposits (Figure 4).

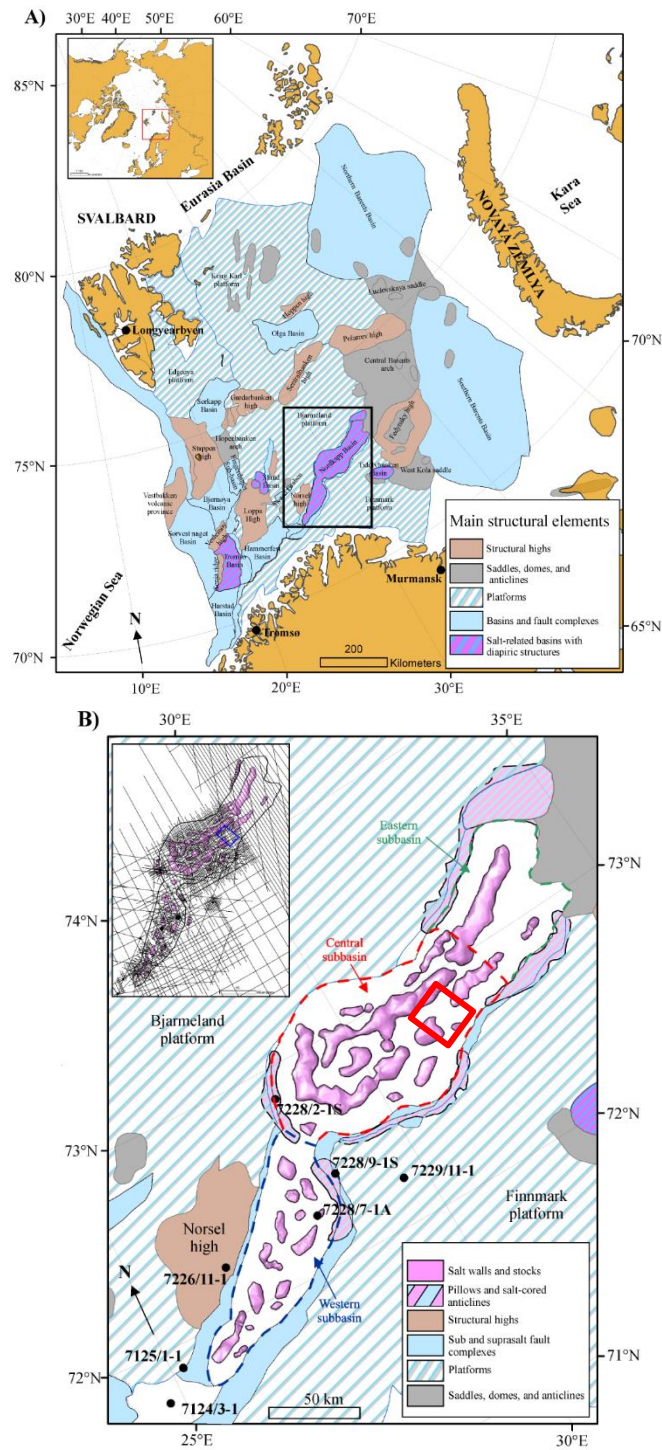
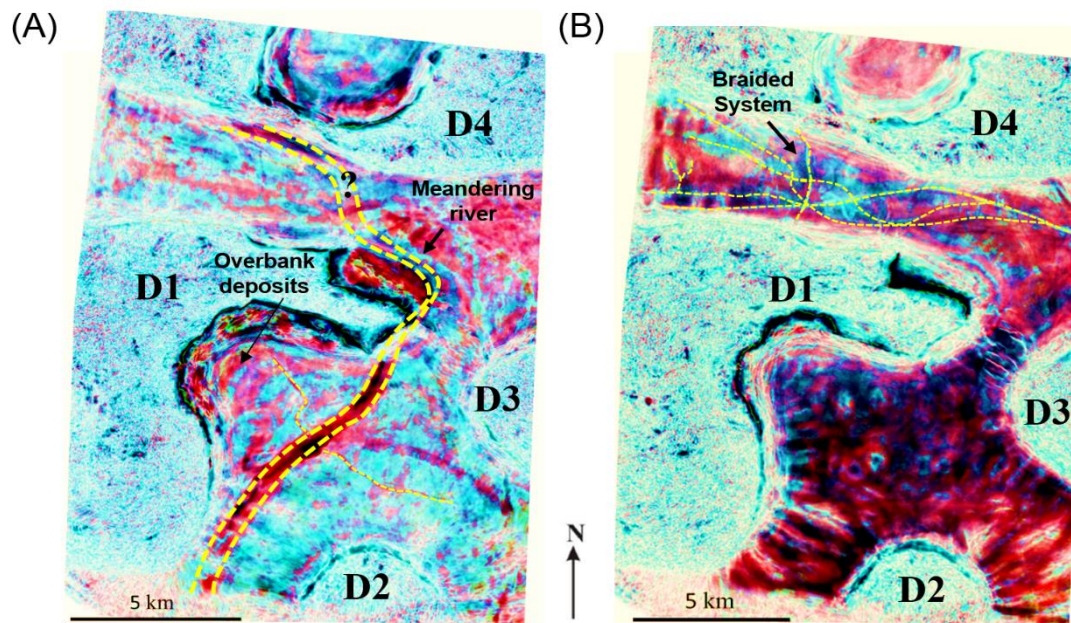


Figure 3. (A) Distribution of basins with salt diapirism induced by the mobilization of Pennsylvanian to lower Permian evaporites within the western Barents Sea. (B) Structural elements of the western Barents Sea region with focus on the Nordkapp Basin. The basin is divided in three sub-basins: western, central, and eastern sub-basins. The study area is underexplored. Black dots are explored wells. Red rectangle shows the location of the full azimuth 3D cube used in this study. Modified after Rojo et al., 2019.



Data courtesy of WesternGeco Multiclient

Figure 4. Depth slices showing the position of channels respect to the salt diapirs. (A) Depth slice 1872 m displays a meandering river with adjacent overbank deposits. (B) Depth slice 2048 m shows the braided system along the northwestern minibasin.

Interpretation of key reflectors (sequence boundaries) in this dataset and their geometries near the diapirs, are the main task of this thesis. The principal challenges that may deter accomplishing these interpretations are: (1) the presence of vertical salt structures in the basin (i.e. salt diapirs). This creates areas of noise and low seismic amplitude because of the particular acoustic properties of salt, resulting in an uncertain interpretation adjacent to salt diapirs, and increasing the risk of misinterpreting structures (Swanston et al., 2011), and (2) the lack of local analyses of diapir growth. Because of this, the 4D growth history of salt diapirs and its impact on the distribution of Mesozoic sediments in the Nordkapp Basin remain poorly understood.

The main objectives of this thesis are: (1) provide a growth history of salt diapirs during the Triassic and (2) understand the influence of salt diapir growth on the distribution of Triassic fluvial systems in the central sub-basin of the Nordkapp Basin. This can help to understand the impact of halokinesis on sedimentation and the petroleum system of the Nordkapp Basin. With this purpose, I use the $\Delta d/d$ (d: depth) method (Bischke, 1994) on the interpreted horizons from the full-azimuth seismic cube.

1.1. Background of salt and salt-related basins.

1.1.1. SALT.

Salt rocks are composed mainly of salt minerals as halite (NaCl), anhydrite (CaSO₄) and gypsum (CaSO₄.2H₂O). These minerals reflect the conditions of their depositional environment including water type, temperature, salinity and basin architecture (James and Dalrymple, 2010). Salt has low mechanical strength, low permeability, and high thermal conductivity. It has a density of 2160 kg/m³ and is almost incompressible, resulting in an almost constant density with depth that is very different from the surrounding overburden (Fossen, 2010). Thus, at certain depth, the density of the overburden exceeds the density of salt, and the salt becomes buoyant and gravitational unstable (Jenyon, 1986). This fact, together with other factors such as differential sedimentary loading and faulting (Hudec and Jackson, 2007) contribute to salt flow and the formation of structural traps, reservoirs in surrounding minibasins, and top and side seals due to the impermeability of the salt (Fossen, 2010). Additionally, the high thermal conductivity of salt influences heat flow, producing cooling of the sediments underlying and flanking the salt diapir, while the sediments above the diapir are heated. This can retard source rock maturation in deep source rocks below the diapir, as well as it affects reservoir diagenesis (Archer et al., 2012; Jackson and Hudec, 2017).

1.1.2. SALT STRUCTURES: GEOMETRY AND CLASSIFICATION

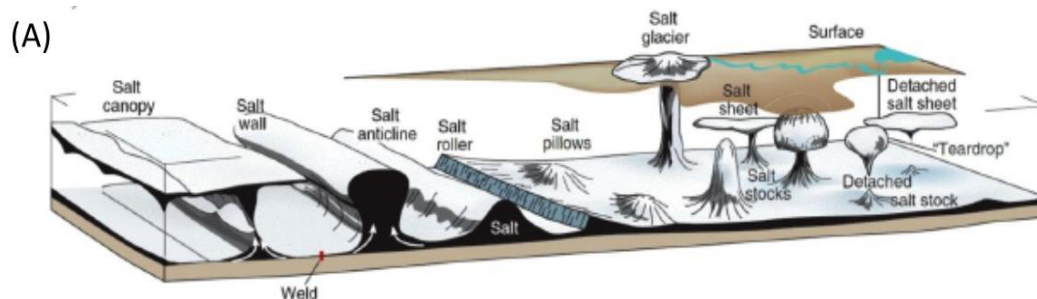
Salt mobilization directly influences the geometry of salt structures. Most of these structures are illustrated in Figure 5A. The morphology of salt structures depends on factors such as strength of the overburden, temperature of the salt, salt source layer thickness, tectonic regime, and sedimentation or erosion rate (Fossen, 2010). In the study area, the dominant salt structures are wall-like diapirs, parallel to the basin margins (Koyi et al., 1996). According to several authors (e.g. Giles and Lawtom, 2002; Hudec and Jackson, 2007; Koyi et al., 1998) one of the most common criteria to explain the shape of salt diapirs is the relationship between the rates of sediment accumulation (A) and salt supply (S) (Figure 5).

1.1.3. DIAPIRISM FORMATION PROCESSES

Salt diapir is a term used for any salt structure, linear or circular in map view, which forms by piercing into the overburden (Schultz-Ela et al., 1993). Therefore, the strength of the overburden restricts the flow of the salt. Fracturing and faulting weakens the overburden and benefits the upward movement of salt (Vendeville and Jackson, 1992). On the other hand, friction along the boundaries of the salt is important, since it restricts the salt movement. Friction plays a significant role in determining the thickness of the salt diapir (Hudec and Jackson, 2007).

Several models explain salt mobilization and formation of salt diapirs. They suggest that diapirism can be triggered by a variety of mechanisms including buoyancy contrasts (Trusheim, 1960), differential loading (Ge et al., 1997; Warsitzka et al., 2013),

and extension or contraction driven by tectonics or gravity gliding (Vendeville and Jackson, 1992b, a; Koyi et al., 1993a; Nilsen et al., 1995; Stewart et al., 1997a).



(B)

Longterm Relative Rates	Characteristics	Fixed Reference Line
<p>Expansion of diapir</p> <p>$R_{net} > A_{sed}$</p>	<ul style="list-style-type: none"> Diapir expansion, flaring and subsequent divergent migration of depocenters. Potential surface glacial flow (development of salt glaciers or salt overhangs). Overtuned beds & repeated sections. Offstepping halokinetic sequence stacking. 	
<p>Vertical rise of diapir</p> <p>$R_{net} = A_{sed}$</p>	<ul style="list-style-type: none"> Vertical salt structures without depocenter migration. Sediment aggradation and vertical beds. High angle unconformities around the salt structure. Aggrading halokinetic sequence stacking. 	
<p>Reduction of diapir</p> <p>$R_{net} < A_{sed}$</p>	<ul style="list-style-type: none"> Diapir contraction with triangular shapes as salt pillows and salt rollers. Sediment onlap and overlap the diapir with convergent vertical migration of depocenters. Low-angle angular unconformities. Onstepping halokinetic sequence stacking. 	

Figure 5(A) Salt structures classification (Fossen (2010)). (B) Evolution of salt diapirs and related halokinetic sequences as function of sedimentation rate vs salt-supply rate. Modified from Guiles and Lawton (2002).

Active diapirism versus passive diapirism

Traditionally, the growth of a salt diapir is thought to be developed in three different stages (Figure 6). The first stage is active diapirism (Trusheim, 1960; Hudec and Jackson, 2007; Fossen, 2010), which is an upwards salt movement caused by differential, thermal or displacement loading. In this stage, a salt pillow develops, which

is responsible for doming and erosion of overburden layers, resulting in a planar to convex and commonly symmetric structure (Figure 6.2). During this phase, salt tends to flow towards the salt pillow. Thus, the source layer is depleted and small minibasins form. These minibasins are known as primary rim synclines, which are filled by growth strata sediments thinning towards the salt structure.

The second stage occurs as the diapir completely pierces its overburden and is exposed at the surface (Figure 6.3). This stage is known as passive diapirism or downbuilding (Hudec and Jackson, 2007). During passive diapirism, a second generation of rim synclines are created due to the mini-basin infill load. This leads to salt movement towards the diapir and the depletion of the source layer. As salt may rise through thousands of meters (Hudec and Jackson, 2007), the secondary rim synclines can occupy larger areas and generate the most extensive depocenters of growth strata adjacent to the salt diapir.

In the last stage, the diapir stops rising since the source layer is completely depleted and the salt supply ends. This results in the burial of the salt diapir and growth strata deposition within the third generation of rim synclines (Figure 6.4).

Reactive diapirism during thick-skinned extension.

The phase of reactive diapirism takes place during extension (Rojo et al., 2019). First, the suprasalt faults creates space of accommodation in the suprasalt which will be filled by sediments, what induces differential loading of the salt and cause its mobilization. Second, the thick-skinned extension stretches the overburden and makes it weaker, allowing salt extrusion and passive diapirism (Figure 7).

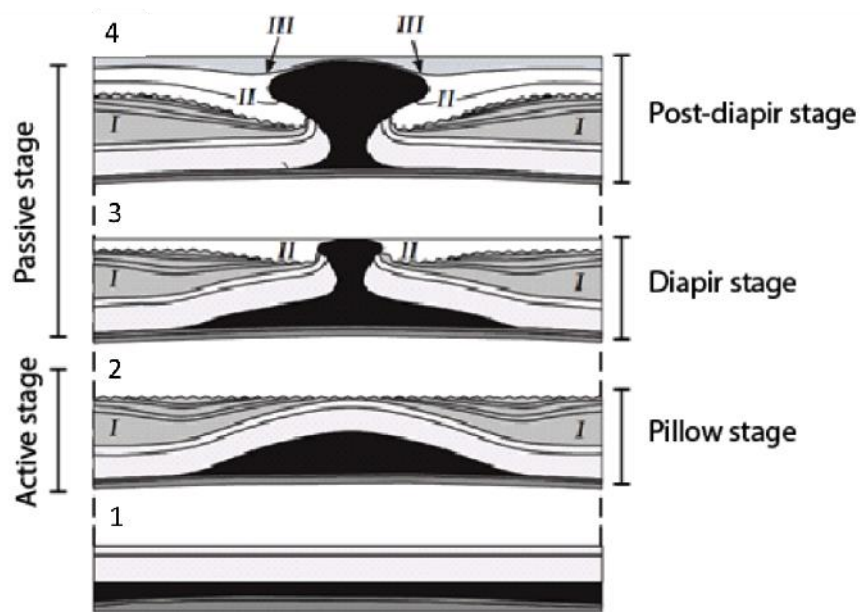


Figure 6. Salt diapir growth by Trusheim (1960). I: Primary rim synclines. II: Secondary rim synclines. III: Tertiary rim synclines.

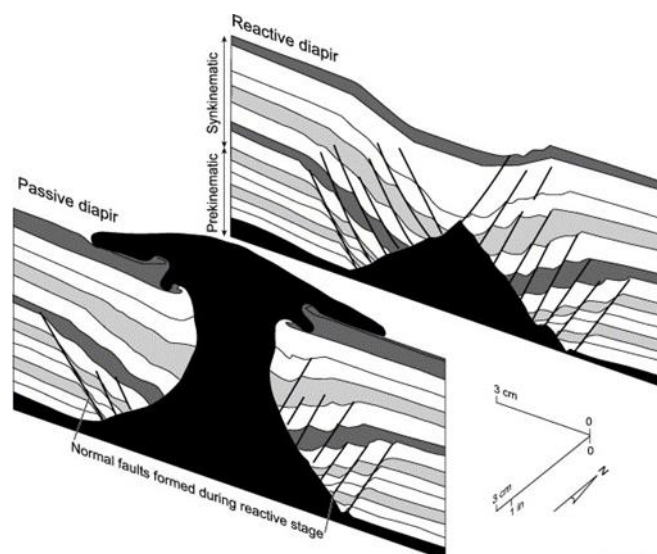


Figure 7. Profiles of a diapir formed in an extensional model. The northern section intersects a reactive diapir. In the southern section, the diapir evolved further to form a passive diapir (Hudec and Jackson, 2007).

Contractional diapirism

During shortening, pre-existing diapirs are also affected. Thus, salt diapirs can continue to grow due to upwards salt movement that promotes doming and the formation of salt glaciers (Figure 8A), where the salt displaced from the squeezed feeder flows out over the surface (Hudec and Jackson, 2007). This diapirism process is called contractional diapirism and is present in many basins that experienced contraction after extensional events (Hudec and Jackson, 2007; Fossen, 2010). In such areas, it is common to find salt structures like teardrop diapirs, whose upper part is detached from the source layer (Figure 8B). The waist of the structure is pinched off during the shortening episode and the salt is expelled upwards enhancing the vertical diapir rise with the formation of an arched roof.

Diapir Collapse or fall during thick-skinned extension

In some cases, the same extension that initiates and enhances the growth of salt structures can also make diapirs fall once the salt supply from its source is restricted (Perez-Garcia et al., 2013). Then, the diapirs sag and fall. A sign of diapir fall or diapir collapse are indentation and/or graben formation of overlying strata and horn-like cups of salt at the crest of the salt below each bounding fault of the indentation as residual structure, whose apices record the original height of the diapir crest (Vendeville and Jackson, 1992b; Figure 9).

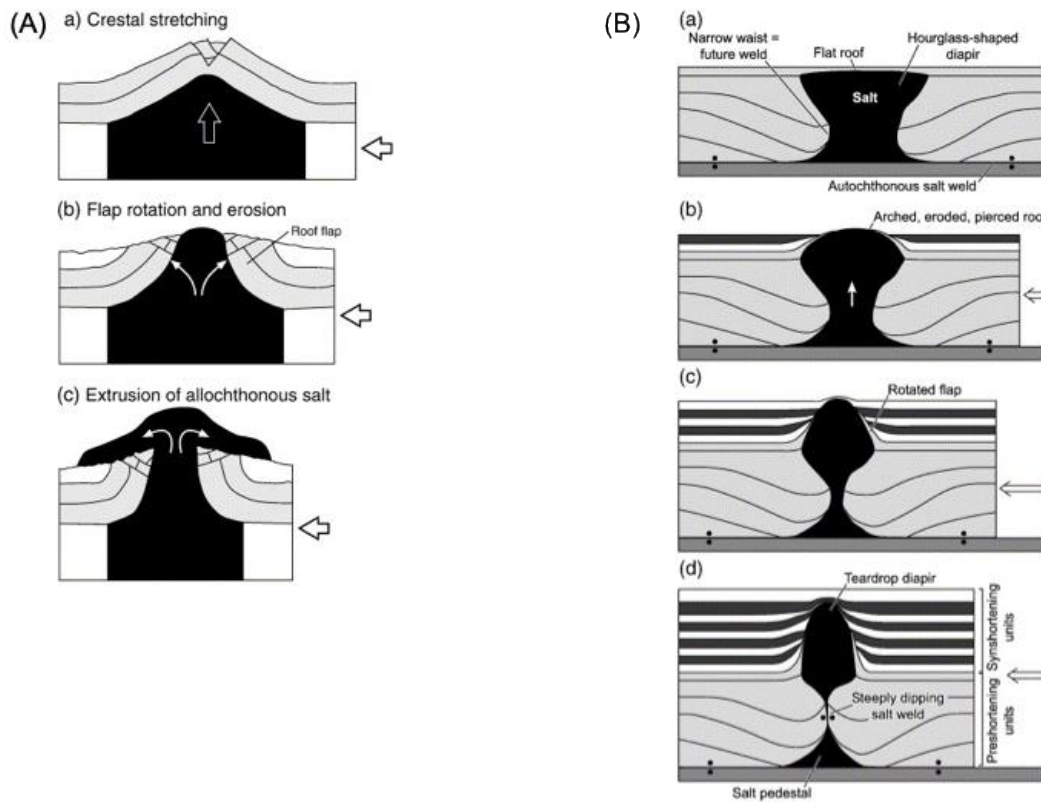
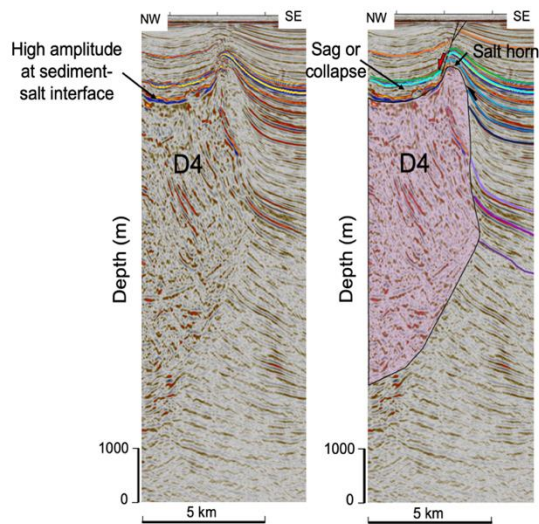


Figure 8 Contractional diapirism. (A) Reactivated salt diapir growing during shortening. (a) The roof is faulted and thinned. (b) Active diapir rise due to the combination of roof thinning and pressurization of the salt. The rotation and erosion of the diapir crest occurs as salt diapir pierce through the overburden. (c) The diapir extrudes at the surface and forms a salt glacier (Hudec and Jackson, 2007). (B) Contractional diapirism that may create salt structures like teardrop diapirs.



Data courtesy of WesternGeco Multiclient

Figure 9. Diapir Collapse. Left: Uninterpreted detail of the salt diapir collapse and its sediment overburden separated by a high amplitude reflector. Right: Interpreted detail of sag or collapse of diapir D4 showing a salt horn and the fault associated to the flank of the salt diapir.

2. GEOLOGICAL SETTING

2.1. Introduction

The Barents Sea comprises the shelf area between the Kola Peninsula to the S, the shelf edge towards the Norwegian Sea to the W, Svalbard to the NW, Franz Josef Land to the NE, and Novaya Zemlya to the E (Henriksen et al., 2001b, Figure 10). The study area is the Nordkapp Basin in the southwestern Barents Sea (Koyi and Talbot et al., 1996). This basin is bordered to the NW by the Bjarmeland platform and the Norsel high, and to the SE by the Finnmark platform. The Nordkapp Basin consists of three subbasins: (1) a 150 km (93 mi) long and 25-50 km (16-31 mi) wide NE-SW subbasin to the west, bounded by the Nysleppen fault complex in the north and the Måsoy fault complex in the south (Figure 10); (2) a 100 km (62 mi) long and 60-80 km (37-50 mi) wide E-W trending subbasin in the central part, this subbasin is limited to the north by the Nysleppen fault complex and the Thor Iversen fault complex in the south (Gabrielsen et al., 1990; Gabrielsen et al., 1992; Jensen and Sørensen, 1992; Nilsen et al., 1995; Koyi and Talbot, 1996), and (3) a 120 km (75 mi) long and 50 km (31 mi) wide NE-SW subbasin to the east. The Nordkapp Basin is an elongated salt-related basin characterized by the presence of salt structures such as salt walls, stocks, and teardrop diapirs which are surrounded by withdrawal minibasins.

The geological features of the Nordkapp Basin are the result of the combination of major tectonic and climatic events that occurred in the Barents Sea, which controlled the initiation, growth and reactivation of the salt diapirs.



Figure 10. Structural elements of the Southern Barents Sea region. Modified after Mattingdal et al., 2015

2.2. Stratigraphical and structural evolution of the Nordkapp Basin

Late Paleozoic

The initial configuration of the Nordkapp Basin corresponds to a NE-SW graben and half graben architecture, in response to regional extension in the Barents Sea. This process occurred during the Late Devonian and mid Carboniferous because rifting developed a wide rift zone in the southern Barents Sea, and strike-slip faults in the north (Faleide et al., 2015). A result of this tectonic event is the development of major rift-basins like the Bjørnøya, Fingerdjupet, Maud, Nordkapp, Ottar and Trømso Basins (Faleide et al., 2015).

The Billefjorden Group contains the oldest sediments in the basin, making up the pre-salt succession (Bugge et al., 2002). This sedimentary succession was deposited during the Late Devonian-Early Carboniferous under tropical humid conditions and comprise nonmarine synrift alluvial-fluvial coaly sediments (Stemmerik & Worsley, 2005; Worsley, 2008) (Figure 11). At the end of this period, plate tectonics caused the movement of Pangea towards warmer latitudes leading to a climatic shift to arid conditions, followed by an ongoing regional sea-level rise with associated deposition of syn-rift to early post-rift halite-dominated layered evaporite sequences (LES) in the basin axis, whereas carbonate and gypsum-rich LES were deposited at basin boundaries which comprise the Gipsdalen Gp (Stemmerik et al., 1999; Stemmerik and Worsley, 2005; Henriksen et al., 2011b; Nordaunet-Olsen, 2015; Figure 11). From the Middle to Late Permian, cold-water carbonates and siliceous shales were deposited due to the movement of Pangea towards colder latitudes in addition that the Uralian Orogeny cut off the input of warm water to the Barents Sea (Ehrenber et al., 2001; Worsley, 2008;

Figure 11). These Late Paleozoic sediments are considered as post-salt strata, and they were deposited before salt mobilization, which occurred mainly during the Triassic (Jensen and Sørensen, 1992; Koyi et al., 1995; Nilsen et al., 1995).

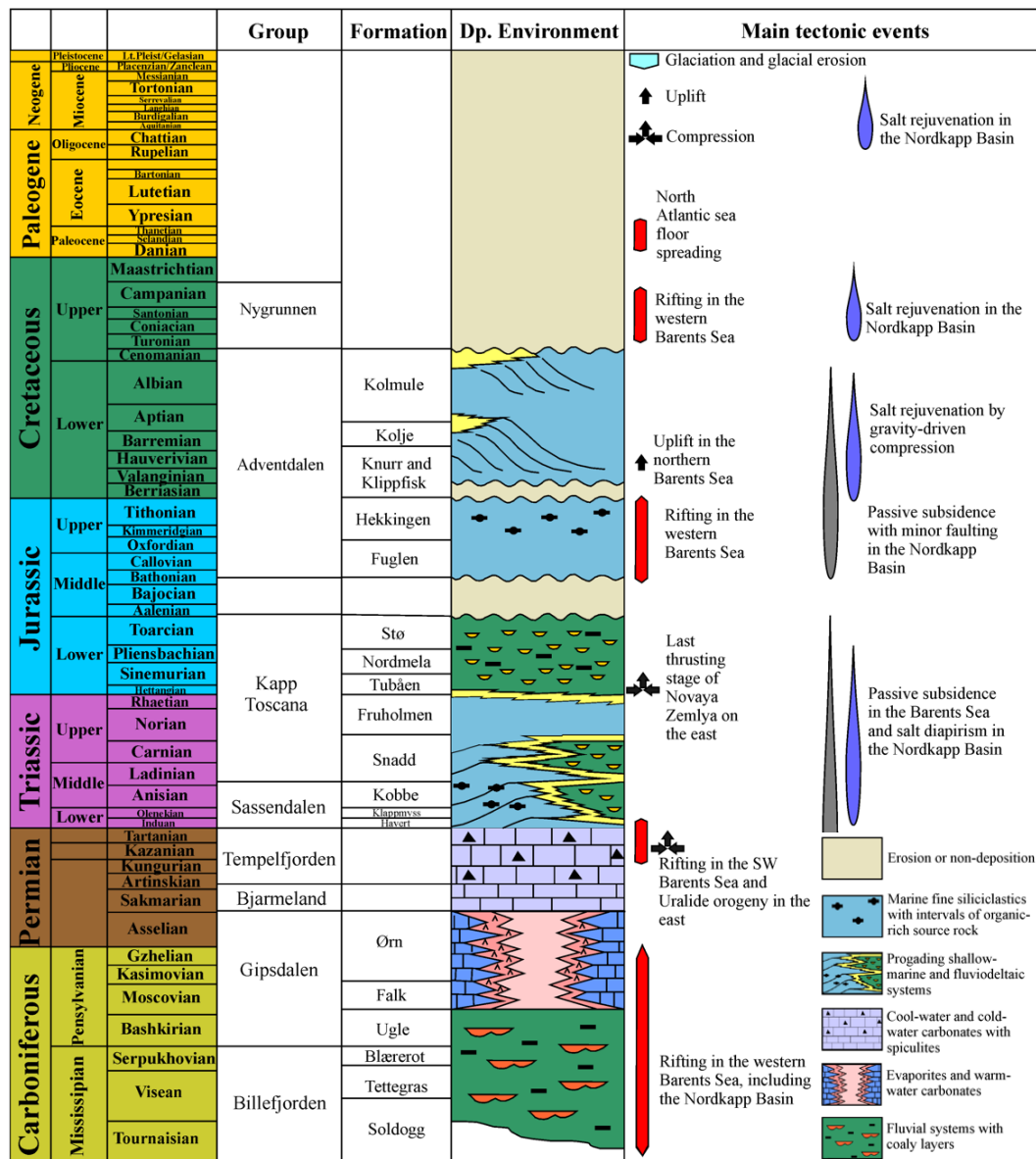


Figure 11. Tectono-stratigraphic chart of the Nordkapp Basin (Rojo et al., 2019)

Triassic-Early Jurassic

In the western Barents Sea, the Triassic was tectonically a quiet period with passive regional subsidence (Gabrielsen et al., 1993; Henriksen et al., 2011b) that results in a deposition of approximately 4-7 km of Triassic strata (Ritzmann & Faleide 2009). According to some authors (e.g. Jensen and Sørensen et al., 1992; Koyi et al., 1993b; 1995b; Nilsen et al., 1995), halokinetic movements started in the Nordkapp Basin during the Early Triassic creating a complex network of Triassic minibasins up to 5-6 km thick, flanked by salt diapirs. Some studies suggest that diapirism was triggered either by (1) NW-progradation of a clastic wedge sourced from the Uralides favouring differential loading and diapirism formation (Dengo and Røssland (2013) and Rowan and Lindsø (2017), and/or (2) regional extension that contributed to upwards salt movement and the subsequent creation of salt structures (Jensen and Sørensen, 1992; Koyi et al., 1993b; Koyi et al., 1995b; Nilsen et al., 1995; Rojo and Escalona, 2018), which continued throughout the Middle Triassic to Jurassic. According to previous works such as Nilsen et al. (1995), diapir growth was triggered by basinward suprasalt gliding and contraction after the Middle Triassic depletion of the underlying salt.

During the Triassic, the sedimentation in the Barents Sea was marked by large fluvio-deltaic systems that prograded to the north and west, mainly sourced from the Uralian Mountains (Glørstad-Clark et al., 2010). The sedimentary Triassic succession in the Nordkapp Basin (Figure 11) is comprised of: (1) Havert-Klappmyss Fm., described as Lower Triassic open marine to prodelta facies. (2) Kobbe Fm. deposited during the Middle Triassic as shallow marine to deltaic sediments, and (3) Snadd Fm., comprising Upper Triassic fluviodeltaic deposits (e.g. Bugge et al., 2002; Rojo and Escalona; 2018)

(Figure 11). Henriksen et al. (2011b) and Anell et al. (2014) suggest that in the Late Triassic-Early Jurassic, this progradational wedge composed of fluviodeltaic sediments turned into more condensed shallow marine and fluviodeltaic deposits (Tubåaen, Nordmela and Stø Fm.), reflecting a more complex drainage system.

Late Jurassic - Early Cretaceous

In this period, Atlantic rifting migrated towards the north (Gernigon et al., 2014), affecting the Barents Sea region with different intensity. The southwest Barents Sea developed major rift basins and highs, such as Bjørnøya, Tromsø and Harstad basins, whereas areas towards (e.g. the Nordkapp Basin) underwent passive subsidence with minor faulting (Faleide et al., 2008). These conditions promoted the deposition in the basin of marine fine-grained siliciclastics (Fuglen Fm.) followed by marine organic-rich sediments (Hekkingen Fm.) (Henriksen et al., 2011b; Figure 11).

During the Early Cretaceous, continued rifting and seafloor spreading resulted in extensive magmatism and uplift of the northern part of the Barents Sea Sea (Gjelberg and Steel, 1995; Grogan et al., 2000; Grantz et al., 2011; Corfu et al., 2013). This resulted in clinoform progradation towards the south of the Barents Shelf. In the Nordkapp Basin, the sedimentation was characterized by shelf to deep water deposits (Marin et al., 2017).

From differences observed in the thicknesses of the Lower Cretaceous growth strata in the Nordkapp Basin, the diapir growth is thought to be continued either by salt supply from underneath (Koyi et al., 1993, 1995b), or gravity-induced contraction (Nielsen et al., 1995).

Late Cretaceous – Cenozoic

Previous studies (e.g. Gabrielsen et al., 1993; Nielsen et al., 1995; Henriksen and Vorren, 1996) suggest that salt growth in the Nordkapp Basin was steady during the Late Cretaceous due to the opening of the Atlantic Ocean. This event promoted gravitational gliding, which led to squeeze of the diapirs and their subsequent growth. In the Cenozoic, salt reactivation took place due to a regional contraction in the Barents Shelf. In addition to diapir rejuvenation in the Nordkapp Basin, shortening also caused inversion and reactivation of previous faults (Jensen and Sørensen, 1992; Koyi et al., 1995b; Nilsen et al., 1995; Rojo and Escalona, 2018; Figure 11). This period was additionally characterized by several episodes of uplift and erosion, with uplift increasing from south to north and east to west (Feleide et al., 1993 a,b; Wood et al., 1989; Henriksen et al., 2011). Because of this, most of the Upper Cretaceous-Cenozoic strata have been eroded (Figure 11). Baig et al., (2016), Henriksen et al., (2011a), and Ohm et al., (2008) estimate that the regional uplift eroded approximately 1300-1500 m of Cenozoic and Mesozoic strata. In the study area, Quaternary strata overlay unconformably the deformed Lower Cretaceous (Figure 11).

3. DATASET AND METHODOLOGY

3.1. Dataset

The dataset used in this study was provided by WesternGeco Multiclient. It includes a full azimuth 3D cube that covers an area of approximately 500 km² in the eastern part of the central sub-basin (**Error! Reference source not found.B**). The seismic data is in true vertical depth (TVD) and displays high-quality seismic imaging around the diapirs, allowing a better interpretation of the study area with especial focus on the minibasins. However, there are some uncertainties related to: (1) the unclear base of the salt structures that makes difficult to map the size and shape of diapirs (Figure 12A), and (2) the presence of acquisition artifacts that may influence on the interpretation. On cross sections, the affected reflectors seem to be faulted by non-existing faults and even like channels traces on depth-slices (Figure 12B).

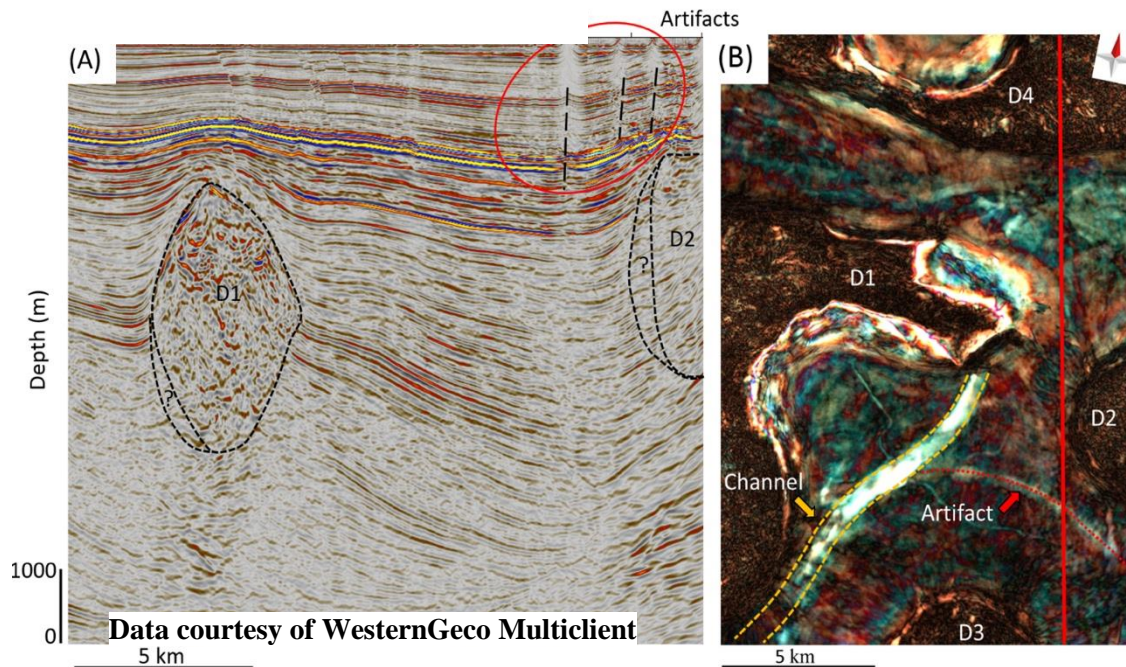


Figure 12. (A) Cross section showing uncertainty on the size and shape of salt diapirs and artifacts that resemble faults. (B) Depth-slice (1872m) displaying artifact (red dotted line) close to a channel (yellow discontinuous-line). Red line marks the position of the cross section. Red arrow on Figure 12A shows the height at which the depth slice intersects the cross section.

Due to the underexplored nature of the study area, no wells are available. Thus, the growth history of salt diapirs and its influence on the distribution of Triassic fluvial system is deduced from the Δd /depth method using pseudo-wells (Bischke, 1994).

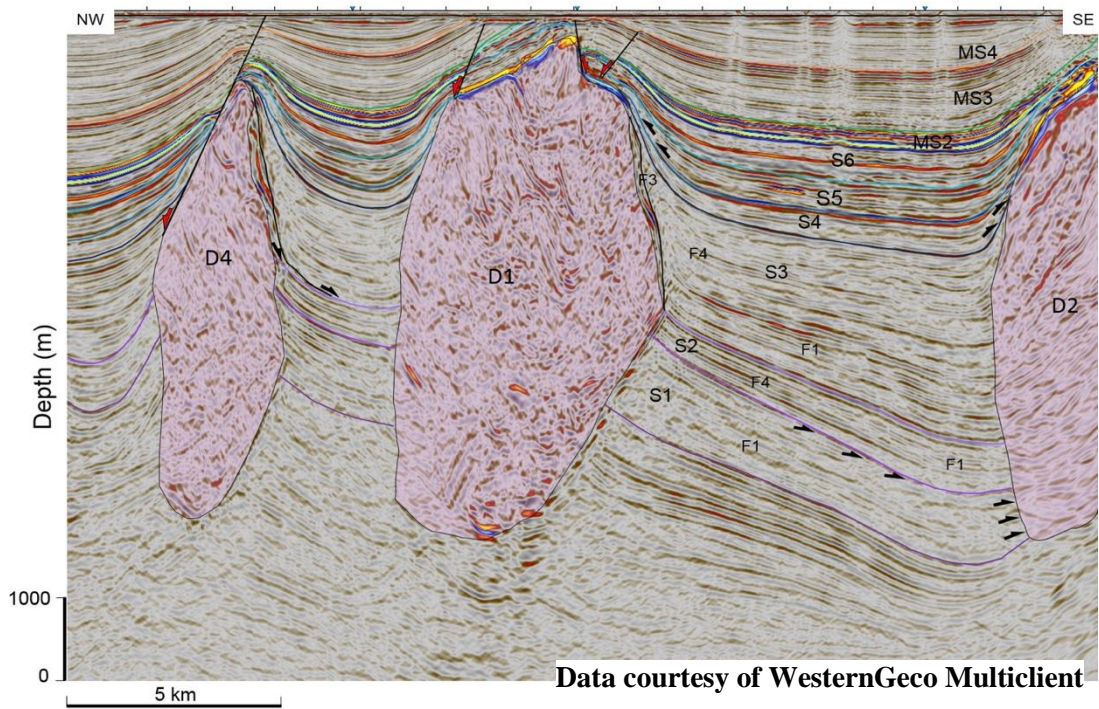
3.2. Methodology

3.2.1. SEISMIC INTERPRETATION

There is some uncertainty on the interpretation of the horizons since no well has been drilled within the study area, thus no well correlations are possible. The interpretation is based on previous works of Rojo et al., 2019 and Rojo and Escalona (2018). Considering this, 19 horizons were interpreted, with emphasis on those that are sequence boundaries (Table 1; Figure 13). All seismic horizons were picked on peaks and manually mapped in those areas close to the diapirs in order to avoid misinterpretations, but also the autotrack tool was used over zones where the seismic quality allowed.

Megasequences		Pick	Continuity	Amplitude	Color
MS4	Cenozoic	Peak	Continuous	High	Orange
MS3	Cretaceous	Peak	Continuous	High	Green
MS2	Jurassic	Peak	Continuous	High	Cian
MS1	S6 - Upper Triassic	Peak	Continuous	High	Light blue
	S5 - Upper Triassic	Peak	Continuous	High	Blue
	S4 - Middle Triassic	Peak	Continuous	High	Dark blue
	S3-Lower to Middle Triassic	Peak	Semicontinuous	Medium	Light purple
	S2 - Lower Triassic	Peak	Discontinuous	Medium	Dark purple
	S1 - Lower Triassic	Peak	Discontinuous	Medium	Purple

Table 1. Summary of seismic horizons that bound the megasequences.



- Legend
- MS4 — Cenozoic
 - MS3 — Cretaceous
 - MS2 — Jurassic
 - MS1
 - S6 - Upper Triassic
 - S5 - Upper Triassic
 - S4 - Middle Triassic
 - S3 - Lower to Middle Triassic
 - S2 - Lower Triassic
 - S1 - Lower Triassic

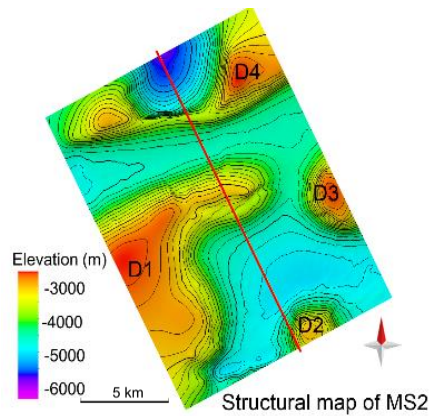


Figure 13 Cross section displaying the interpreted seismic horizons truncating against the salt diapirs: D4, D1 and D2 (from the NW to the SE). The inset structural map on the bottom left shows the location of this seismic line in the study area within the central sub-basin of the Nordkapp Basin. MS1 = megasequence 1; MS2 = megasequence 2; MS3 = megasequence 3; MS4 = megasequence 4; S1 = sequence 1; S2 = sequence 2; S3 = sequence 3; S4 = sequence 4; S5 = sequence 5; S6 = sequence 6.

The salt structures were mapped using Multi-Z interpretation and different depth-slices that helped to control the salt-sediment interface. Commonly, salt interpretation is a challenge due to the imaging problems related to the large impedance contrast between sediments and salt, especially in areas of steep dip (e.g., salt flanks; Figure 14A). However, the seismic data used in this thesis display an unusual high quality seismic imaging that allowed a robust and accurate seismic interpretation near the salt diapirs (Figure 14B).

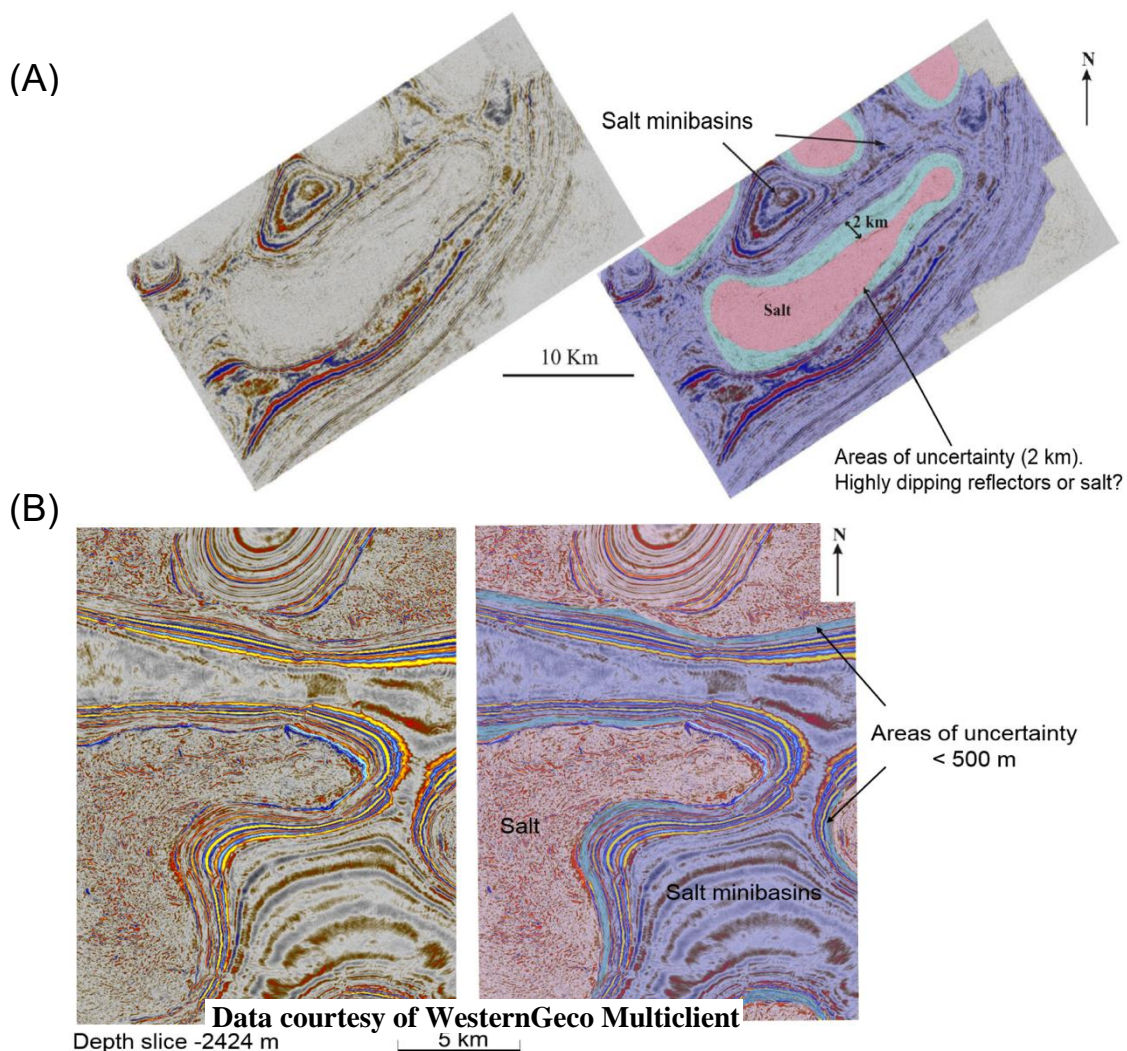


Figure 14. A) Time slice of the SW sub-basin of Nordkapp Basin (from Rojo, 2015), showing areas of uncertainty where the salt-sediment interface is not clear. (B) Depth slice within the study area displays the high quality seismic imaging that allows a more accurate interpretation close to diapirs.

3.2.2. STRATIGRAPHIC FRAMEWORK.

The stratigraphic framework of the minibasins infill in the Nordkapp Basin was established by using sequence stratigraphy principles. In this way, the sedimentary succession was divided into megasequences (MSes) according to Van Wagoner et al., 1990 and Canteneanu et al., 2011. These MSes are stratigraphic units bounded by subaerial unconformities and their correlative surfaces (Van Wagoner, et al., 1990) that normally range between 40 and 80 My. The MSes are bounded by the Base Lower Jurassic, Base Cretaceous unconformity (BCU), Base Cenozoic, and Base Quaternary (seabed) (Rojo et al., 2019). Since this thesis focuses on the Triassic interval, a further subdivision into sub-sequences was performed using flooding surfaces as sequence boundaries (Figure 15Figure 13). All the interpretations are based on previous works (e.g. Rojo and Escalona, 2018 and Rojo et al., 2019) and seismic observation.

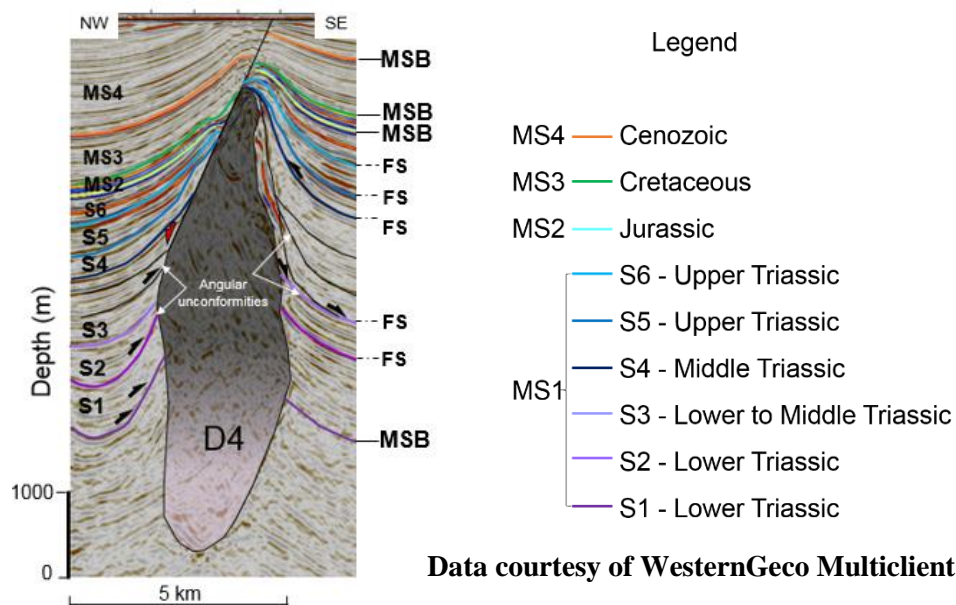


Figure 15. Detailed seismic analysis of the Triassic succession based on previous works (Rojo et al 2019) and observations of these seismic units, growth strata, onlaps, downlaps, and truncations, which were interpreted to establish the major periods of salt mobilization and quiescence. Triassic sequences are bounded by angular unconformities close to the diapir that become laterally flooding surfaces towards the southeast.

3.2.3. Δd /DEPTH METHOD.

What it is - The $\Delta d/d$ (d : depth) method is based on a stratigraphic correlation of the growth sedimentary section (Bischke, 1994). The law of superposition states that sediments are deposited in a systematic manner in a growth section, which records the continuous history of structures and the dynamic processes that affect them. Growth structures form as sediments are deposited near active faults, mobile salt or in subsiding basins. Thus, the Nordkapp Basin is a good place to apply this method.

How the method is obtained - The $\Delta d/d$ plots are constructed from the measurements made by stratigraphic correlating of horizons between two wells and measuring the difference in vertical distance in sequence tops between the wells. The differences in vertical distance (Δd) are plotted in relation with the vertical depth (d) in the structurally higher or reference well (Figure 16).

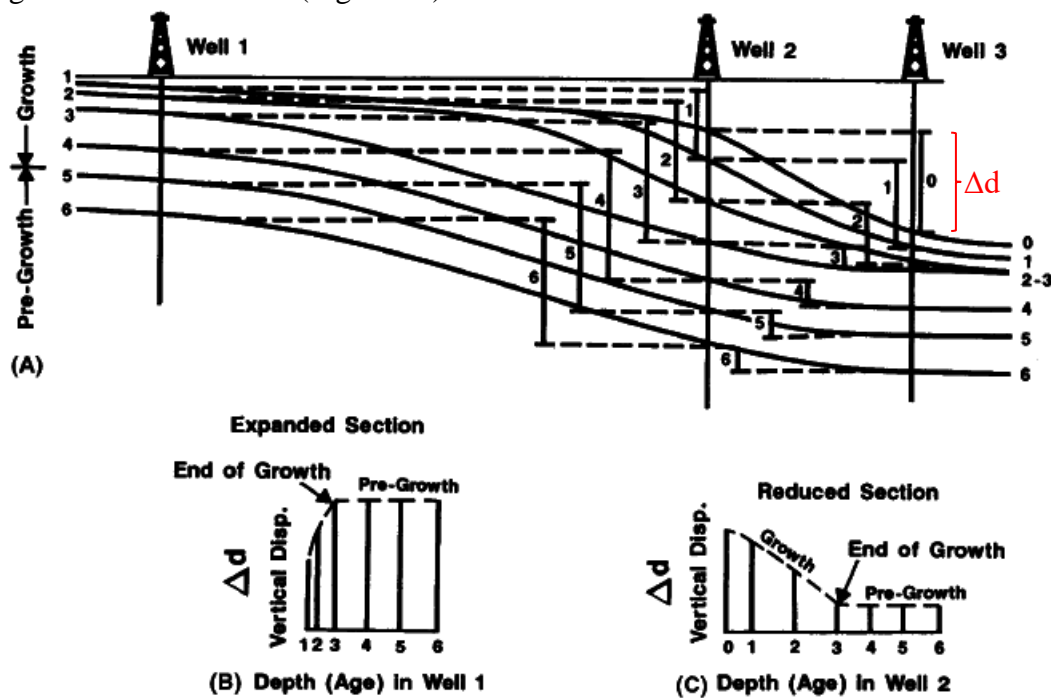


Figure 16. (A) Delta prograding over pre-growth section causing sediment accumulation at different levels that allows horizon correlation in order to construct the $\Delta d/d$ diagram. (B) The slope records the growth from the structurally higher well 1 to well 2. A positive slope or discontinuity indicates expanded sections. While (C) a negative slope or discontinuity indicates the presence of a condensed or reduced section (from the structurally lower well 2 to well 3). Flat slopes show pre-growth intervals (Bischke, 1994).

How the method works - Correlations obtained from the growth section graphically depict the growth history of the structures. Monotonic or linear correlation growth curves (Suppe et al., 1992; Bischke, 1994) indicate that sediments are deposited systematically with no growth changes (i.e., sediment deposition was not affected by neither sequence boundaries, disconformities nor active faults).

On the contrary, a deviation from the linear trends of the sediment growth might indicate stratigraphic miscorrelations (Figure 17).

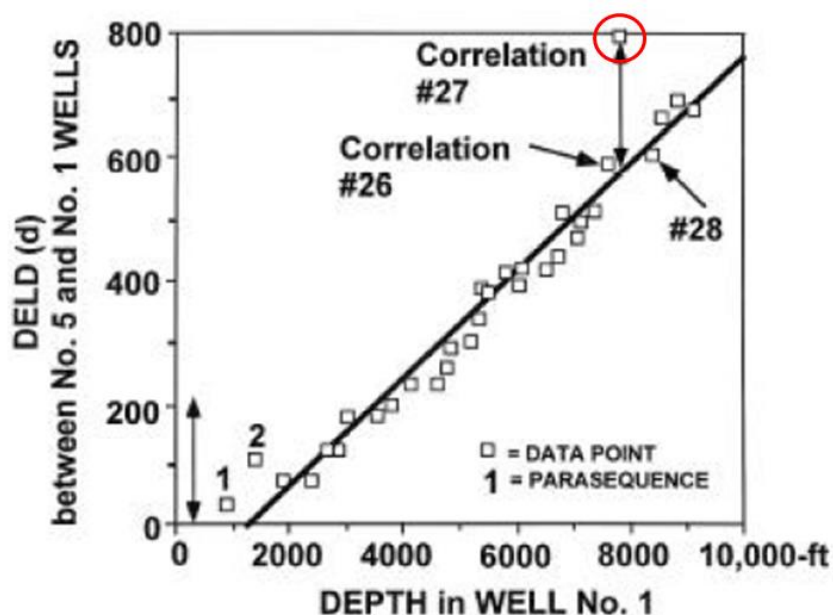


Figure 17. Linear Δd /depth diagram for two wells showing a rough linear correlation of the data points with an exception for correlation 27, which indicates a miscorrelation (red circle). Modified after Bischke, 1994.

Applications – The $\Delta d/d$ plots analysis is an excellent technique since the growth plot obtained are used to (Bischke et al., 1994):

- Locate sequence boundaries and subtle stratigraphic traps.
- Identify and solve correlation problems in areas of rapidly changing lithology.

- Determine high growth or potential thick sand rich intervals on seismic profiles.
- Establish the time of structural growth and fault timing.
- Check interpretation for consistency.
- Identify problems that may go unrecognized using standard interpretation techniques

Another feature of these diagrams is the possibility to identify unconformities from observation of onlaps and downlaps. Onlaps tend to create a positive slope or discontinuity (Figure 18A), while downlaps develop a negative slope or discontinuity (Figure 18B).

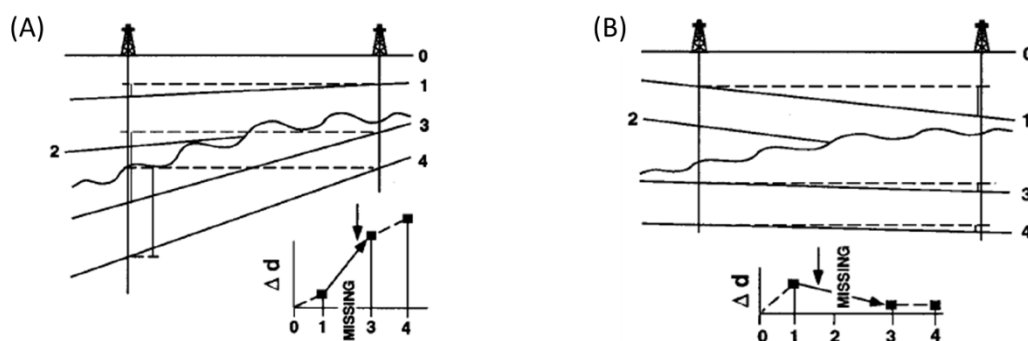


Figure 18. Large unconformities can produce positive or negative slopes that resemble faults. (A) Onlap create a positive slope, while (B) downlap generates a negative slope. As a rule, unconformities tend to remain in the same stratigraphic level. In this case, both profiles show missing sections between horizon 1-3 levels. Thus, this feature is interpreted as an unconformity instead of a fault (Bischke, 1994).

Bischke, 1991 describes a practical example to understand how the method works (Figure 19). This example, from the northern Gulf of Mexico, involves a salt-related structure. The growth of salt diapirs leads to stratigraphic units onlapping the flanks of the diapirs, which creates large unconformities with missing sections that can resemble growth faults. As stated above, distinguishing faults from unconformities may be difficult in some cases. However, the $\Delta d/d$ technique with knowledge of the local

geology can help to solve this problem. This method seems to be valid as long as unconformities do not dip more than 40 degrees and eliminate more section in the downdip direction.

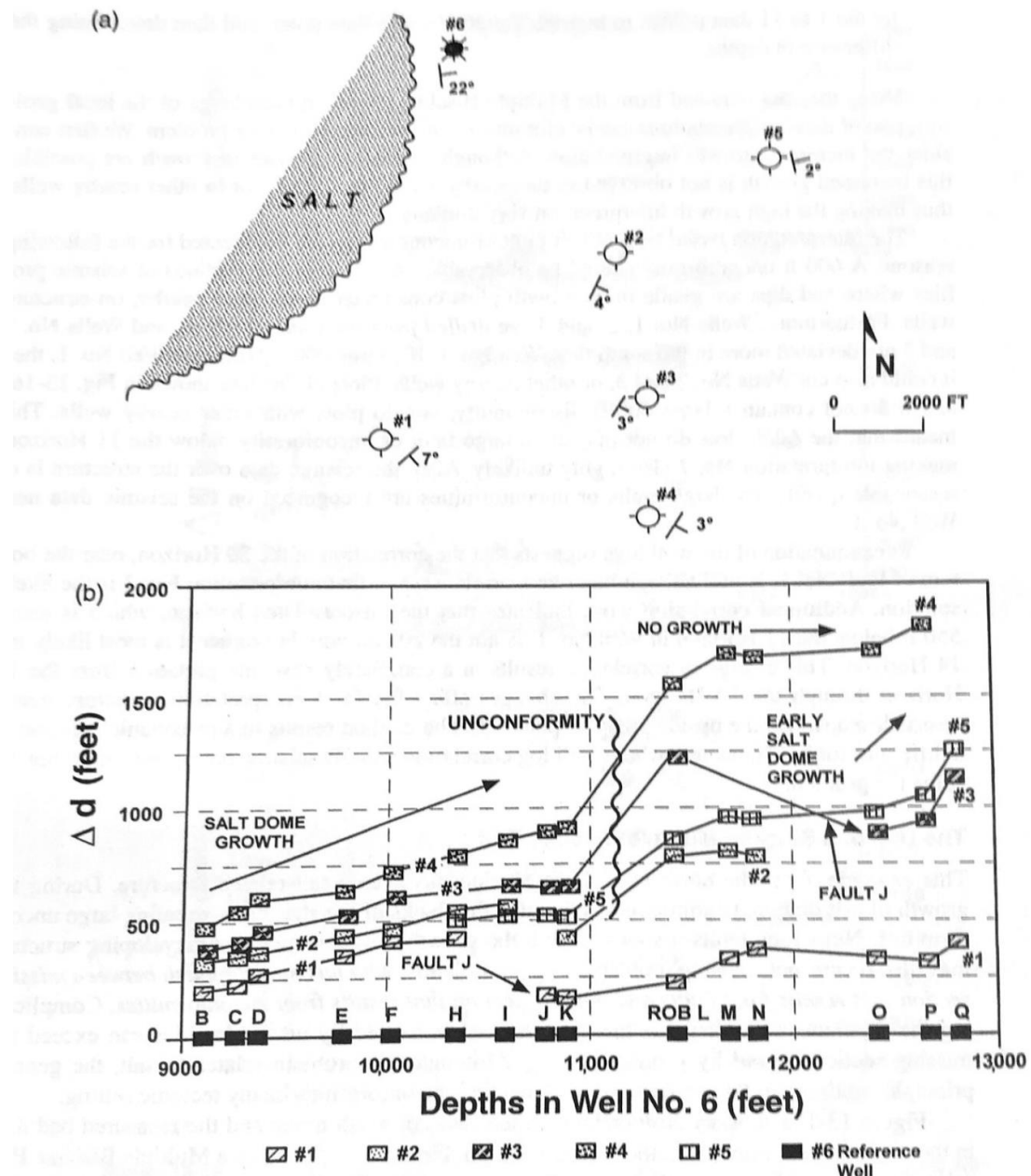


Figure 19. (A). Map showing strike and dip on the Rob L horizon on the flank of a salt diapir in the northern Gulf of Mexico, USA. In this environment, geoscientist have difficulties attributing missing section to faults or to large unconformities. (B) The MBP for the structurally higher reference Well No. 6 versus the five off-structure comparison wells. A large unconformity is interpreted above the Rob L horizon. In Well No. 1 and 3 the Fault J produces about 250 and 340 ft of missing section, respectively (Bischke, 1994).

Figure 19A shows well locations on the flank of a salt diapir and the measured bed dips in the wells at a stratum called the Rob L Horizon. Figure 19B shows a Multiple Bischke Plot (MBP) using the structurally higher Well No.6 as a reference well. All the data from the off-structure wells can be plotted on the same diagram since every well has been compared to Well No.6. On the x-axis the Horizons B through Q in each well have been plotted.

The salt structure experienced two growth stages: (1) the intervals between B and M Horizons and (2) the section between the O and Q Horizons. The interval from M to O Horizons indicates a little growth. Wells No. 1 and 3 display negative discontinuities that represent missing section, resulting from either a fault in the lower well (Figure 16C) or downlap (Figure 18). As downlap is rare on the flanks of salt diapirs, it is more likely that these discontinuities or displacements are the result of a fault in the structurally lower well rather than an unconformity. Correlation to other off-structure wells confirms that the missing sections in Wells No. 1 and 3 on the MBP are due to Fault J.

A positive discontinuity above Rob L Horizon exists in every well included in Figure 19. The missing section pointed out by that positive slope remains in the same stratigraphic level, thus it evidences an unconformity.

In the central sub-basin of the Nordkapp Basin and specifically in the interpreted seismic cube, the $\Delta d/d$ method was applied. To gain a better understanding of the growth of every salt diapir, multiple Bischke Plots (MBP) were performed using 42 pseudo-wells displayed in Figure 20. Distinction between faulting and unconformities is based on seismic interpretation (recognition of onlaps and downlaps) and previous works (Rojo and Escalona 2018).

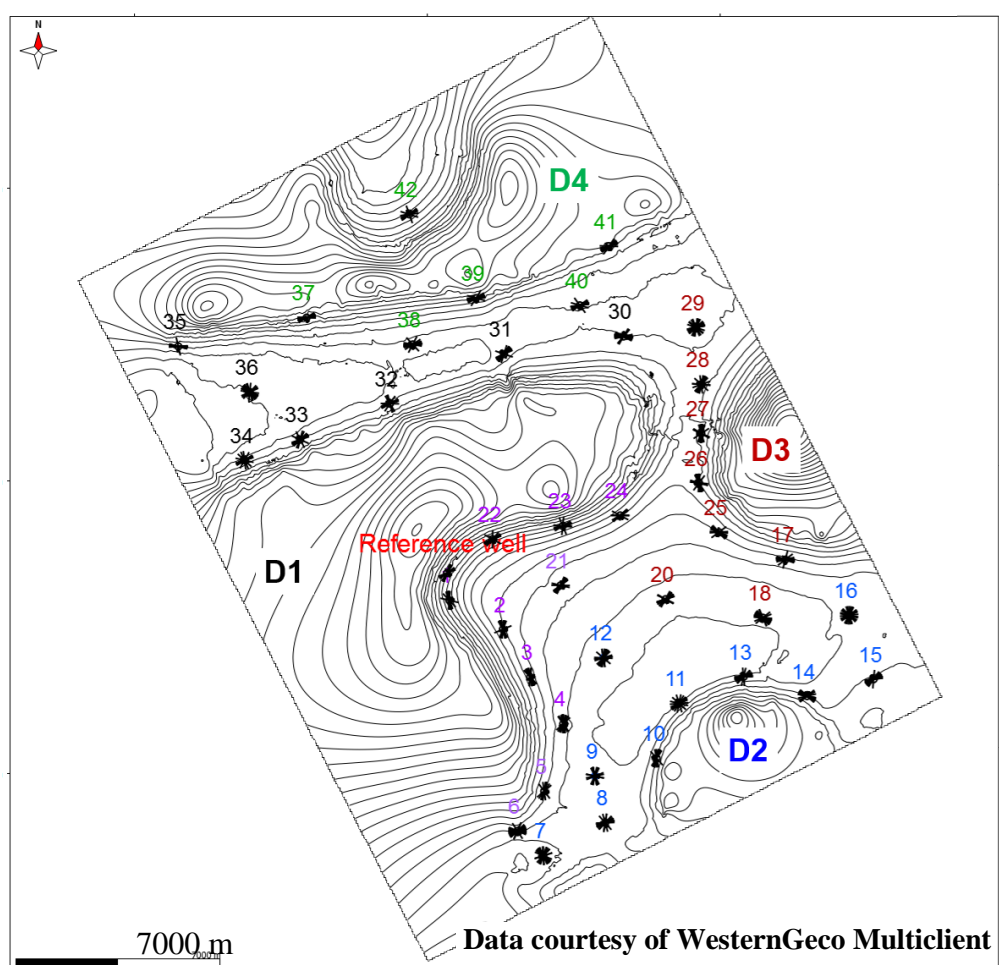


Figure 20. Structural map showing the location of the 42 pseudo-wells around the salt diapirs (D1, D2, D3 and D4) in the salt-bearing minibasins. Pseudo-wells labeled in different colors for each diapir; D1 flank SE in purple; D1 flank NW in black, D2 in blue; D3 in brown and D4 in green.

4. RESULTS

4.1. Seismic Facies: Description and Interpretation.

The Nordkapp Basin comprises several minibasins infilled with sediments, which have different seismic response. Thus, these sediments influence the seismic reflection characteristics such as the reflection terminations and amplitudes. Six seismic facies were recognized (Table 2). Due to the underexplored nature of the study area, no wells are available. Therefore, all interpretations of these facies are based exclusively on (1) their seismic reflection characteristics and (2) the previous work of Rojo and Escalona (2018) and Rojo et al., 2019.

SEISMIC FACIES F1

Description

Seismic facies F1 appear like semicontinuous, rough regular seismic events with locally distributed medium- to low-amplitude seismic events (Table 2). It is bounded at its top and base by well-defined, continuous and high-amplitude reflectors.

Interpretation

Semicontinuous, parallel to chaotic seismic events represent outer shelf to prodelta depositional environments.

SEISMIC FACIES F2

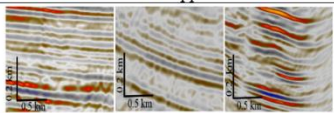
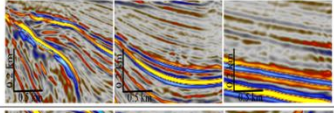
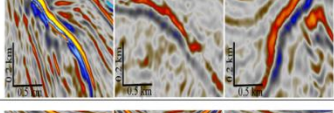
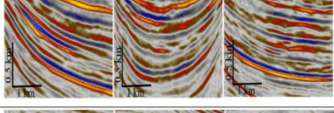
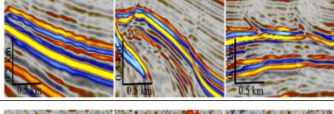
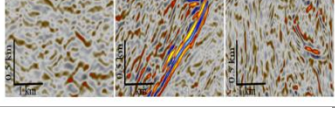
Description

These facies show a wedge-shaped architecture with semicontinuous, parallel, gently inclined, low-amplitude seismic events downlapping an angular unconformity (Table 2).

Top of seismic facies F2 appears as a medium- to high-amplitude seismic event that is overlapped by semicontinuous, medium-amplitude reflectors.

Interpretation

Based on the presence of dipping seismic events within this interval, the sediments are thought to prograde towards the southeast within a sigmoidal clinoform (Figure 21.), which shows foreset angles of less than 4 degrees.

Seismic Facies	Seismic Reflection characteristics	Interpretation (based on recent works by Rojo and Escalona (2018) and Rojo et al., 2019)	Examples of seismic facies in the Nordkapp Basin
F1	Semicontinuous, quite regular, medium- to low-amplitude seismic events. Lateral change to regular and high-amplitude seismic events.	These semicontinuous and parallel seismic events represent outer shelf to prodelta depositional environments.	
F2	Semicontinuous, parallel, gently inclined, low-amplitude seismic events, downlapping a basal unconformity.	Sediments prograding to the southeast within a sigmoidal clinoform, which shows foreset angles of less than 4 degrees.	
F3	Inclined, semicontinuous, medium to high-amplitude seismic events downlapping a basal unconformity. The top is a high-impedance seismic event.	Gravity flows adjacent to the salt structures.	
F4	Marked continuous to semicontinuous, parallel, high- to medium-amplitude seismic events. In certain areas, these regular seismic events turn into irregular events.	Based on the stratigraphical record these seismic facies could be interpreted as fluviodeltaic deposits.	
F5	Very high-amplitude, continuous and parallel seismic event.	From a regional correlation, seismic F5 comprises the BCU and it may be interpreted as massive marine organic-rich shales.	
F6	Chaotic seismic events with medium to low-amplitudes, changing to high-amplitude reflectors, as they are inclined.	Deformed layered evaporate sequences	

Data courtesy of WesternGeco Multiclient

Table 2. Summary of the different seismic facies in the minibasins of the study area. All facies interpretations are based exclusively on seismic interpretation and previous work of Rojo and Escalona (2018) and Rojo et al., 2019

SEISMIC FACIES F3

Description

Seismic facies F3 display a wedge-shape that comprises inclined, semicontinuous, medium- to high-amplitude seismic events, downlapping a basal unconformity (Table 2). The top of seismic facies F3 is normally defined by high-amplitude reflectors overlapped by medium- to low-amplitude seismic events (Figure 21).

Interpretation

Regarding its architecture seismic facies F3 is interpreted as gravity flows adjacent to salt structures.

SEISMIC FACIES F4

Description

These facies comprise marked continuous to semicontinuous, parallel, high- to medium-amplitude seismic events. In certain areas, these regular seismic events turn into less regular seismic events of seismic facies F1.

Interpretation

Based on stratigraphical record, these seismic facies could represent fluvial deposits (Table 2). From a depth slice analysis of spectral decomposition, some fluvial systems are recognized within these seismic facies (Figure 22). A meandering channel crosses the southeastern minibasin from north to south. This river goes between diapirs D1 and D2 and is more proximal to diapir D1. On its western side, overbank deposits are visible (Figure 22). Towards the center of the study area, where diapirs D1 and D3 are in front

of each other, the river system rounds the diapir D1 to cross the northwestern minibasin bounded by diapirs D1 and D4, in order to reach the flank of diapir D4 (Figure 22, left). This braided river system runs along the northwestern minibasin keeping a straight trajectory between diapirs D1 and D4 (Figure 22, right).

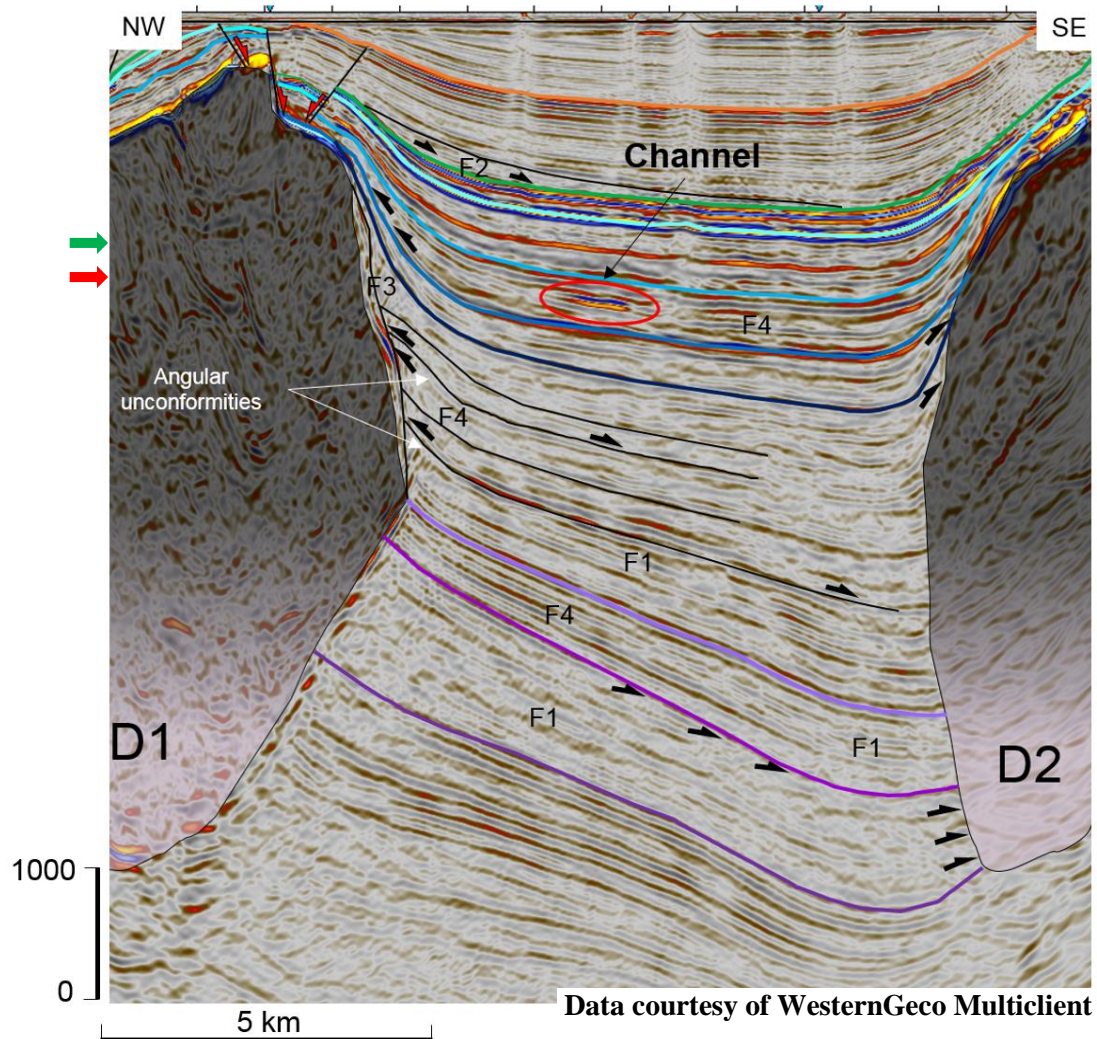
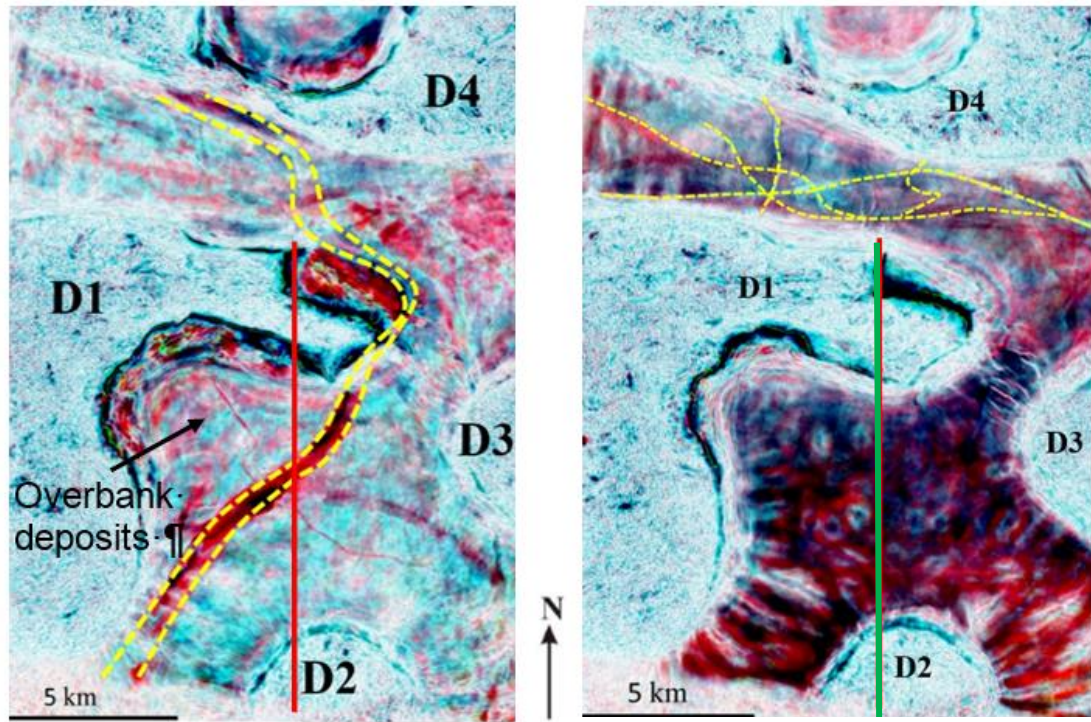


Figure 21. Seismic line showing the different seismic facies in the minibasin of the study area. Seismic facies F4 and F1 are the dominant in the study area. Seismic facies F1 become seismic facies F4 which onlaps onto seismic facies F3. Seismic facies F2 downlaps onto the basal unconformity (green line). Note the high-amplitude reflector between the seismic facies F4 indicating the presence of a channel. Arrows indicates the position of depth slices of Figure 22.



Data courtesy of WesternGeco Multiclient

Figure 22. Depth slices showing the position of channels respect to the salt diapirs. (Left) Depth slice 1872 m displays a meandering river with adjacent overbank deposits. (Right) Depth slice 2048 m shows the braided system along the northwestern minibasin. Red and green lines indicate the position of seismic line of Figure 21.

4.2. Structural maps of study area

This section describes the structural maps of those horizons interpreted as sequences boundaries with emphasis on Triassic and Jurassic sequences. The seismic cube shows four salt diapirs named diapirs D1, D2, D3 and D4. Diapirs D1 and D3 are in the central zone of the data set, diapir D2 is in the east, and diapir D4 is in the west.

TOP SEQUENCE S1: LOWER TRIASSIC

The major diapirs recognized here are diapirs D4 and D1 (Figure 23). Diapirs D2 and D3 are barely visible at this level. Diapir D4 is in the north and extends from east to west. It represents the maximum elevation point located to the northwesternmost part. Diapir D1 occupies the central part but without reaching great elevations. The area between both diapirs is the northwestern minibasin, which is shallower (around -5000m) than the southeaster minibasin ($> -7000\text{m}$).

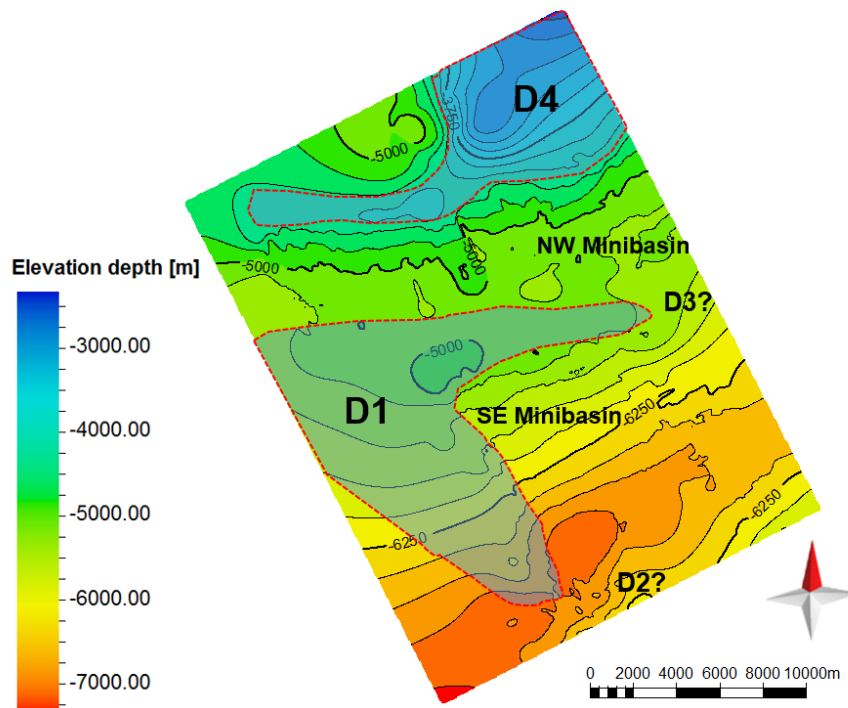


Figure 23. Top Sequence S1 elevation structural map showing the extension of salt diapir D4 in the north and diapir D1 in the central part. Note diapirs D2 and D3 are not recognized at this level.

BASE SEQUENCE S3: LOWER TO MIDDLE TRIASSIC

Diapir D1 is the dominant structural element in the Lower to Middle Triassic interval. It reaches higher elevation compared with its stage in the Lower Triassic (Figure 24). Diapir D4 remains its height and continues extending towards the west. The crest of both diapirs reach the seabed (0 m). Diapir D3 also show an important elevation but diapir D2 is still not visible. Southeastern minibasin appears at deeper level than northwestern minibasin.

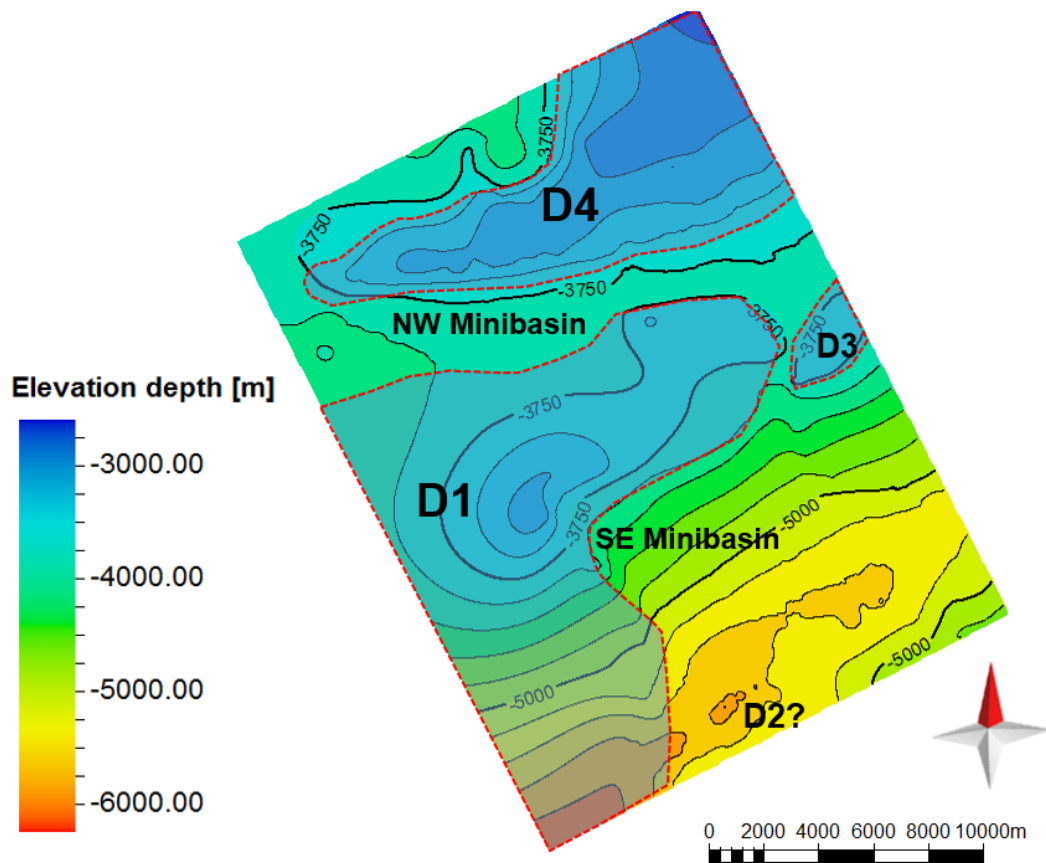


Figure 24. Base Sequence S3 structural map. Diapirs D1 and D4 are longer and diapir D3 is already visible while diapir D2 does not appear in this period. .

TOP SEQUENCE S5: MIDDLE TRIASSIC

Middle Triassic structural map shows an area dominated by the four well-defined salt diapirs; D1-D4 (Figure 25). All salt structures except diapir D2 reach the seabed at their tops. Note the deepest part (> 2400 m) located in the north, which is enclosed by the elongated diapir D4. Southeastern minibasin is the second deeper and the northwestern minibasin is the shallower.

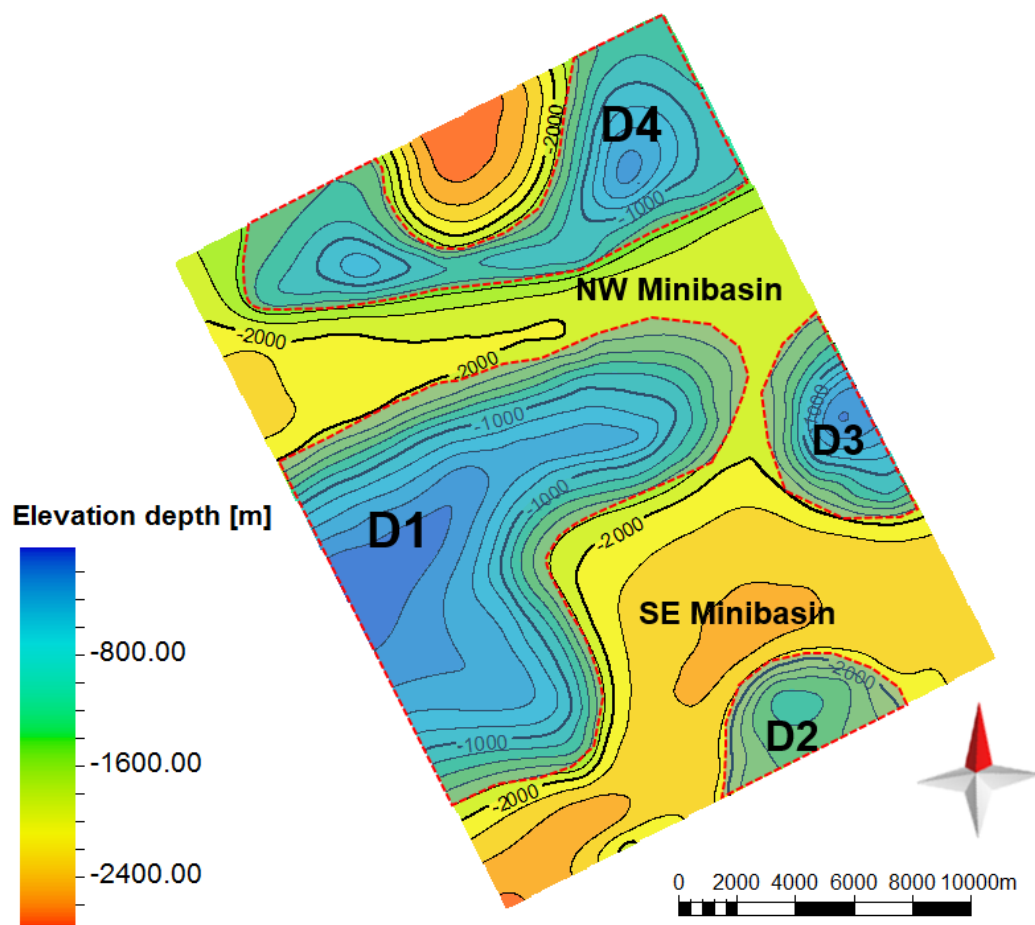


Figure 25. Structural depth map showing all salt diapirs: D1-D4. Note the deepest point in the north.

Structural maps of sequences S4 and S6 are not included since both of them display similar characteristics of S5 structural map.

TOP MEGASEQUENCE MS2: JURASSIC

All salt structures show great heights up to reach the seabed at their tops. However, they are thinner and minibasins between those structures widen. This is especially evident for diapir D4, which is very thin in its central part (Figure 26). The deepest point remains in the northernmost part (> -2000 m) but the northwestern minibasin is at the shallower level around -1250 m.

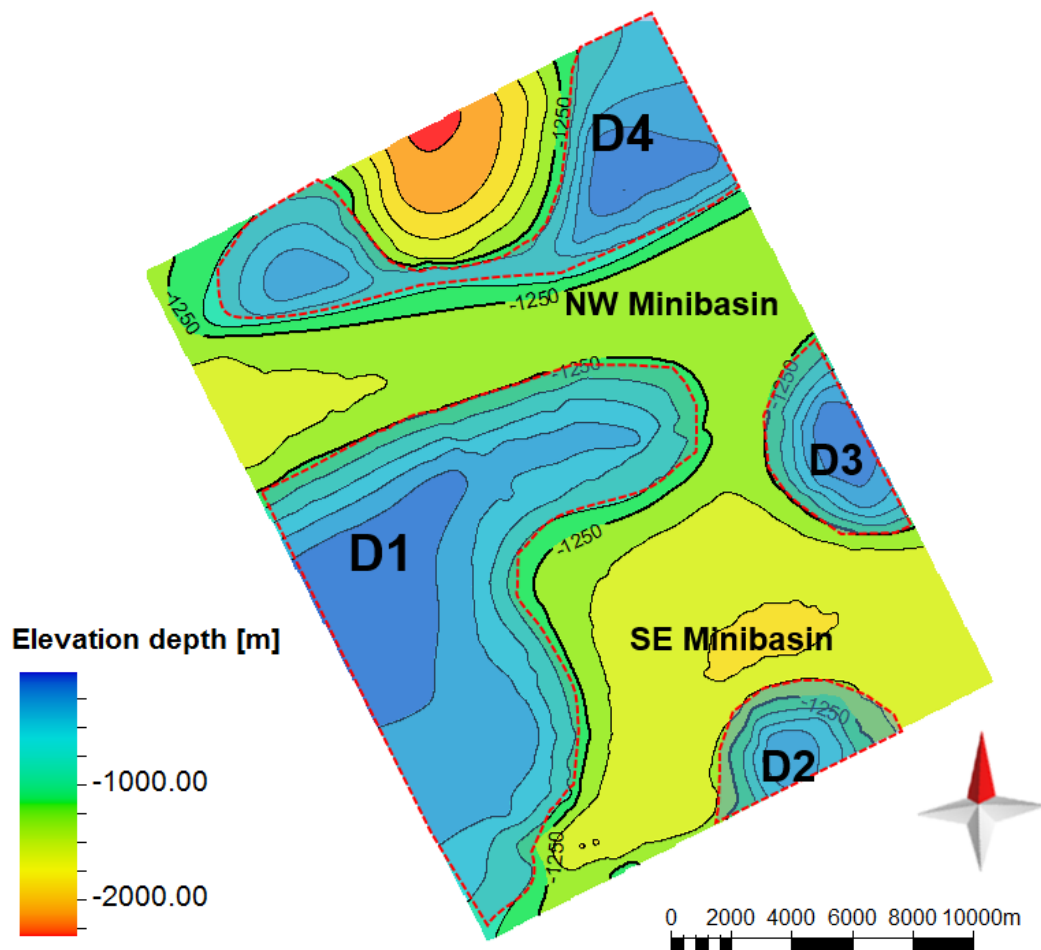


Figure 26. Top Megasequence MS2 elevation map showing the structural configuration of the study area in the Jurassic. All four diapirs reach the seabed at their top. Minibasins widen due to diapirs are thinner.

4.3. Thickness maps of sequences in the central sub-basin

SEQUENCE S1: LOWER TRIASSIC

The thickest strata between sequences S1 and S2 are located around the southeast flank of Diapir D1. In this part, from flank SE of diapir D1 to diapir D2, the enclosed minibasin displays the large depocenter compared to the southeastern minibasin (Figure 27). The zone between diapirs D1, D3 and D4 also shows deep strata due to the accommodation space created by the presence of those diapirs.

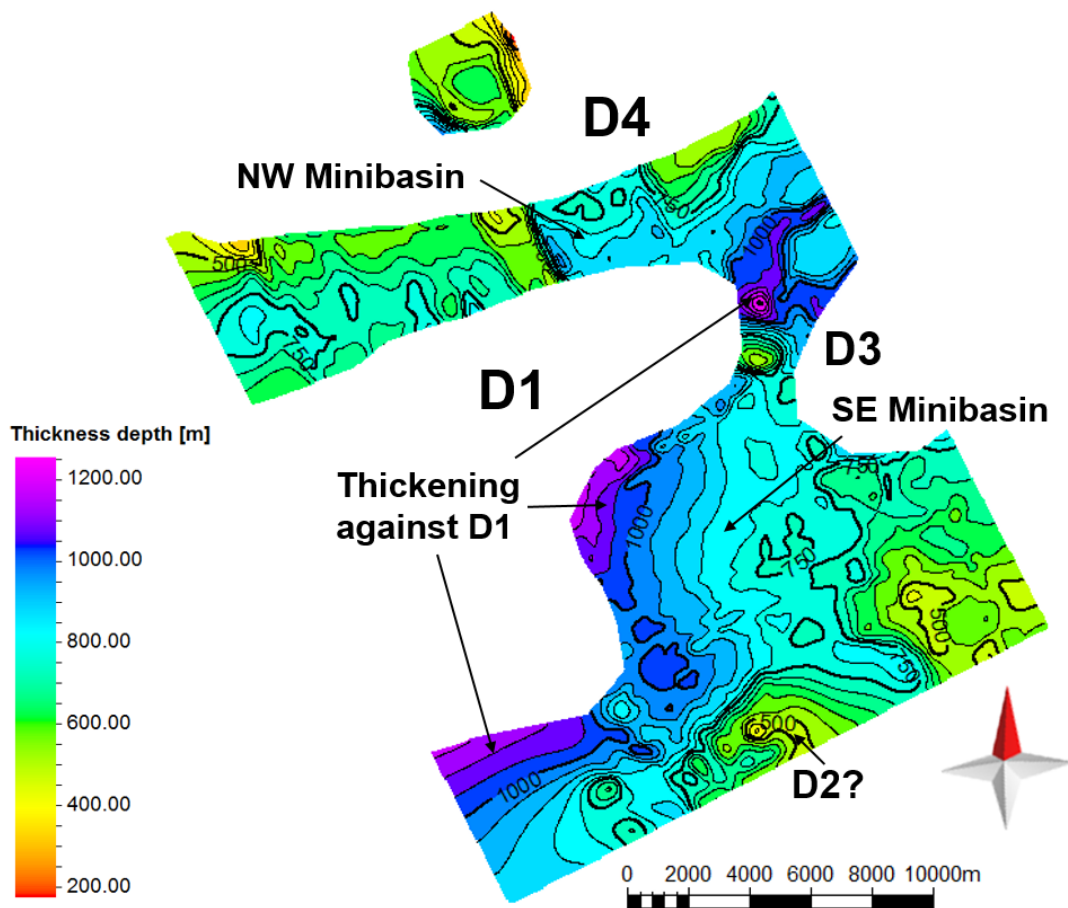


Figure 27. Depth thickness map of sequence S1 (Lower Triassic). Strata around diapir D1 thicken against the southeastern flank. SE minibasin displays the deepest strata.

SEQUENCE S3: LOWER TO MIDDLE TRIASSIC

Thickness variation of this unit is small and the most significant thickening occurs towards the southeast on the southeastern minibasin along the eastern flank of salt diapir D1 (Figure 28). The strata in the northwestern minibasin thin from the basin axis to flanks of diapirs D1 and D4. This trend is also observed between diapirs D1 and D3.

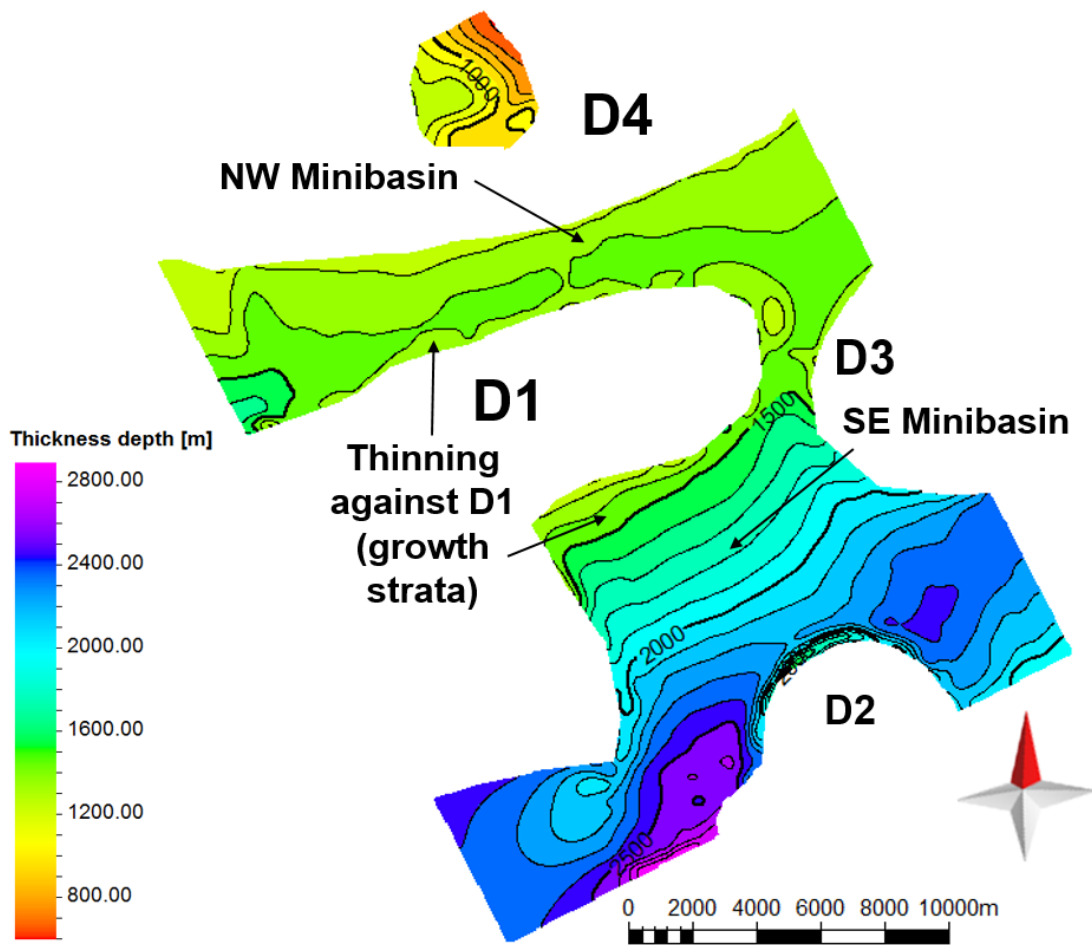


Figure 28. Thickness map of sequence S3. Largest depocenter is located in the southernmost part. Towards the north, strata thin against diapirs D1, D3 and D4.

TOP SEQUENCE S5: MIDDLE TRIASSIC

Clear evidence of thinning near salt diapirs is observed (Figure 29). The truncation of growth strata are limited to a narrow section of 1 km length. Thickness variation is roughly homogeneous.

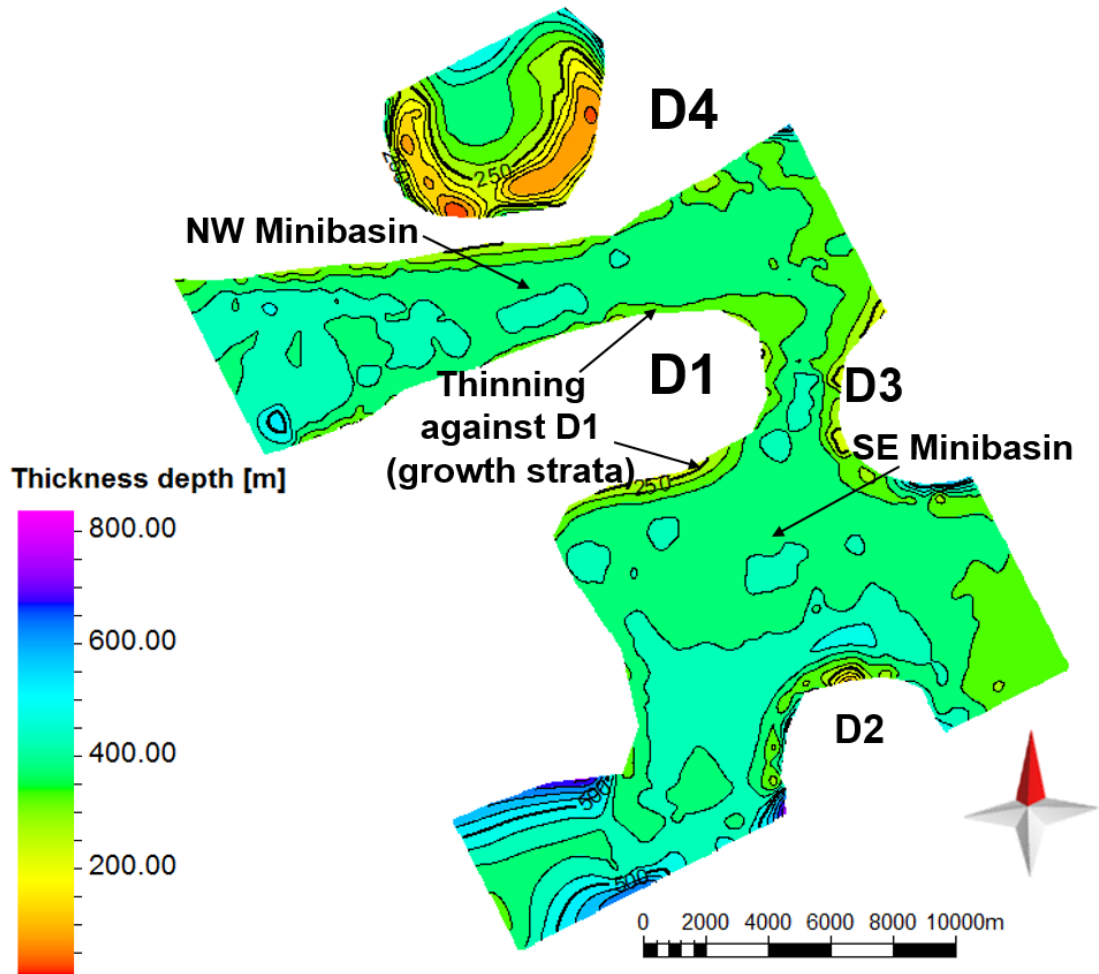


Figure 29. Depth thickness map of sequence S5 showing thinning towards diapirs. During Middle Triassic thickness variations are roughly constant..

TOP MEGASEQUENCE MS2: JURASSIC

Jurassic strata show constant thickness along both minibasins. The marked thickness variation is concentrated around diapirs flanks and within minibasin enclosed by diapir D4 in the northernmost part (Figure 30).

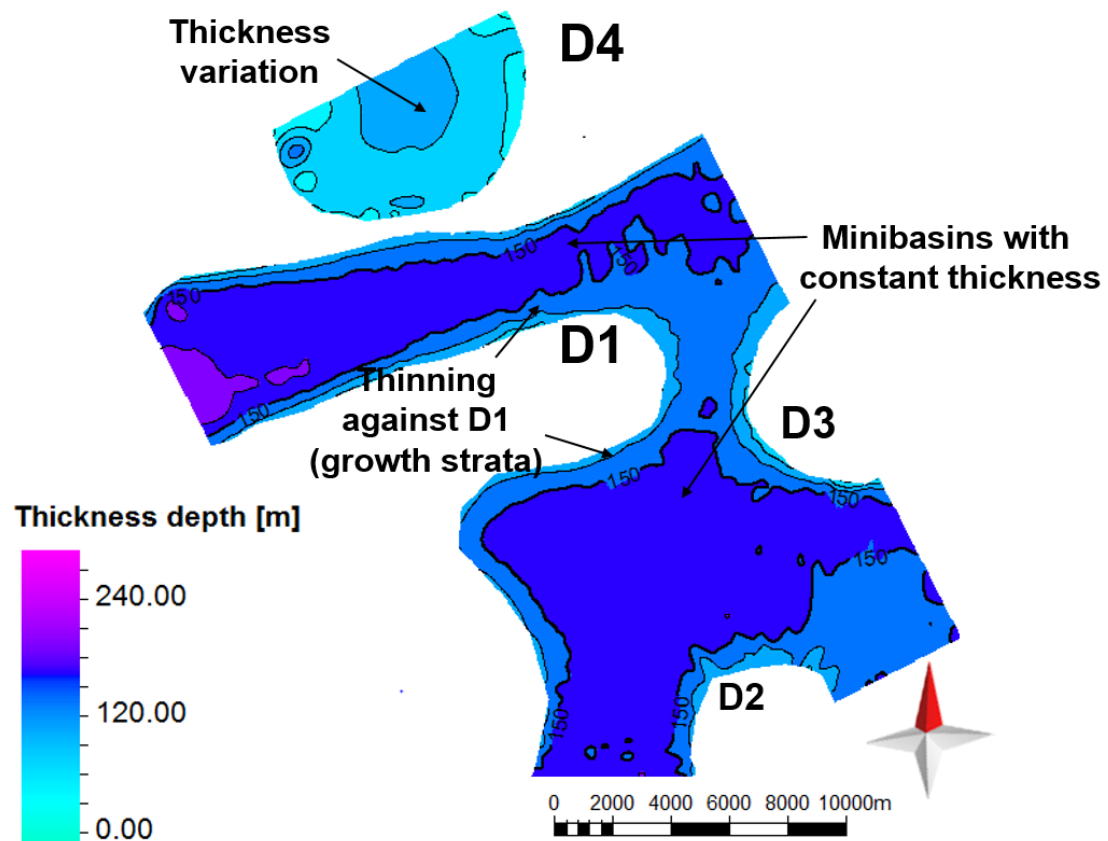


Figure 30. Thickness map of megasequence MS2 showing constant thickness in both minibasins. In the northern part, note the thickness variation of minibasin enclosed by diapir D4.

4.4. Basin profiles of the central sub-basin

The interpreted stratigraphic sequence is between the base Lower Triassic and the base Quaternary (seabed). The sedimentary succession was divided into megasequences (MSes). Since this thesis focuses on the Triassic interval, a further subdivision into subsequences (S) was performed in this interval (Table 1). In this section, three profiles crossing the sub-basin are presented and described. The position of these profiles is shown in Figure 31. The seismic profiles display the structural configuration of the basin with emphasis on the salt structures and the surrounding minibasins.

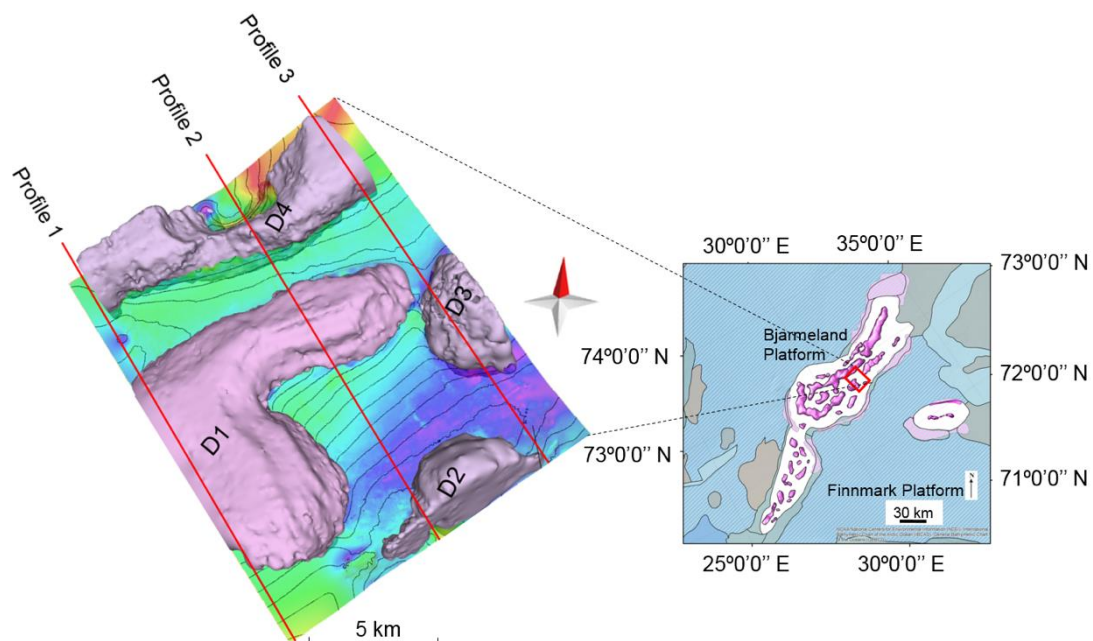


Figure 31. Left: Structural maps of sequence S3 showing the location of profiles through the interpreted salt diapirs D1, D2, D3 and D4. Right: insert map showing the distribution of salt structures within the Nordkapp Basin. Red rectangle indicates the extent of the study area.

PROFILE 1 (FOCUSED ON SEQUENCE S1)

The easternmost part of the study area is dominated by the presence of two salt diapirs: diapir D1 and D4, which are separated by well-defined salt-bearing minibasins (Figure 32). The teardrop diapir D1 is the largest salt structure and it is situated in the basin centre (Figure 31). Diapir D4 is an elongated salt wall that spans west to east showing collapse evidence towards the east, which led to the formation of a large depocenter in this area (Figure 27).

All the sequences, except the deeper sequences S1 and S2, get thinner towards the salt bodies where they are upturned and truncated within a distance of less than 2 km (Figure 32). Sequences S1 and S2 in the southeastern minibasins, show a shift in salt withdrawal resulting in a minibasin inversion, i.e., S1 strata are thickening towards the diapir D1 while S2 strata are thinning towards D1. This process may have led to the formation of a turtle structure. The minibasin inversion is recognized not only in the seismic profile but also in the corresponding depth thickness map of S1 (Figure 27). Between sequences S1 and S2, an angular unconformity is recognized because the reflectors are truncated against the top of S1. Growth strata occur from sequence S4 (Middle Triassic). Jurassic strata are truncated against the diapir D4, which indicates that diapir growth continued during this period. Towards the SE, megasequences 3 and 4 display evidence of growth strata, which are truncated and overlain at the top by Quaternary sediments (Figure 32).

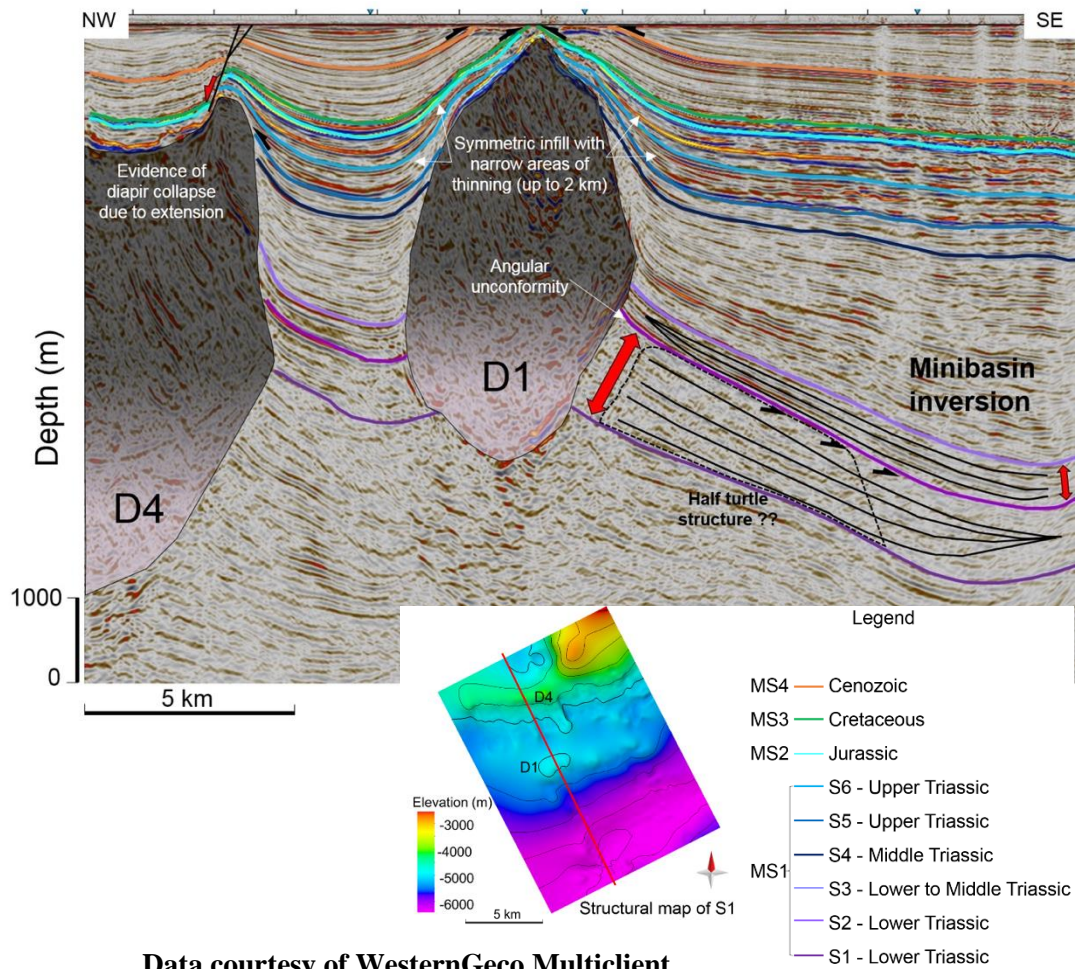
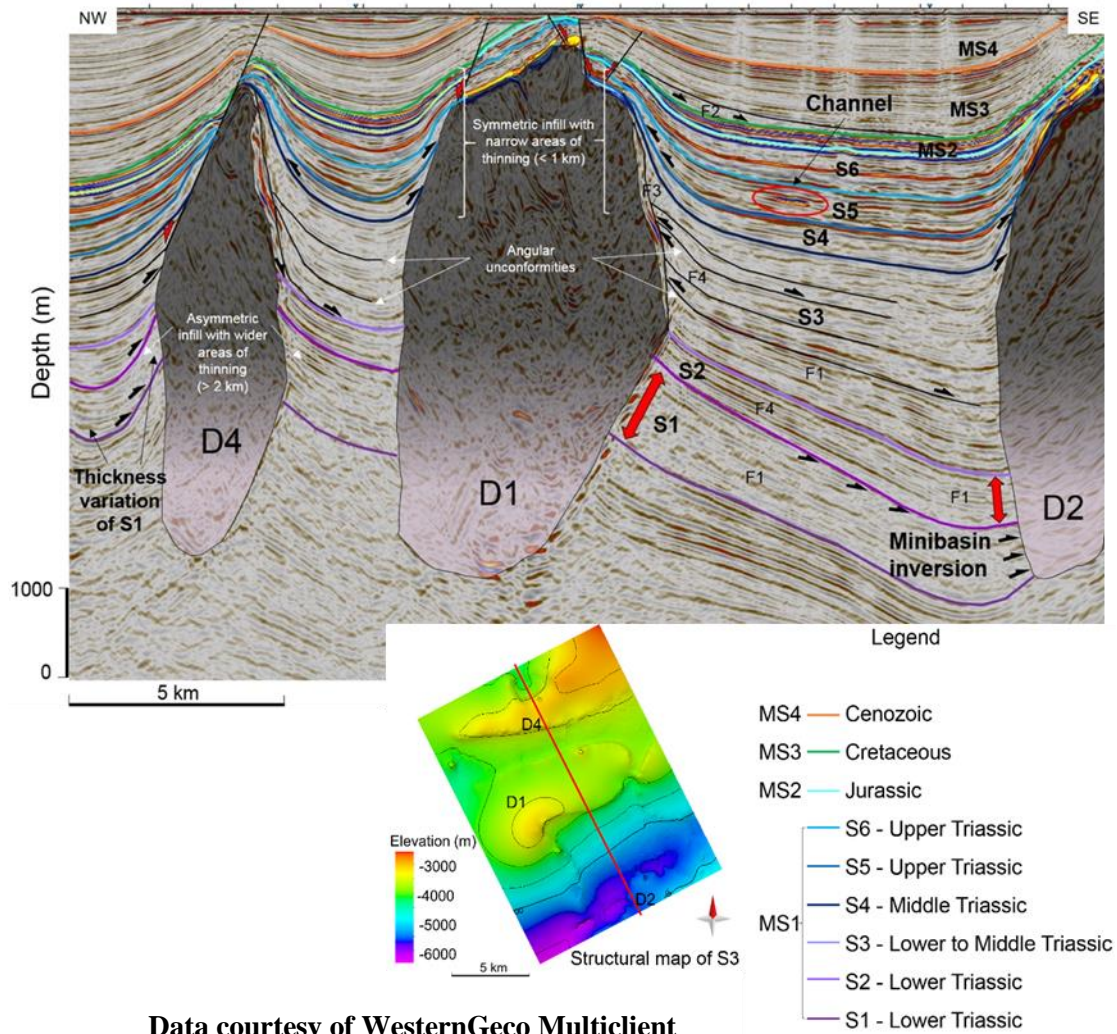


Figure 32. Profile 1 showing the stratigraphic and structural configuration of the study area within the central sub-basin in the Nordkapp Basin. The inset structural map of sequence S1 on the bottom left shows the location of this seismic line. Evidence of salt tectonic is observed from the Middle Triassic until Quaternary (e.g. truncation and thinning occurring at the top of S4). In the SE flank of salt diapir D1, Triassic sequence S1 and S2 are delimited by an angular unconformity that becomes conformable towards the NW. MS1 = megasequence 1; MS2 = megasequence 2; MS3 = megasequence 3; MS4 = megasequence 4; S1 = sequence 1; S2 = sequence 2; S3 = sequence 3; S4 = sequence 4; S5 = sequence 5; S6 = sequence 6.

PROFILE 2 (FOCUSED ON SEQUENCE S3)

Farther east close to the center of the study area, three salt diapirs are identified (Figure 33). The major structure, diapir D1, limits with diapir D4 to the NW and diapir D2 to the SE. These salt structures are separated by well-defined minibasins that show evidence of salt growth. All diapirs are buried by Middle Triassic deposits, which are affected by normal faults at the top of diapirs D4 and D1. Above diapirs D1 and D2, megasequences MS2, MS3 and MS4 are truncated and overlain at the top by Quaternary strata (Figure 33). Every minibasin comprises sedimentary sequences that are truncated against salt bodies.

Overall, this profile roughly shows the same structural configuration as profile 1. Growth strata occurs from the sequence S4 (Middle Triassic). Sequence S3 is characterized by the presence of a large number of angular unconformities. Within this sequence, seismic facies F1 laterally become seismic facies F4, and onlaps onto seismic facies F3 towards the salt diapirs. On the other hand, sequence S5 displays seismic facies F4, which contains channels highlighting the presence of fluvial systems (Figure 33 and Table 2). Above the Jurassic strata, well-defined southward progradation of seismic facies F2 is observed within the Lower Cretaceous unit (Table 2). The strata configuration around the diapir D1 is quite similar onto both diapir flanks. Onto the western flank of diapir D4, the deeper, surrounding sequences S1 and S2 thin unequally within wide areas (>2km) compared to its eastern flank, while diapir D1 flanks are surrounded by sequences that thin symmetrically within a distance of less than 1 km from the salt body. In the northwestern minibasin, sequence S1 shows evidence of thickness variation (Figure 33).



Data courtesy of WesternGeco Multiclient

Figure 33. Profile 2 displays the stratigraphic and structural configuration of the study area within the central sub-basin in the Nordkapp Basin. The inset structural map of the sequence S3 on the bottom left shows the location of this seismic line. Salt diapirs growth occur from the Lower Triassic until Quaternary (e.g. truncation and thinning occurring at the top of S1 and S4). The largest depocenter is located in the SE minibasin, in which a shift in salt withdrawal caused the minibasin inversion. Note the marked thickness variations of S3 in each minibasin and the presence of channels in S5. MS1 = megasequence 1; MS2 = megasequence 2; MS3 = megasequence 3; MS4 = megasequence 4; S1 = sequence 1; S2 = sequence 2; S3 = sequence 3; S4 = sequence 4; S5 = sequence 5; S6 = sequence 6

PROFILE 3

Easternmost seismic line crossing through diapirs D4 and D3 (Figure 34). Both salt bodies reach the Quaternary deposits. These younger strata truncate Middle Triassic and Jurassic sediments.

Growth strata evidences appear from the sequence S1 (Lower Triassic) in the northwestern minibasin. On the contrary, in the southeastern minibasin thickness variations of S1 is smaller (Figure 34). The thickness variation of S1 in the northwestern minibasin is directly related to salt diapir growth.

As a rule, all sequences get thinner towards salt bodies where they are truncated and onlapped within a distance of less than 2 km from the salt structures (Figure 34). However, sequences S1, S2 and S3 following the opposite tendency; they get thicker towards the teardrop salt diapir D3 (Figure 34). Around the salt structure D3, a symmetric infill is observed and, the strata are thinning within a narrow area (up to 2 km). This seismic line displays an area of uncertainty at the base of diapir D4 regarding its dimensions (shape and size).

An erosive unconformity exists between Triassic and Jurassic strata, reflectors downlap onto the top of Triassic deposit. This unconformity is well-defined in the MBP because it marks a change in growth trend.

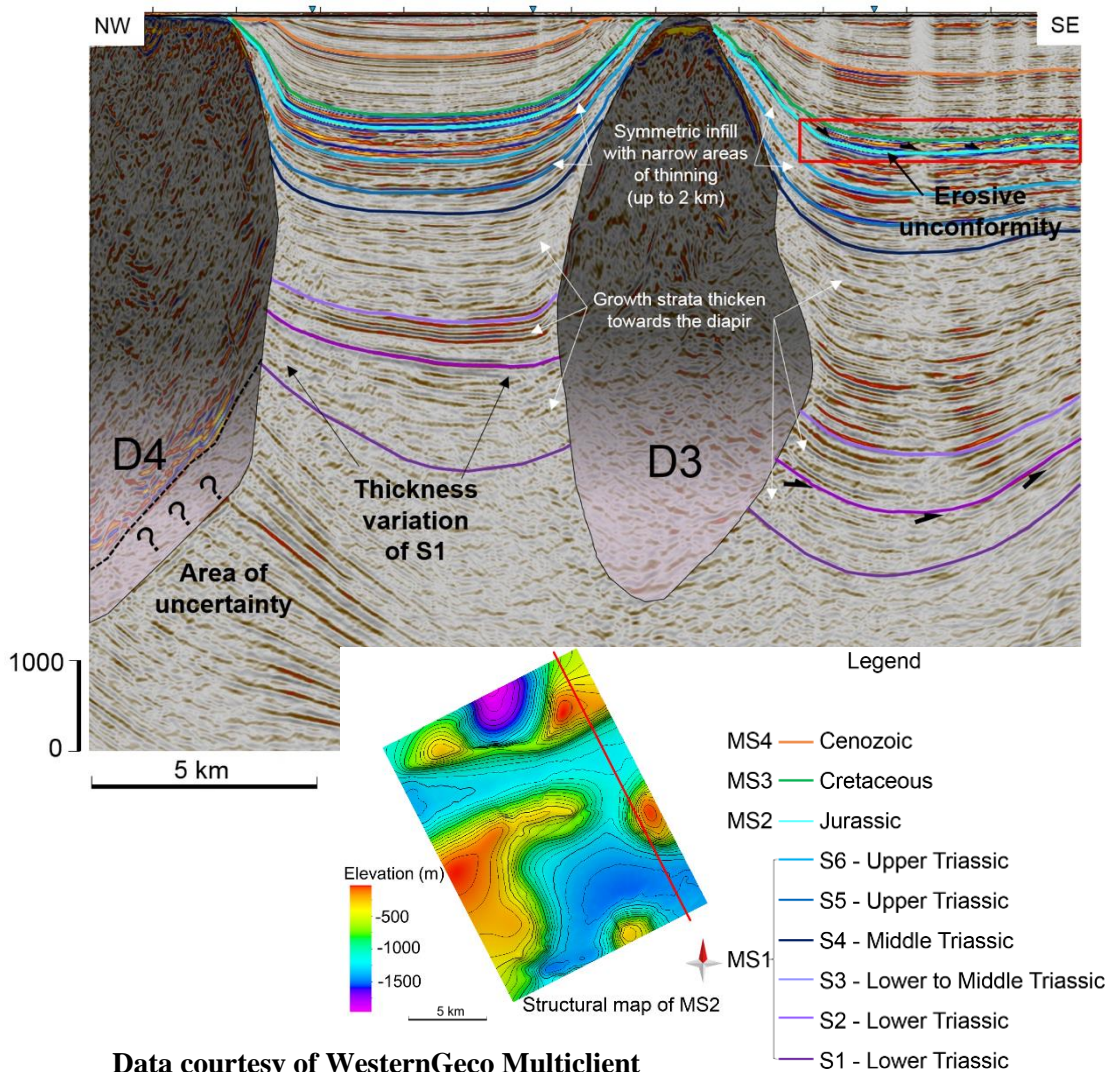


Figure 34. Profile 3 showing the stratigraphic and structural configuration of minibasins enclosed by diapirs D4 and D3. The inset structural map of megasequence MS2 on the bottom left shows the location of the profile. Halokinesis is observed from Lower Triassic until Quaternary (e.g. thickness variation of S1). Note that the largest depocenter is located in the SE minibasin. Triassic strata are separated from Jurassic strata by an unconformity. MS1 = megasequence 1; MS2 = megasequence 2; MS3 = megasequence 3; MS4 = megasequence 4; S1 = sequence 1; S2 = sequence 2; S3 = sequence 3; S4 = sequence 4; S5 = sequence 5; S6 = sequence 6.

4.5. Minibasin Stratigraphy of the central sub-basin

MEGASEQUENCE 1: LOWER TRIASSIC-UPPER TRIASSIC

Megasequence 1 (MS1) comprises six subsequences (S1-S6) in the Triassic section. MS1 is delimited at its base by the Lowermost Triassic units, which cannot be identified in this data set. The top is bounded by the base Jurassic, which is represented by a high-amplitude seismic event (Figure 32). This event is regionally interpreted as an erosive unconformity, formed by the decrease in subsidence in the western Barents Sea during the last thrusting stage of Novaya Zemlya on the east (Buitter and Torsvik, 2007; Anell et al., 2014)

Sequence 1: Lower Triassic

Description

Sequence 1 (S1) is bounded by continuous, quite regular and medium- to low-amplitude seismic reflectors both at the base and at the top. This sequence comprises seismic facies F4, which laterally changes to regular and high-amplitude seismic facies F1.

On the southeastern minibasins, S1 thickens towards the salt body in the northwest (Figure 32). Internally, parallel reflectors are truncated against the salt body and towards the top.

Interpretation

According to Glørstad-Clark et al. (2010), S1 could be part of the Lower Triassic (Lower Havert Fm.). The internal parallel configuration of S1 could indicate no halokinesis, but the beds thickening towards the northwest suggest early salt movement.

Sequence 2: Lower Triassic

Description

Sequence 2 (S2) is delimited at its top and base by continuous, high-amplitude seismic reflectors, which are characteristics of seismic facies F4. These seismic events become more irregular and discontinuous towards the diapir D2 (Figure 34).

On the northwestern minibasin, S2 displays growth strata that are gently upturned and truncated against the salt diapir D4 (Figure 34). This sequence thickens towards the southeast from diapir D4 to diapir D3. However, to the west of diapir D3 the thickness of this sequence remains constant (Figure 34).

Interpretation

Based on Glørstad-Clark et al. (2010), this section is part of the latest Lower Triassic (upper Havert Fm.). It displays evidence of salt growth, as for example, the presence of growth strata and truncations against the salt structures (Figure 34).

Sequence 3: Lower-Middle Triassic

Description

Based on seismic interpretation, S3 is bounded at its top and base by continuous, high- to medium-amplitude seismic events, quite similar to the underlying S2. On the northwestern minibasin, S3 becomes unconformable and more reflective near the salt diapirs D4 and D1, to conformable towards the minibasin (Figure 33). Around the salt diapir D4, growth strata and truncations are observed (Figure 33). However, the thickness variation of this unit is small and the most significant thickening occurs towards the southeast on the southeastern minibasin along the eastern flank of salt diapir

D1 (Figure 33). Here, seismic facies F3 displays inclined, semicontinuous, medium to high-amplitude seismic events downlapping the basal unconformity.

Interpretation

According to Rojo and Escalona et al., 2018, S3 could cover the Klappmyss and Kobbe Fms. (Figure 11). This sequence comprises angular unconformities near salt diapirs (Figure 33). These unconformities are the result of erosion of the salt highs. Based on seismic observation, the transition of F1 in the base to F4 towards the top, suggests a transition from prodelta to shallow marine depositional environments (F1 and F3) to a fluviodeltaic system (F4).

Sequences 4, 5, and 6: Middle to Upper Triassic

Description

Based on seismic interpretation, these sequences are bounded by high-amplitude seismic events, which represent unconformities close to the salt structures, but they become conformable towards the minibasins (Figure 33). S6 and S5 comprise high-amplitude seismic events (seismic facies F4) that are overlaid by low-amplitude seismic reflector F1, which is the dominant seismic facies within S4. At glance, S4 to S6 show a transition from semicontinuous, regular, medium- to low-amplitude seismic events of F1 to the continuous, high-amplitude seismic events of F4.

On these sequences, clear evidence of thinning near salt diapirs is observed (Figure 34). The upturn and truncation of growth strata are limited to a narrow section of 1 km length. This section tends to be characterized by low-amplitude seismic events and noise. However, the seismic data display a high-quality seismic imaging that allowed a

more accurate seismic interpretation and the recognition of fluvial systems as meandering channels within S5 (Figure 33).

Comparing depth-thickness maps, sequences S4-S6 display 400 m thick minibasins (Figure 29) in comparison with S3 (Figure 28).

Interpretation

Sequences 4-6 are interpreted to cover the interval between the upper Kobbe, Snadd and Fluholmen Fms. (Figure 11). Salt growth is responsible for the erosion of diapir-induced highs which are recognized by the presence of narrow angular unconformities near the salt diapirs (Figure 33). Based on previous work in the southwestern and central part of the Nordkapp Basin by Rojo and Escalona (2018), these sequences transition from shallow marine environments at the base to prodelta depositional environments, with the presence of meandering channels in S5.

4.6. Diapir growth according to Multiple Bischke Plots (MBP) during Triassic.

Bischke and Tearpock (1994) stated that the $\Delta d/d$ plots analysis is an excellent technique since the growth plots obtained give valuable information that is used to locate sequence boundaries and subtle stratigraphic traps, to identify and solve correlation problems in areas of rapidly changing lithology, to determinate high growth or potential thick sand rich intervals on seismic profiles, to stablish the time of structural growth and fault timing and to check interpretation for consistency. All this has implications for hydrocarbon exploration since higher growth rates correlate with oil formation, migration and entrapment (Tearpock et al., 1993).

In order to investigate the diapir growth rate of each diapir located in the study area, six $\Delta d/d$ plots were constructed from measures made by stratigraphic correlations of seismic horizons interpreted on a 3D full azimuth seismic data set in the central sub-basin, between 42 pseudo-wells located in the area of interest.

In the first MBP, (Figure 35), the growth diapirs is analyzed in general, comparing all diapirs with each other. To construct this plot, Well 1 is used as reference well respect to 42 wells located near the other diapirs (Figure 20). The MBP of Figure 35 display 42 $\Delta d/d$ curves corresponding to the 42 pseudo-wells used.

Interpretation of MBP

A positive slope will show either (1) a steeper slope that would indicate an expanded section formed in an unstable or growth tectonic environment, e.g. diapirs during the Lower-Middle Triassic interval (Figure 35), or (2) a smaller or approximately flat slope implying a stable pre-growth tectonic environment, e.g. during Cretaceous and Cenozoic times (Figure 35). On the contrary, a negative slope or discontinuity on these plots will indicate the presence of a condensed or reduced section, implying thinning of strata due to changes such as the switch in salt withdrawal during the Early Triassic (Figure 35)

Abrupt changes in growth occur across sequence boundaries, which are interpreted as unconformities from seismic interpretation of downlaps and onlaps in the basin profiles 1-3 (Figure 33).

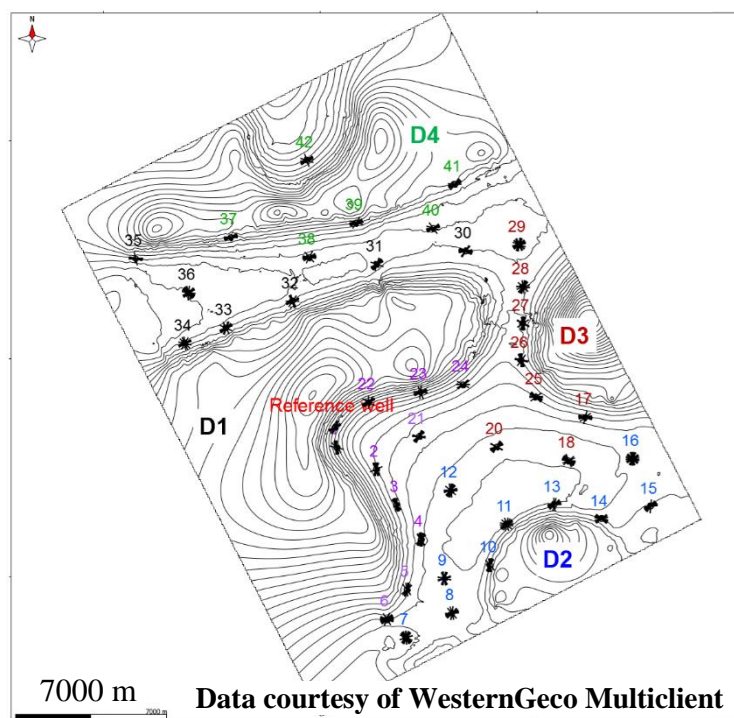
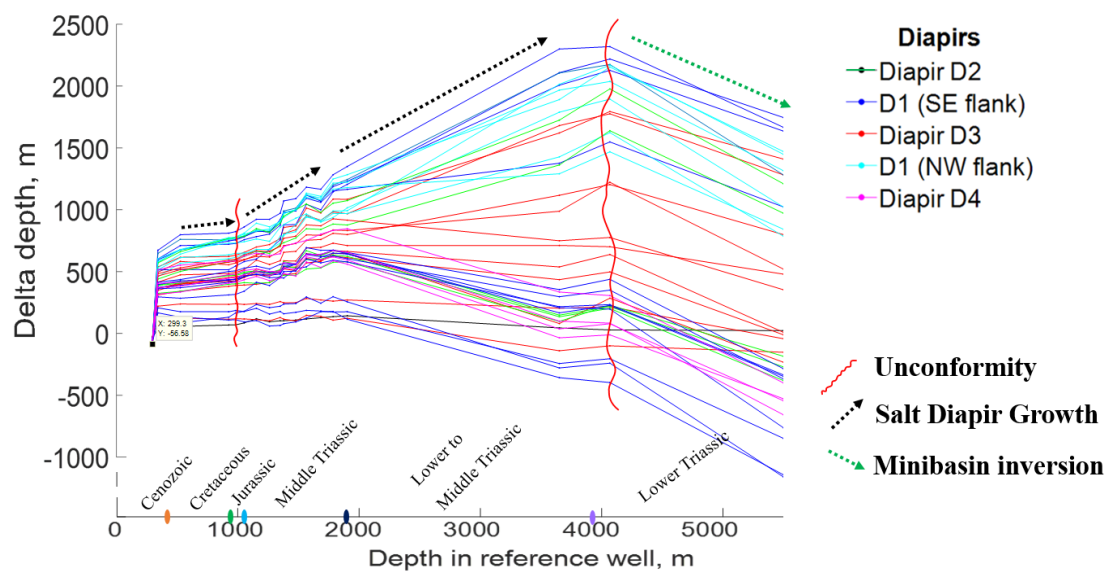


Figure 35. . Top: graph showing the Multiple Bischke Plot for the structurally higher Reference Well No.1 respect to 42 wells around every salt diapir. Bottom: the inset map (

) displays the structural configuration of the study area. The MBP depicts the overall growth trend for each diapir. During the Lower Triassic, diapirs D2 and D3 show a greater growth than diapir D1 and D4. Through the Lower-Middle Triassic, the growth trend is the same, SE salt structures keep growing more than NW diapirs. In the Middle Triassic-Jurassic, migration of depocenters occurred because of diapirs located to the NW (D1 and D4) grew more than diapirs D2 and D3 in the SE due to the salt depletion in this part. Two unconformities are identified between (1) Lower Triassic sequences S1 and S2, and (2) Middle Triassic and Jurassic strata. Minibasin inversion observed

DIAPIR GROWTH: EARLY TRIASSIC

Observation:

Important thickness variations and growth strata are observed in the lowest part of MS1 (Figure 36). A growth tendency is recognized on the MBP by a positive slope into the Lower Triassic interval. This is especially visible into the southeastern minibasin close to D2 and D3, where the larger depocenter is located. The depth thickness map indicates that the passive growth of salt diapirs took place earlier in the southeastern minibasins than in the northwestern minibasins (Figure 27).

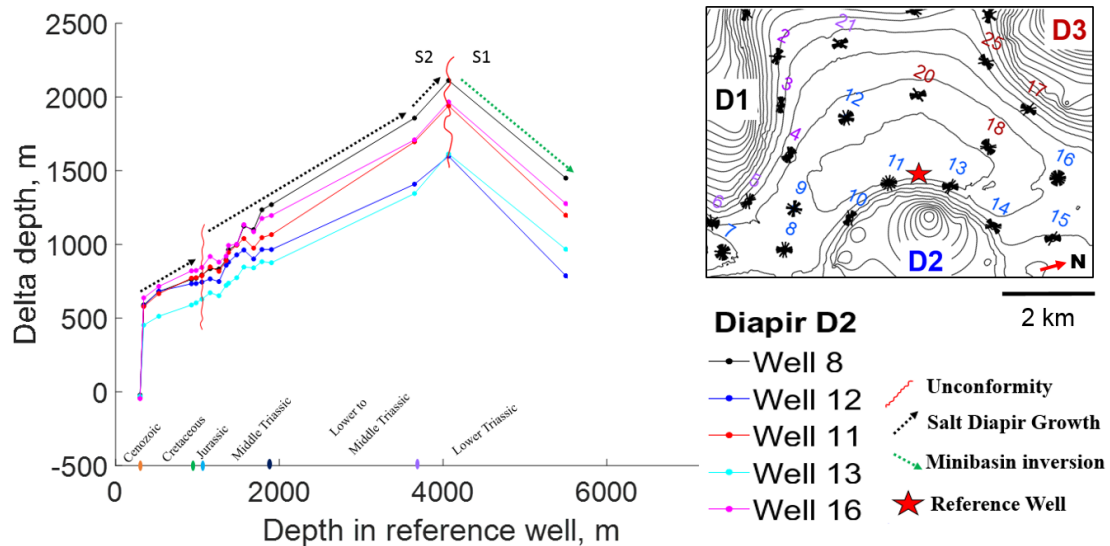


Figure 36. MBP for diapir D2 showing the minibasin inversion during Lower Triassic. A general growth trend driven by passive diapirism is recognized after the unconformity between sequences S1 and S2. The inset map displays the position of wells respect to the reference well, which is located closer to diapir D2.

Interpretation

Evidences of thickness variation and growth strata into the MS1 supports the theory of a syn-kinematic sedimentation (Rojo and Escalona et. al., 2019) during the Early Triassic that is influenced by halokinetic movement (Figure 35 **Error! Reference source not found.**). Towards the east, the void created by tectonic subsidence was infilled by Lower Triassic NNW-prograding fluviodeltaic systems that causes a differential loading at the basin axis and salt expulsion towards the North (Figure 37FH). Based on the MBP, the thick-skinned extension allowed the rise of salt structures by passive diapirism, being less regular and discontinuous towards the northwestern minibasin that is affected by diapir D1. However, the rest of diapirs show more regular and continuous growth rates (Figure 35). The evacuated salt due to the subsalt faulting led to the shift in salt withdrawal from the Early to Middle Triassic, what explains the minibasin inversion observed in the southeastern minibasins (Figure 32). This change in the environmental condition is represented on the MBP as a negative slope, what indicates that strata are thinning as they go away from salt bodies (Figure 35).

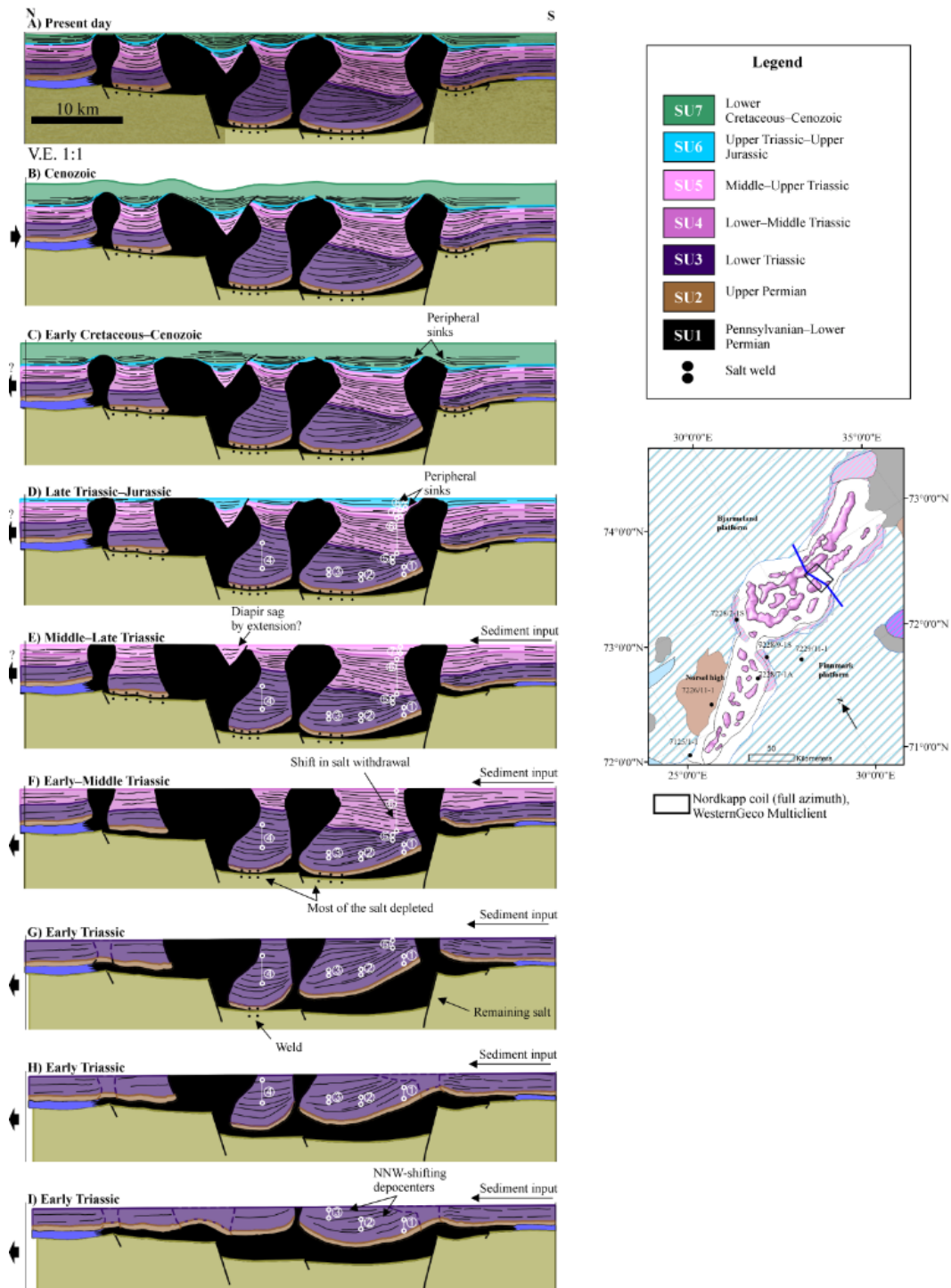


Figure 37. Two-dimensional (2-D) cross section restoration taken from Rojo and Escalona et al., 2019 corresponding to the study area of this master thesis. (G-I) Early Triassic minibasins inversion due to the sub-salt faulting responsible for the salt evacuation and the subsequent shift in salt withdrawal. (E-F) Early to Middle Triassic diapir collapse or sag in response to minor movement of sub-salt. (C-E) Middle Triassic-Jurassic depocenters migrating from the SE to the NW. (D) Late Triassic gravity gliding to induce contractional diapirism and to form teardrop diapirs. (C) Early Cretaceous-Cenozoic regional shortening leading to the rejuvenation and growth of salt diapirs.

DIAPIR GROWTH: EARLY TO MIDDLE TRIASSIC

Observation:

S3 comprises evidences of halokinesis (e.g. large thickness variations). As result of this, salt minibasins flanked by salt diapirs were forming. The growth trend is recognized on the $\Delta d/d$ plots as a marked positive slope (growth ranges around 1000 m; Figure 35). However, in the northwester part, the sediment growth decreases since the slopes turning into more and more negative towards the north, the transition from a positive to negative slope is evidence on Figure 35. The minor growth rate is also visible in the depth-thickness map (Figure 27). Furthermore, this area underwent extensional events that caused the collapse of diapir D4 (Figure 38), creating salt minibasins at its crest surrounded by the remaining salt horns. Within this depocenter, growth strata onlap towards the SW-NE fault-related to collapse.

Interpretation:

Because of halokinetic movement, the minibasin flanked by the diapirs D1 and D2 in the southeater part, displays a large depocenter of up to 2000 m of sediment accumulation (Figure 27). The minor sediment growth in the northwester part is due to the salt diapirs D3 and D4 grew less in comparison to the diapirs D1 (Figure 27). Thus, the available accumulation space was also small. The enclosed minibasin by the reaming salt horns of diapir D4 was progressively filled by prograding shallow-marine and fluviodeltaic sediments.

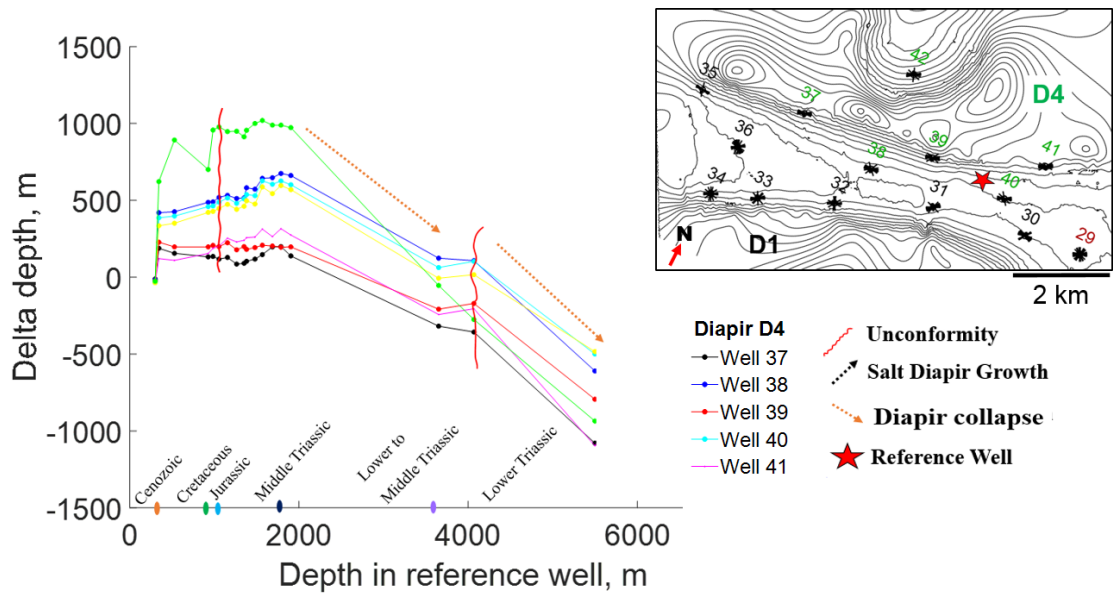


Figure 38. Graph showing the growth rate of diapir D4. Observing the general negative trend of the $\Delta d/d$ curves the growth rate relate to this salt structure is the lowest compared with the others diapirs due to diapir D4 underwent an extension episode that led to diapir collapse (Figure 37E-F).

DIAPIR GROWTH: MIDDLE TRIASSIC-JURASSIC

Observation:

Migration of depocenter from the SE to the NW. Towards the south, S4, S5 and S6, are onlapping the diapirs flanks (Figure 33). On the $\Delta d/d$ graphs the sediment growths are showed as small changes in the slope; with a positive trend for the NW flank of the diapir D1 (Figure 39), whereas onto its SE flank the slope turns into flat compared with the diapir D3 trend, which is also located in the central part. (Figure 40). In the northwestern part, the collapse of diapir D4 continued and the resulting minibasins kept filling to develop a large depocenter. This process is showed on $\Delta d/d$ plot as a sharp change in slope of the green line about 1000 m in depth (Figure 38).

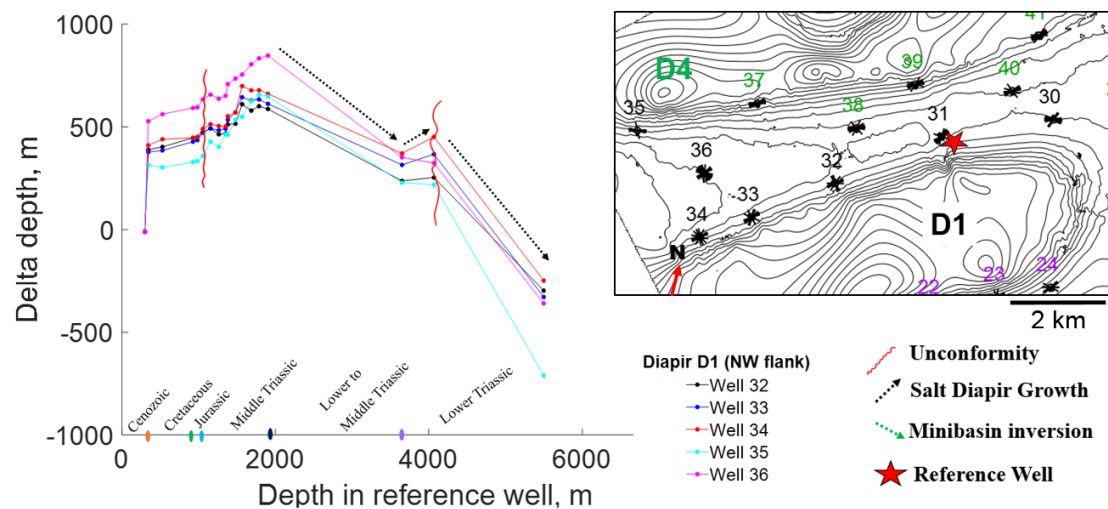


Figure 39. Graph showing the MBP for the NW flank of diapir D1, according to the negative slope of its $\Delta d/d$ curves, in this zone diapir D1 grew less than southeastern salt structures during the Triassic period.

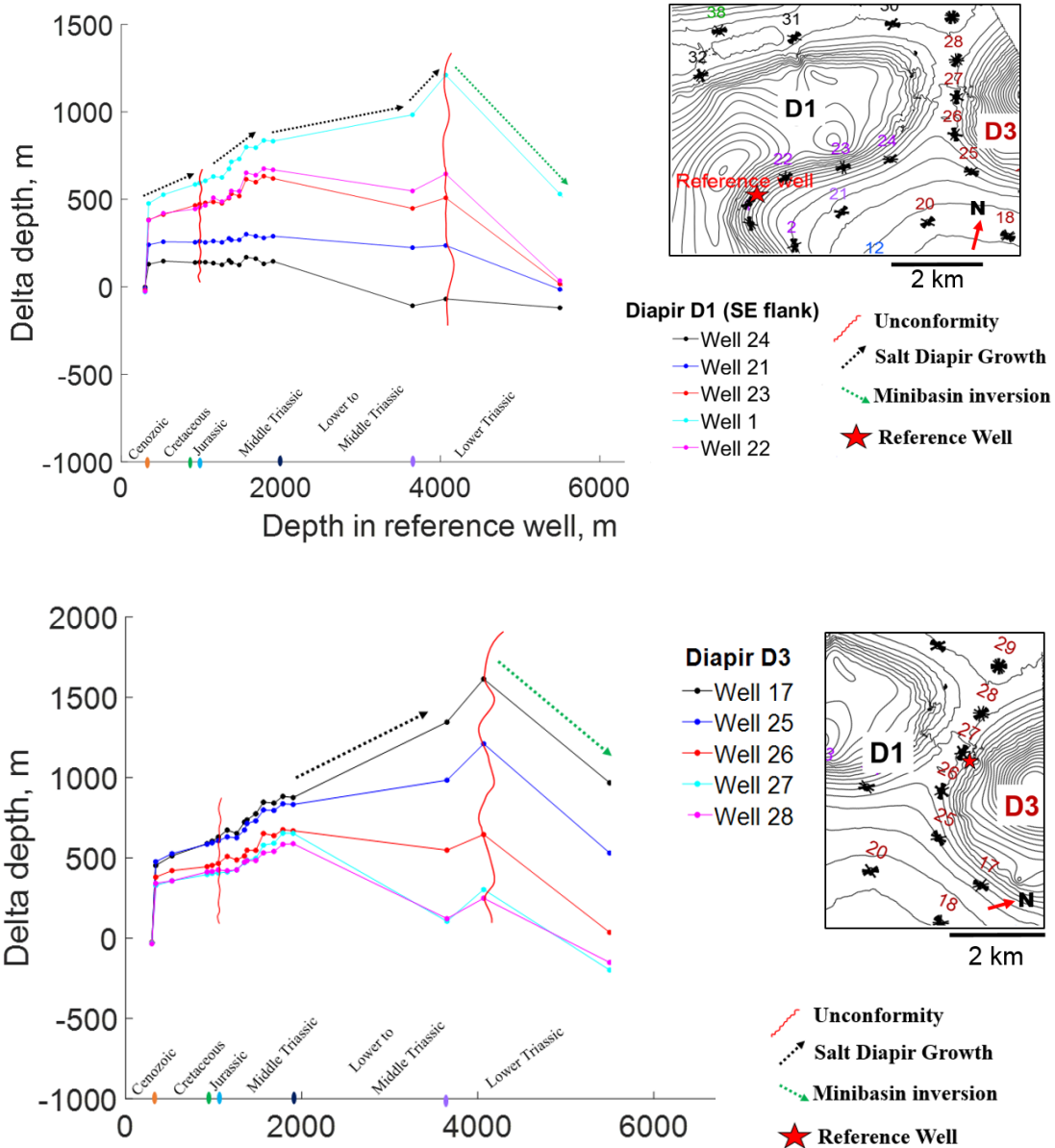


Figure 40. (Top) MBP for diapir D1 (SE flank) showing a positive growth trend during the Triassic interval compared with its NW flank (**Error! Reference source not found.**), although $\Delta d/d$ curves of wells located towards the N (wells 22-24) are adopting a negative trend what means a smaller growth rate in this region. (Bottom) Plot of $\Delta d/d$ curves related to diapir D3. Note the marked positive slope in contrast diapir D1, which indicates that diapir D3 has a greater growth rate than diapir D1 on its SE flank.

Interpretation:

During this period, most of the underlying salt was depleted with the exception of the northeastern part, where the expulsion of the salt continued causing a sediment loading, which induced the migration of depocenters from the SE to the NW (Figure 37E). That is why the trend in the NW flank of diapir D1 is positive indicating a salt growth by passive diapirism (Figure 39). On the contrary, on its SE flank the small thickness variations of the S4, S5 and S6 can be attributed to minor extension (Figure 37D-E). These different slopes around diapir D1 indicate that (1) towards the southeastern minibasin diapir D1 grew less than diapir D2 and D3 (Figure 40). (2) On the NW flank, the positive trend shows a greater growth of diapir D1 compared to diapir D4, which was undergoing collapse. According to Rojo et al. (2019), the minor extension resulted in a triggering towards the basin with the gravity gliding of suprasalt strata what induced a contractional diapirism that can create salt structures such as teardrop diapirs. The salt motion occurred during this time seems to influence on the distribution of fluvial systems located into S5; this matter will be discussed above.

5. DISCUSSIONS

5.1. Diapir growth history in the central sub-basin

The overall growth history of salt diapirs in the central sub-basin deduced from observations and interpretation of seismic data and Multiple Bischke Plots (MBP) comprises three main episodes: (1) the minibasins inversion during the Lowest-Early Triassic due to a shift in loading. This phenomenon is observed both on the $\Delta d/d$ plots (Figure 41) and on seismic lines (Figure 33), where MS1 thickens towards the salt diapirs D1 instead of thinning (Figure 37G-I), (2) Passive diapirism affecting all diapirs (Figure 37E-H) and, (3) a regional shortening event and diapir rejuvenation that led to teardrop diapirs (Figure 37C-D).

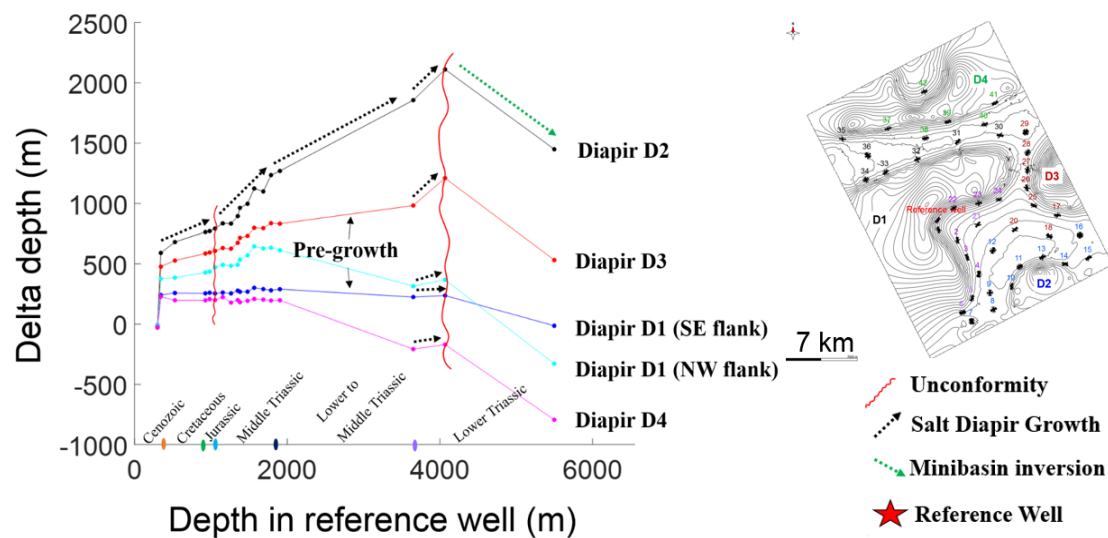


Figure 41. Graph showing the Multiple Bischke Plot for the structurally higher Reference Well No.1 respect to five wells around every salt diapir. The MBP depicts the overall growth trend for each diapir. During the Lower Triassic, diapirs D2 and D3 show a greater growth than diapir D1 and D4. Through the Lower-Middle Triassic, the growth trend is the same, SE salt structures keep growing more than NW diapirs. In the Middle Triassic-Jurassic, migration of depocenters occurred because of diapirs located to the NW (D1 and D4) grew more than diapirs D2 and D3 in the SE due to the salt depletion in this part. Two unconformities are identified between (1) Lower Triassic sequences S1 and S2, and (2) Middle Triassic and Jurassic strata. Minibasin inversion observed in Lower Triassic sequences.

5.2. Influence of the diapirs growth on the distribution of Triassic fluvial systems.

The Nordkapp Basin study results of great interest since it involves halokinetics and fluvial systems, what allows the opportunity to investigate how channels are affected by rising of salt structures because they are intensely sensitive to minor changes of both slope and sediment load (Damuth et al., 1998; Gee et al., 2007). Due to this study uses high-resolution 3D seismic data (full azimuth); two different fluvial systems are identified: the segment of a meandering channel and braided channels (Figure 42). After performing attribute analyses and the Bischke method $\Delta d/d$, the results suggest that the fluvial systems observed into the S5 (Middle Triassic) show evidences that they overcome the influence of the diapirs growth. In this way, it is observed that diapir D1 exerts the major influence on the meandering channel into the southeaster minibasin which is also enclosed by diapirs D2 and D3. As these diapirs show a greater growth rate than diapir D1 (Figure 41), the channel tends to migrate towards the last one but no big influence is recognized in its SE flank. This indicates that the depositional rate was higher compared to the salt diapir growth rate. However, the salt movements started to slow down greatly in the southern part and the diapir D1 reached a point to the NW in where it grew more and exceeded the depositional rate, what caused the channel bypassed the diapir D1 in order to make it to the diapir D4 (Figure 42). The segment of this meandering channel that crossed the northwestern minibasin was eroded by the following braided system that was flowing along the minibasin. Even all diapirs show a general trend to rise. The growth rate varies from one diapir to each other, what influences on the channels dynamic i.e., salt diapirs control the distribution of surrounding depositional environments and sediments. This difference in growth rate

for every diapir is illustrated on Figure 42 as red arrows. Thus, as bigger the arrow is; higher growth rate.

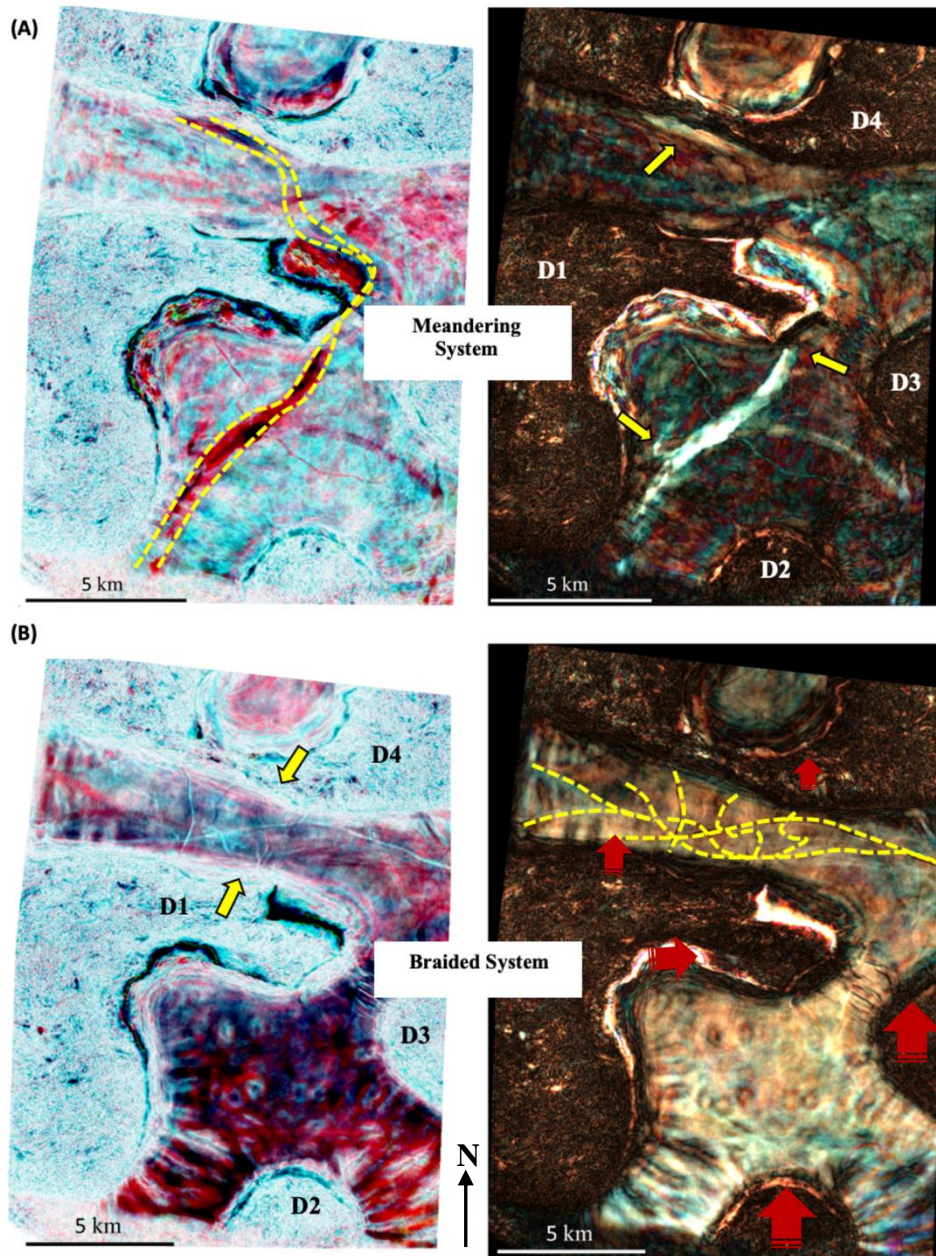
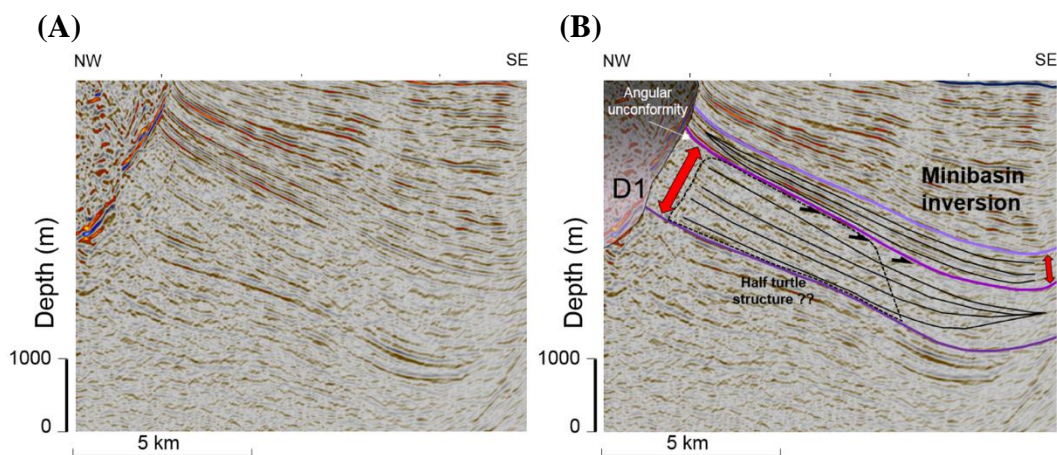


Figure 42. Depth slice an **Data courtesy of WesternGeco Multiclient 5 strata (Middle Triassic)**. (A) Depth slices at 1872 m showing the trajectory of the meandering channel bypassing the diapir D1 to reach the diapir D4. (B) Depth slice at 1872 m displays the braided system along the NW minibasin enclosed by D1 and D4.

5.3. Implication in the petroleum system.

Analysing how much a diapir grows compared with the others may be a useful tool in order to predict the location of the highest growth or the highest petroleum potential intervals. This is like that, because a salt-sediment interaction exists and influences on the distribution of surrounding depositional environments and sediments. Then, under conditions of low growth for a diapir, submarine channels tend to locate close to the diapirs and even can bypass them. This has important implications for hydrocarbon exploration since in a scenario of low diapir growth there is a higher chance of potential reservoirs on diapir flanks. In addition, the Bischke method helps to gain insight into the stratigraphic and structural configuration of the area analyzed; helping to identify important angular unconformities, which might act as stratigraphic traps. An example of this is recognized within Lower Triassic sequences S1 and S2, between these sequences, an unconformity results from the formation of a turtle structure (Figure 43).



Data courtesy of WesternGeco Multiclient

Figure 43. (A) Uninterpreted seismic analysis of the Lower Triassic. (B) Interpreted detailed seismic analysis showing the angular unconformity between Lower Triassic sequences S1 and S2, that resulted from the formation of a half turtle structure.

6. CONCLUSIONS

The Multiple Bischke Plots (MBP) display $\Delta d/d$ curves that depict the growth history of a section of sediments readily to interpret. It is used in this thesis to analyse the growth history of the four salt diapirs located in the central sub-basin of the confined salt-bearing Nordkapp Basin. Each single diapir shows a different growth rate. The analysis of these growth trends has allowed on the one hand, understanding the distribution and configuration of the Triassic sediments, which are affected by the salt bodies and on the other hand, providing a growth history for these salt diapirs. The importance of this study is because of the salt-sediment interaction analysis has relevant implications for hydrocarbon exploration since these researches help to predict the location of the highest petroleum potential intervals.

In this thesis, six MPB or $\Delta d/d$ graphs have been plotted after performing a detailed seismic interpretation of a region in the center sub-basin of the Nordkapp Basin, which was focused on the Triassic period. Every MBP corresponds to one diapir. From these plots and together with knowledge of regional geology some useful information about the growth of sediments and salt structures is deduced:

- 1) Diapirism was triggered by thick skinned extension (Rojo et al., 2019). First, the suprasalt faults creates space of accommodation in the suprasalt which will be filled by sediments, what induces differential loading of the salt and cause its mobilization. Second, the thick-skinned extension stretches the overburden and makes it weaker, allowing salt extrusion and passive diapirism.

- 2) Diapirs growth trend is roughly common for all diapirs. However, it is important to keep in mind that not all salt structures formed in the same time and way, i.e. salt withdrawal is different in each period. Lower Triassic intervals show a great salt evacuation that leads the rise of salt structure mainly in the SE part (Diapirs D2 and D3). During the Early to Middle Triassic minor salt movement occur, what results in the collapse of diapir D4. Middle Triassic-Jurassic interval displays a depocenter migration, diapirs towards the NW grew greater than those located in the SE part. The Late Triassic gliding is responsible for the contractional diapirism to generate teardrop diapirs. Episodes of shortening are recognized during the Cretaceous and Cenozoic times that allows the rejuvenation and growth of salt diapirs.

- 3) The fluvial systems identified in the study area (i.e. meandering and braided systems) are being affected by the salt diapirs growth. From observation of depth slices, it can be recognized that channels go along places where diapir growth is low in order to keep an equilibrium stage.

7. REFERENCES

- Anell, I., A. Braathen, and S. Olaussen, 2014, The Triassic–Early Jurassic of the northern Barents Shelf: A regional understanding of the Longyearbyen CO₂ reservoir: *Norsk Geologisk Tidsskrift*, v. 94, p. 83–98.
- Baig, I., J. I. Faleide, J. Jahren, and N. H. Mondol, 2016, Cenozoic exhumation on the southwestern Barents Shelf: Estimates and uncertainties constrained from compaction and thermal maturity analyses: *Marine and Petroleum Geology*, v. 73, p. 105–130.
- Bischke, R. E., 1994, Interpreting Sedimentary growth Structure from Well Log and Seismic Data (With Examples): *AAPG Bulletin*, v. 78, p. 873-892.
- Bischke, R. E., W. Finley, and D. J. Tearpock, 1999, Growth Analysis ($\Delta d/d$): Case Histories of the Resolution of Correlation Problems as Encountered while Mapping around Salt: *Gulf Coast Association of Geological Societies Transactions*, v. XLIX, p. 102-110.
- Bugge, T., G. Elvebakk, S. Fanavoll, G. Mangerud, M. Smelror, H. M. Weiss, J. Gjelberg, S. E. Kristensen, and K. Nilsen, 2002, Shallow stratigraphic drilling applied in hydrocarbon exploration of the Nordkapp Basin, Barents Sea: *Marine and Petroleum Geology*, v. 19 p. 13-37.
- Buiter, S. J., and T. H. Torsvik, 2007, Horizontal movements in the eastern Barents Sea constrained by numerical models and plate reconstructions: *Geophysical Journal International*, v. 171, p. 1376–1389.
- Carter, R. C., M. R. Gani, T. Roesler, and A. k. Sarwar, 2016, Submarine channel evolution linked to rising salt domes, Gulf of Mexico, USA: *Sedimentary Geology*, v. 342, p. 237–253.
- Catuneanu, O., W. E. Galloway, C. G. S. C. Kendall, A. D. Miall, H. W. Posamentier, A. Strasser, and M. E. Tucker, 2011, Sequence stratigraphy: Methodology and nomenclature: *Newsletters on Stratigraphy*, v. 44, p. 173–245.
- Corfu, F., S. Polteau, S. Planke, J. I. Faleide, H. Svensen, A. Zayoncheck, and N. Stolbov, 2013, U–Pb geochronology of Cretaceous magmatism on Svalbard and Franz Josef Land, Barents Sea Large Igneous Province: *Geological Magazine*, v. 150, p. 1127–1135.
- Dengo, C., and K. Røssland, 1992, Extensional tectonic history of the western Barents Sea, in R. M. Larsen, H. Brekke, B. T. Larsen, and E. Talleraas, eds., *Structural and tectonic modelling and its application to petroleum geology*: Oslo, Norway, Norwegian Petroleum Society, v. Special Publication 1, p. 91–107.

- Faleide, J. I., K. Bjørlykke, and R. H. Gabrielsen, 2015, Geology of the Norwegian Continental Shelf, *in* K. Bjørlykke, ed., *Petroleum Geoscience*: Berlin Heidelberg, Springer p. 603–637.
- Faleide, J. I., F. Tsikalas, A. J. Breivik, R. Mjelde, O. Ritzmann, O. Engen, J. Wilson, and O. Eldholm, 2008, Structure and evolution of the continental margin off Norway and the Barents Sea: *Episodes*, v. 31, p. 82-91.
- Fossen, H., 2010, *Structural Geology*: Cambridge: New York, Cambridge University Press.
- Gabrielsen, R., O. Kløvján, A. Rasmussen, and T. Stølán, 1992, Interaction between halokinesis and faulting: Structuring of the margins of the Nordkapp Basin, Barents Sea region, *in* H. B. B. Larsen, B. Larsen, and E. Talleraas, ed., *Structural and tectonic modelling and its implication to petroleum geology*: Oslo, Norway, Norwegian Petroleum Society Special Publication 1, p. 121-131
- Gabrielsen, R. H., I. Grunnaleite, and S. Ottesen, 1993, Reactivation of fault complexes in the Loppa High area, southwestern Barents Sea, *in* E. B. T. O. Vorren, Ø. A. Dahl-Stammes, E. Holter, B. Johansen, E. Lie, and T. B. Lund, ed., *Arctic geology and petroleum potential*: Oslo, Norway, Norwegian Petroleum Society Special Publication 2, p. 631–641.
- Ge, H., M. P. Jackson, and B. C. Vendeville, 1997, Kinematics and dynamics of salt tectonics driven by progradation: *AAPG Bulletin*, v. 81, p. 398–423.
- Gernigon, L., M. Brönnner, D. Roberts, O. Olesen, A. Nasuti, and T. Yamasaki, 2014, Crustal and basin evolution of the southwestern Barents Sea: from Caledonian orogeny to continental breakup: *Tectonics*, v. 33, p. 347-373.
- Giles, K. A., and T. F. Lawton, 2002, Halokinetic sequence stratigraphy adjacent to the El Papalote diapir, northeastern Mexico: *AAPG Bulletin*, v. 86, p. 823–840.
- Giles, K. A., and M. G. Rowan, 2012, Concepts in halokinetic sequence deformation and stratigraphy, *in* S. G. A. G. I. Alsop, A. J. Hartley, N. T. Grant, and R. Hodgkinson, ed., *Salt tectonics, sediments and prospectivity*, v. 363: London Special Publications 2012, Geological Society, p. 7–31.
- Gjelberg, J., and R. J. Steel, 1995, Helvetiafjellet Formation (Barremian-Aptian), Spitsbergen: characteristics of a transgressive succession, *in* V. L. F. R. J. Steel, E. P. Johannesson, and C. Mathieu, ed., *Sequence stratigraphy on the Northwest European margin*: Oslo, Norway, Norwegian Petroleum Society Special Publication 5, p. 571–593.

- Glørstad-Clark, E., J. I. Faleide, B. A. Lundschieen, and J. P. Nystuen, 2010, Triassic seismic sequence stratigraphy and paleogeography of the western Barents Sea area: *Marine and Petroleum Geology*, v. 27, p. 1448–1475.
- Grantz, A., P. E. Hart, and V. A. Childers, 2011, Geology and tectonic development of the Amerasia and Canada Basins, Arctic Ocean, *in* A. F. E. A. M. Spencer, D. L. Gautier, A. V. Stoupakova, and K. Sørensen, ed., *Arctic petroleum geology*, v. 35: London, Geological Society, p. 771-799.
- Grogan, P., K. Nyberg, B. Fotland, R. Myklebust, S. Dahlgren, and F. Riis, 2000, Cretaceous magmatism south and east of Svalbard: evidence from seismic reflection and magnetic data: *Polarforschung*, v. 68, p. 25-34.
- Henriksen, E., H. Bjørnseth, T. Hals, T. Heide, T. Kiryukhina, O. Kløvjan, G. Larssen, A. Ryseth, K. Rønning, and K. Sollid, 2011a, Uplift and erosion of the greater Barents Sea: Impact on prospectivity and petroleum systems, *in* A. F. E. A. M. Spencer, D. L. Gautier, and a. K. S. A. V. Stoupakova, eds., *Arctic petroleum geology*, v. 35: London, Geological Society, p. 271–281.
- Henriksen, E., A. Ryseth, G. Larssen, T. Heide, K. Rønning, K. Sollid, and A. Stoupakova, 2011b, Tectonostratigraphy of the greater Barents Sea: Implications for petroleum systems, *in* A. F. E. A. M. Spencer, D. L. Gautier, A. V. Stoupakova, and K. Sørensen, ed., *Arctic petroleum geology*, v. 35: London, Geological Society, , p. 163–195.
- Henriksen, S., and T. O. Vorren, 1996, Early Tertiary sedimentation and salt tectonics in the Nordkapp Basin, southern Barents Sea: *Norsk Geologisk Tidsskrift*, v. 76, p. 33–44.
- Hudec, M. R., and M. P. Jackson, 2007, Terra infirma: Understanding salt tectonics: *Earth-Science Reviews*, v. 82, p. 1–28.
- Jackson, M. P., and M. R. Hudec, 2017, *Salt Tectonic: Principles and Practice*, Cambridge University Press.
- James, N. P., and R. W. Dalrymple, 2010, *Facies Models 4* Geological Association of Canada.
- Jensen, L. N., and K. Sørensen, 1992, Tectonic framework and halokinesis of the Nordkapp Basin, Barents Sea, *in* H. B. R. M. Larsen, B. T. Larsen, and E. Talleraas, ed., *Structural and tectonic modelling and its application to petroleum geology*: Oslo, Norway, Norwegian Petroleum Society Special Publication 1, p. 109–120.
- Jenyon, M. K., 1986, *Salt Tectonics*, Elsevier.
- Koyi, H., 1998, The shaping of salt diapirs: *Journal of Structural Geology*, v. 20, p. 321–338.

- Koyi, H., M. K. Jenyon, and K. Petersen, 1993a, The effect of basement faulting on diapirism: *Journal of Petroleum Geology*, v. 16, p. 285–312.
- Koyi, H., C. J. Talbot, and B. Torudbakken, 1995a, Analogue models of salt diapirs and seismic interpretation in the Nordkapp Basin, Norway: *Petroleum Geoscience*, v. 1 p. 185–192.
- Koyi, H., C. J. Talbot, and B. O. Tørudbakken, 1993b, Salt diapirs of the southwest Nordkapp Basin: Analogue modelling: *Tectonophysics*, v. 228,, p. 167–187.
- Koyi, H., C. J. Talbot, and B. O. Tørudbakken, 1995b, Salt tectonics in the Northeastern Nordkapp basin, southwestern Barents Sea, *in* D. G. R. M. P. A. Jackson, and S. Snelson, ed., *Salt tectonics: A global perspective: AAPG Memoir 65*, p. 437–447.
- Marin, D., A. Escalona, H. Nøhr-Hansen, K. Sliwinka Kasia, and A. Mordasova, 2017, Sequence stratigraphy and lateral variability of Lower Cretaceous clinoforms in the southwestern Barents Sea: *AAPG Bulletin*, v. 101, p. 1487–1517.
- Mattingsdal, R., T. Høy, E. Simonstad, and H. Brekke, 2015, An updated map of structural elements in the southern Barents Sea.
- Nilsen, K. T., Vendeville, B. C. , and J.-T. Johansen, 1995, Influence of regional tectonics on halokinesis in the Nordkapp Basin, Barents Sea, *in* D. G. R. M. P. A. Jackson, and S. Snelson, ed., *Salt tectonics: A global perspective, AAPG Memoir 65*, p. 413–436.
- Nordaunet-Olsen, E., 2015, Controls on Upper Paleozoic carbonate build-up development in the south central Norwegian Barents Sea: Master's thesis thesis, University of Stavanger, Stavanger, Norway, 154 p., 154 p p.
- Ohm, S. E., D. A. Karlsen, and T. Austin, 2008, Geochemically driven exploration models in uplifted areas: Examples from the Norwegian Barents Sea: *AAPG Bulletin*, v. 92, p. 1191–1223.
- Rojo, L. A., N. Cardozo, A. Escalona, and H. Koyi, 2019, Structural style and evolution of the Nordkapp Basin, Norwegian Barents Sea, *In press*.
- Rojo, L. A., and A. Escalona, 2018, Controls on minibasin infill in the Nordkapp Basin: Evidence of complex Triassic Synsedimentary deposition influences by salt tectonic: *AAPG Bulletin*, v. 101, p. 1239-1272.
- Rojo, L. A., A. Escalona, and L. Schulte, 2016, The use of seismic attributes to enhance imaging of salt structures in the Barents Sea: *First Break*, v. 34, p. 41-49.
- Rowan, M. G., K. A. Giles, T. E. Hearon IV, and J. C. Fiduk, 2016, Megaflaps adjacent to salt diapirs: *AAPG Bulletin*, v. 100, p. 1723–1747.

- Rowan, M. G., T. F. Lawton, K. A. Giles, and R. A. Ratliff, 2003, Near-salt deformation in La Popa basin, Mexico, and the northern Gulf of Mexico: A general model for passive diapirism: *AAPG Bulletin*, v. 87, p. 733–756.
- Rowan, M. G., and S. Lindsø, 2017, Salt tectonics of the Norwegian Barents Sea and Northeast Greenland Shelf A2 *in* J. I. Soto, *in* J. F. Flinch and G. Tari. , ed., *Permo-Triassic salt provinces of Europe, North Africa and the Atlantic Margins*: Amsterdam, Elsevier, p. 265–286.
- Schultz-Ela, D. D., B. C. Vendeville, and M. P. Jackson, 1993, Mechanics of active salt diapirism: *Tectonophysics*, v. 228, p. 275-312.
- Stemmerik, L., G. Elvebakk, and D. Worsley, 1999, Upper Palaeozoic carbonate reservoirs on the Norwegian arctic shelf; delineation of reservoir models with application to the Loppa High: *Petroleum Geoscience*, v. 5, p. 173–187.
- Stemmerik, L., and D. Worsley, 2005, 30 years on-Arctic Upper Palaeozoic stratigraphy, depositional evolution and hydrocarbon prospectivity: *Norsk Geologisk Tidsskrift*, v. 85, p. 151–168.
- Stewart, S., A. Ruffell, and M. Harvey, 1997, Relationship between basement-linked and gravity-driven fault systems in the UKCS salt basins: *Marine and Petroleum Geology*, v. 14, p. 581-604.
- Suppe, J., G. T. Chou, and S. C. Hook, 1992, Rates of folding and faulting determined from growth strata, *in* K. R. McClay, ed., *Thrust tectonics*: New York, Chapman and Hall, p. 105-121.
- Swanston, A. M., M. D. Mathias, and B. C. A., 2011, Wide-azimuth TTI imaging at Tahiti: Reducing structural uncertainty of a major deepwater subsalt field: *Geophysics*, v. 76, p. WB67-WB78.
- Tearpock, D., and R. E. Bischke, 1991, *Applied subsurface geological mapping*: New York, Prentice-Hall.
- Tearpock, E., R. E. Bischke, and J. L. Brewton, 1993, *Quick look techniques and pitfalls in prospect evaluation*, Subsurface Consultants & Associates.
- Trusheim, F., 1960, Mechanism of salt migration in northern Germany: *AAPG Bulletin*, v. 44, p. 1519-1540.
- Van Wagoner, J. C., R. M. Mitchum, K. M. Campion, and V. D. Rahmanian, 1990, Siliciclastic sequence stratigraphy in well logs, cores, and outcrops: concepts for high-resolution correlation of time and facies., v. 7, *American Association of Petroleum Geologists*.

- Venus, J., N. Mountney, and W. McCaffrey, 2015a, Syn-sedimentary salt diapirism as a control on fluvial system evolution: an example from the proximal Permian Cutler Group, SE Utah, U.S.A. : Basin Research, v. 27, p. 152-182.
- Venus, J. H., N. P. Mountney, and W. D. McCaffrey, 2015b, Syn-sedimentary salt diapirism as a control on fluvial system evolution: An example from the proximal Permian Cutler Group, SE Utah, USA: Basin Research, v. 27, p. 152-182.
- Warsitzka, M., J. Kley, and N. Kukowski, 2013, Salt diapirism driven by differential loading—Some insights from analogue modelling: Tectonophysics, , v. 591, p. 83-97.
- Worsley, D., 2008, The post-Caledonian development of Svalbard and the western Barents Sea: Polar Research, v. 27, p. 298-317.